

BARREL RIGIDITY, HEME DISTORTION, LIGAND PROTECTION, AND NITRIC
OXIDE INTERACTIONS WITH HEME IN NITROPHORIN 4

by

Angela Michelle Amoia

A Dissertation Submitted to the Faculty of the
DEPARTMENT OF BIOCHEMISTRY & MOLECULAR BIOPHYSICS
DEPARTMENT OF MOLECULAR & CELLULAR BIOLOGY

In Partial Fulfillment of the Requirements
For the Degree of

DOCTOR OF PHILOSOPHY
WITH A MAJOR IN
BIOCHEMISTRY AND MOLECULAR & CELLULAR BIOLOGY

In the Graduate College

THE UNIVERSITY OF ARIZONA

2006

THE UNIVERSITY OF ARIZONA
GRADUATE COLLEGE

As members of the Dissertation Committee, we certify that we have read the dissertation prepared by ANGELA M. AMOIA

entitled BARREL-RIGIDITY, HEME DISTORTION, LIGAND PROTECTION, AND NITRIC OXIDE INTERACTIONS WITH HEME IN NITROPHORIN 4

and recommend that it be accepted as fulfilling the dissertation requirement for the Degree of DOCTOR OF PHILOSOPHY

Date: November 02, 2006
Dr. William R. Montfort

Date: November 02, 2006
Dr. Megan McEvoy

Date: November 02, 2006
Dr. Matthew Cordes

Date: November 02, 2006
Dr. Ann Walker

Date: November 02, 2006
Dr. Nancy Horton

Date: November 02, 2006
Dr. Elizabeth Vierling

Final approval and acceptance of this dissertation is contingent upon the candidate's submission of the final copies of the dissertation to the Graduate College.

I hereby certify that I have read this dissertation prepared under my direction and recommend that it be accepted as fulfilling the dissertation requirement.

Date: November 02, 2006
Dissertation Director: Dr. William R. Montfort

STATEMENT BY AUTHOR

This dissertation has been submitted in partial fulfillment of requirements for an advanced degree at The University of Arizona and is deposited in the University Library to be made available to borrowers under rules of the Library.

Brief quotations from this dissertation are allowable without special permission, provided that accurate acknowledgment of source is made. Requests for permission for extended quotation from or reproduction of this manuscript in whole or in part may be granted by the head of the major department or the Dean of the Graduate College when in his or her judgment the proposed use of the materials is in the interests of scholarship. In all other instances, however, permission must be obtained from the author.

SIGNED: ANGELA M. AMOIA

ACKNOWLEDGMENTS

THE MONTFORT LABORATORY. All members, Dr. Bill Montfort – *mentor*, Dr. Sue Roberts – *numerous discussions*, Dr. Andrzej Weichsel – *some data collection, numerous discussions*, Carrie Plummer – *mutant production*, Jacquie Brailey – *protein preparation, heme analog titration, constant encouragement*, Abreeza Zegeer – *some crystallization*, Dr. Estelle Maes – *moral support, training & mentorship in early years, and numerous conversations during her post doc*, Dr. Lauren Murata – *moral support*, Xiaohui Hu – *kinetics and overall knowledge*; **DEPT OF BMB.** Dr. Tom Baldwin – *always looking out for the best for his department*, Olivia Mendoza – *door always open for questions & fashion talk*, Kriss Pope, Jane Dugas, Douglas Starkey, Ron Richards, 5th & 4th Floor Biological Sciences West, Dr. Vahe Bandarian – *teaching colleague and kinetics*; **DEPT OF MCB.** Barb Johnson – *door always open*, Marilyn Kramer – *support and good spirits, always knowing answers*, Dr. Carol Dieckmann – *teaching colleague*, Dr. Kate Dixon – *being supportive and understanding*; **DISSERTATION COMMITTEE.** Dr. Megan McEvoy – *numerous discussions, constant encouragement, teaching colleague*, Dr. Matt Cordes – *mentorship & great bluegrass*, Dr. F. Ann Walker, Dr. Nancy Horton – *teaching colleague*, Dr. Elizabeth Vierling,; **DATA.** Brookhaven National Laboratory (BNL), Argon National Laboratory-Advanced Photo Source (APS), Stanford Synchrotron Radiation Laboratory (SSRL), Pete Dunten – *SSRL remote collection support staff*, Dr. Nikolai Shorkhiev – *–pdb Transform program*, Irina Persikova – *PDB Deposition*, Annie Heroux – *BNL mail-in data collection for apo-rNP4*, Dr. Gordon Tollin – *Cary 300-Bio UV-Visible Spectrophotometer for kinetics*, Dr. Katrina Miranda – *donation of DEA/NO compound, NO discussions*; **FUNDING.** ARCS Foundation, MCB Training Grant (T32 GM08659), National Institutes of Health grant HL62969 to William R. Montfort, Department of BMB; **FAMILY & FRIENDS – WITHOUT THEM THERE WOULD BE NO ME.** Ma (Felicia Ann) & Dad (Louie) Amoia – *no words to describe*, Sam & Magin Amoia – *invitation always open for a visit, constant support & a swift kick when needed*, Gram Longo – *faithfully writing every week since my first week of college*, Mike Foster – *no words to describe*, Freddie ‘Foster’ – *many cuddles & thinking my computer mouse is a toy*, David and Fay Foster, Luna ‘Famoia’ – *our newest member*, Julie Gramaglia – *our treehouse days*, The A. W. Commune [Becca Walker, Anne Walker, Amanda Reynolds, Stacie Gibbins, Sara Giles, Andrea Albright, Cortnie Cherry] – *LOST, being you, girl talk*, The Boys [Tom Hartl, Chris Pappas, Mike Dillinger, Jay Koniscka] – *porch*, Danielle Davidson – *being you & many 17th St chats*, Liz Saunders – *great cooking times*, Laura Van Dorn – *pep talks*, Rafaela Machado – *sushi*, Katie Hamm, Matt & Candice Donaldson, Erin Dolan, Branwen Hall & Jim Spoonemore, Alex Eilts, April Childs, Stryder Meadows, Vegas Crew [Cordones, Ed & Beth, Kirsten & Dan, Alex & Olga] – *pig roast/clam bakes and many good laughs*, Lynn O’Brien, Tim Koenezer, Jack Bopp, Debbie Daley, Michelle Marks, Joseph Lauricella; **Places.** B-Line – *friendliness & not kicking me out all day*, Epic Café – *many morns of grading*, Rincon Apartments – *Margaret, Steve & Lenny for a great place to live*, Tucson Yoga, Body Wisdom Yoga.

DEDICATION

When you get where you are going, don't forget where you came from.

You can't chance or change time.

There are no words to describe what it is like being in the family that I belong. We hold values, morals, strength, and Italian tradition. I have learned and experienced my whole life with my family by my side and they will continue to be the root of my strength. This thesis is dedicated to my *whole family* with special dedication to my grandma, *Dora Longo*, who has faithfully written to me every week since my first week of college, my Mom, *Felicia Ann Amoia*, who, on top of being my best friend, is the strongest, most beautiful woman I know, my Dad, *Louie Amoia*, who is the most noble and humble person I know, and my big brother, *Savino (Sam) Amoia*, who has always been a role model for me and in our older years, always been there when I needed a good swift kick back to reality. Families are ever changing due to birth, marriage, and death. Our family has been blessed with the addition of my wonderful sister-in-law, *Magin Amoia*, and my full-hearted companion, *Mike Foster*. Their patience and gratefulness with life and others should be hallmarked.

You only live once, in this life time anyway. So don't live in chaos.

Live life as it comes day by day, as if it were your last. For one of them will be.

May 06 1993 – treehouse wall in red paint, auburn NY

TABLE OF CONTENTS

LIST OF TABLES	9
LIST OF FIGURES	10
ABSTRACT	11
CHAPTER 1. INTRODUCTION.....	13
1.1. Macromolecular Structure.....	13
1.1.1. Brief history of X-ray crystallography.....	14
1.1.2. General overview of X-ray crystallography.....	16
1.2. Lipocalins.....	18
1.3. Insect Feeding and the Nitrophorins.....	20
1.4. Structural Features of Nitrophorin 4.....	22
1.4.1. Eight-stranded beta-barrel and introduction to beta-barrel Rigidity.....	24
1.4.2. Hydrophobic molecule binding and introduction to heme distortion.....	25
1.4.3. Flexible omega-loop and introduction to ligand protection.....	31
1.4.4. N-terminal helix and a conserved interaction.....	32
1.4.5. Disulfide-bridge pattern.....	33
1.5. Dissertation Outline.....	33
CHAPTER 2. HIGH RESOLUTION STRUCTURE OF APO NITROPHORIN 4: A RIGID BETA-BARREL REMAINS.....	35
2.1. Introduction.....	35
2.2. Materials and Methods.....	36
2.2.1. Expression and purification of Apo rNP4.....	36
2.2.2. Crystallization, data collection and processing.....	36
2.2.3. Structure determination.....	37
2.3. Results and Discussion.....	38
2.3.1. Apo rNP4 remains ordered resulting in a high resolution structure.....	38
2.3.2. Beta-barrel carbon backbone remains rigid and heme binding	

TABLE OF CONTENTS-Continued

pocket is flexible.....	40
2.3.3. Removal of cofactor slightly affects heme contacting residues.....	44
2.3.4. AB and GH loops closed at low pH	48
2.3.5. Apo lipocalins retain general holo protein structure.....	48
2.3.6. Interaction may act to hold rNP4 beta-barrel intact.....	51
CHAPTER 3. HEME DISTORTION IN NITROPHORIN 4: HIGH RESOLUTION STRUCTURES OF HEME ALTERED, and L123V and L133V MUTANT PROTEINS.....	53
3.1. Introduction	53
3.2. Materials and Methods	57
3.2.1. Mutagenesis of proteins	57
3.2.2. Expression, purification, and activity of mutant and analog proteins.....	58
3.2.3. Crystallization, data collection and processing	59
3.2.4. Structure determinations.....	60
3.2.5. Quantifying heme distortion and orientation of imidazole ligand ...	62
3.3. Results	63
3.3.1. Mutations of distal positions L123 and L133.....	63
3.3.2. Alteration to heme at vinyl positions	80
3.4. Discussion	88
3.4.1. NO binding induces increased ruffling in altered proteins	89
3.4.2. Distal ligand orientation and NO anisotropy changed in altered proteins	89
3.4.3. Macrocycle pivots in heme analog structures	92
3.4.4. Increase in ruffling and elimination of saddling in double mutant gives insight into general distortion mechanism in rNP4 heme	93
3.4.5. Proximal histidine orientation may contribute to ruffling in rNP4.....	99
3.4.6. Tuning heme properties to proper biological function	100
CHAPTER 4: LIGAND PROTECTION AND NITRIC OXIDE INTERACTIONS WITH HEME IN NITROPHORIN 4: KINETIC AND STRUCTURAL ANALYSES OF A LOOP MUTANT.....	103

TABLE OF CONTENTS-Continued

4.1. Introduction.....	103
4.2. Materials and Methods.....	107
4.2.1. Mutagenesis.....	107
4.2.2. Expression and purification.....	108
4.2.3. rNP4 AAA crystallization, data collection and processing.....	109
4.2.4. Structure determination.....	109
4.2.5. Kinetics.....	110
4.3. Results and Discussion.....	113
4.3.1. rNP4 AAA (V36A/D129A/L130A) at 1.0 Å.....	113
4.3.2. Fast phase kinetics.....	117
4.3.3. NO decay from NO-protein complex	122
CHAPTER 5: RESEARCH SUMMARY AND FUTURE DIRECTIONS.....	135
5.1. Barrel rigidity.....	135
5.2. Heme distortion.....	136
5.3. Ligand protection and nitric oxide interactions with heme.....	137
APPENDIX A: ABBREVIATIONS.....	139
APPENDIX B: CRYSTAL GROWTH AND PREPARATION; BEAMLIN INFORMATION.....	141
APPENDIX C: FORMAL CORE DIAGRAMS FOR HEME ANALOG STRUCTURES.....	143
APPENDIX D: TEACHING AT THE COLLEGE LEVEL: A SIDE DISH.....	145
D.1. Introduction.....	145
D.2. Pedagogical Advancements.....	145
D.2.1. Certificate in college teaching.....	145
D.2.2. Molecular graphics curriculum development and instruction in Biochemistry Honors 462aH.....	147
D.2.3. The Wakonse Conference on college teaching.....	150
D.2.4. Biological science instructors journal club.....	151
D.3. My Teaching Philosophy.....	151
REFERENCES	160

LIST OF TABLES

TABLE 2.1. Apo rNP4 Data Collection and Refinement Statistics.....	39
TABLE 2.2. Actual Comparison of Apo and Holo Lipocalins in Current Literature	50
TABLE 3.1. UV-Visible Absorption Maxima (nm) for rNP4 and rNP4 Altered Structures at pH 8.0.....	64
TABLE 3.2. Crystallographic Data and Refinement Statistics for rNP4 Mutant Structures.....	66
TABLE 3.3. Coordination Sphere Geometrical Parameters for rNP4 and rNP4 Altered Structures.....	72
TABLE 3.4. Representative Heme Distortions in rNP4 Altered Structures.....	75
TABLE 3.5. Pyrrole Ring Rotation in rNP4 and rNP4 Altered Structures.....	77
TABLE 3.6. Crystallographic Data and Refinement Statistics for rNP4 Heme Altered Structures.....	83
TABLE 3.7. Highlighted Structural Features for rNP4 Altered Proteins.....	88
TABLE 4.1. rNP4 AAA Mutant Data Collection and Refinement Statistics.....	114
TABLE 4.2. Fast Phase NO Rate Constants at 25 °C.....	120
TABLE 4.3. NO-Protein Complex Decay	129
TABLE B.1. Crystal Growth and Preparation Conditions.....	141
TABLE B.2. Beam Line Information.....	142

LIST OF FIGURES

FIGURE 1.1. Overview of rNP4 Structural Features.....	23
FIGURE 1.2. Heme Coordination Sphere for rNP4-NO and rNP4-NH ₃	27
FIGURE 1.3. Schematic Representation of the Ruffling and Saddling Distortions.....	29
FIGURE 2.1. Ribbon Diagram of Apo rNP4.....	41
FIGURE 2.2. Electron Density in Core of Apo rNP4.....	42
FIGURE 2.3. Heme Contacting Residues in Apo and Holo rNP4.....	45
FIGURE 2.4. Collapse of Val 36.....	47
FIGURE 2.5. Tryptophan-Arginine Interaction in rNP4.....	52
FIGURE 3.1. Protein and Heme Alterations in rNP4.....	55
FIGURE 3.2. Electron Density for the rNP4 L123V/L133V Coordination Sphere.....	68
FIGURE 3.3. Thermal Ellipsoid Plots.....	70
FIGURE 3.4. Atomic Deviations from Planarity for Mutant Complexes.....	79
FIGURE 3.5. UV-Visible Spectrum of Heme Analog 1.....	81
FIGURE 3.6. Coordination Sphere Superimposition of Analog Complexes and Wild-Type rNP4.....	85
FIGURE 3.7. Imidazole Rotation.....	91
FIGURE 3.8. Increased Ruffling in rNP4 L123V/L133V.....	96
FIGURE 3.9. Elimination of Saddling in rNP4 L123V/L133V.....	98
FIGURE 4.1. Loop Mutations in rNP4.....	106
FIGURE 4.2. Open Conformation in the rNP4 AAA Mutant.....	116
FIGURE 4.3. Extraction of First Phase Kinetic Rates.....	118
FIGURE 4.4. NO-Protein Complex Decay Experimental Design.....	123
FIGURE 4.5. NO-Protein Decay Under Aerobic Conditions.....	125
FIGURE 4.6. NO-Protein Decay Under Anaerobic Conditions.....	126
FIGURE 4.7. Spectral Matching for rNP4 AAA at pH 5.....	128
FIGURE 4.8. NO-Protein Decay Under Aerobic Conditions (+GSH).....	131
FIGURE 4.9. NO-Protein Decay Under Anaerobic Conditions (+GSH).....	132
FIGURE C.1. Atomic Deviations from Planarity for Analog 1 Complexes.....	143
FIGURE C.2. Atomic Deviations from Planarity for Analog 2 Complexes.....	144
FIGURE D.1. Concept of a Mentor.....	153

ABSTRACT

Nitrophorins are nitric oxide transport proteins that aid in an insect obtaining a blood meal. The nitrophorins from the saliva of *Rhodnius prolixus*, a blood-sucking insect, consist of seven closely related proteins (rNP1-7). These proteins have the classic hallmarks that define the lipocalin protein family: an eight-stranded beta-barrel, binds a hydrophobic molecule, contains a flexible omega loop that lines the entrance to the binding cavity, contains a N-terminal helix and a conserved Trp-Arg/Lys interaction, and a disulfide bridge pattern. This dissertation explores the functional implications of the rNP4 structure. An apo structure of rNP4 to 1.11 Å resolution revealed the beta-barrel of rNP4 remains a rigid structure in the absence of its heme cofactor and is similar to that of holo rNP4. An X-ray crystallographic study of alterations to protein and heme cofactor was used to explore how heme distortion arises. In all altered proteins, local changes were seen at the point of alteration. The protein has evolved so as to have all surrounding contacts, as well as electronic interactions between ligand and heme, contribute to distortion. An omega loop triple alanine mutant of rNP4 that was unable to collapse over the binding cavity was used to investigate ligand (nitric oxide) protection crystallographically and kinetically. A 1.00 Å resolution structure confirmed the mutant protein was unable to collapse. The loop mutant, as well as wild-type protein, display NO binding to heme that was unaffected by oxygen, indicating that NO binds to heme before reacting with surrounding oxygen. NO-protein complex decay was very slow (hours) under conditions where NO was allowed to rebind to heme, highlighting the protection properties of rNP4. In the presence of oxygen and/or glutathione, which can react with

NO, decay was accelerated but still slow (minutes to hours). Taken together, these data suggest that NO binds to the heme iron and then dissociates and associates hundreds of times before reacting with any surrounding compound.

CHAPTER 1

INTRODUCTION

1.1. Macromolecular Structure

Proteins are biological macromolecules, occurring in all cellular compartments. Proteins arise in great variety (kinds and sizes), exhibit diversity in biological function, and are the molecular instruments in which genetic information is expressed. Proteins are all constructed from the same set of 20 amino acids, covalently linked in characteristic linear sequences. Nature is truly remarkable: by joining these 20 amino acids in many different ways and sequences, proteins arise with dramatically different properties and functions.

The functional properties of proteins depend upon their three-dimensional structures. The three-dimensional structure arises from particular sequences of amino acids arranged into linear polypeptide chains that form the compact domains of the specific structure.

To understand the biological function of these building blocks of life, we would like to be able to predict the three-dimensional structure by examining the amino acid sequence. However, this hope has not yet been achieved. Instead, two primary techniques are used to study the atomic-level three-dimensional structures of proteins: X-ray crystallography and Nuclear Magnetic Resonance Spectroscopy (NMR). This and subsequent abbreviations used throughout this dissertation are in Appendix A. Though

there are advantages and disadvantages to both techniques (beyond the scope of this dissertation), together they give different but complementary information about a protein structure. The majority of this dissertation involves the three-dimensional structure of a salivary protein from *Rhodnius prolixus*, nitrophorin 4 (rNP4). The structures were determined using X-ray crystallography and thus, a brief history and overview of this technique follows.

1.1.1. Brief history of X-ray crystallography

X-ray crystallographic studies of proteins began in the mid 1930's with pioneer crystallographers A.H. Palmer, Max Perutz (1914-2002) and John Kendrew (1917-1997). Palmer began crystallization studies of bovine beta-lactoglobulin (β lg), a lipocalin (see Section 1.2.), and was successful with crystallization but not with structure determination [1,2]. Meanwhile, Max Perutz and John Kendrew, a student of Perutz, were diligently working on crystallization and structure determinations of the globins. The structure of myoglobin (Kendrew) was determined first because it is a single polypeptide chain and smaller in size. Hemoglobin (Perutz) followed and was the first structure of an oligomeric protein to be determined. Studies on hemoglobin began in the mid 1930's and the structure was fully determined in 1959. In 1962, Perutz and Kendrew won the Nobel Prize in Chemistry "for their studies of the structures of globular proteins" along side of Maurice Wilkens, James Watson, and Francis Crick "for their discoveries concerning the molecular structure of nucleic acids and its significance for information transfer in living

material” (Nobel Prize in Physiology or Medicine) and John Steinbeck “for his realistic and imaginative writings, combining as they do sympathetic humor and keen social perception” (Nobel Prize in Literature). Also noteworthy by any respectable scientist is the acknowledgment of the pioneer female crystallographer, Rosalind Franklin. Without her work, the structure of DNA would not have been so rapidly published by Watson and Crick. Rosalind passed on in 1958 at the immature age of 37 from ovarian cancer. She received no recognition at the 1962 Nobel Laureate Award Ceremony [3].

Since the first attempt of β lg, many other attempts to determine the structure of β lg resulted with very low maximum resolution (4-6 Å) [4-9]. However, in 1984, Newcomer et al. both crystallized [10] and determined the structure of the first lipocalin, retinol binding protein (RBP), to 3.1 Å resolution using X-ray crystallography [11]. Because of this, RBP has become the prototypic lipocalin. Since then, and only in the past decade (1997), have structures of β lg reached a satisfactory level of quality for examining molecular details (1.8 Å) [12].

Structures of proteins have been determined at an exponential rate starting in the mid to late 1980's and their coordinates have been deposited into the Protein Data Bank (PDB) (www.pdb.org). As of late summer 2006, there were 35,623 protein structures in the PDB and of those, 30,623 were determined by X-ray crystallography.

1.1.2. General overview of X-ray crystallography

The primary method for obtaining the detailed secondary, tertiary, and sometimes quaternary structures of proteins is X-ray crystallography. The purpose of this section is not to give a detailed description of the physical basis of X-ray crystallography, but rather to provide a general understanding of how a structure is determined through the principles and procedures involved.

The general strategy for determining a protein's structure is as follows. Once the protein is expressed and purified, it is crystallized, diffraction data are measured and converted into electron density, a model is made from the electron density produced, and subsequent structure refinement cycles are performed until the model is in satisfactory agreement with the diffraction data.

Crystallization is a crucial and important step because it is the first prerequisite for solving a structure by X-ray crystallography. The X-ray technique depends upon directing a beam of X-rays onto a regular repeating array of many identical molecules so that the X-rays diffract in a pattern for which the structure of an individual molecule can be retrieved [13]. Because of this, crystals must be well ordered and diffract strongly. Crystals are made of repeating units called unit cells. The more identical and the more closely packed together the unit cells are the better diffraction will be. In addition, diffraction is proportional to the abundance of unit cells contained in a crystal, which in turn depends on the volume of the crystal.

One can surmise that growing well ordered globular protein crystals is not an easy task because they are large, spherical, or ellipsoidal objects with irregular surfaces and it is impossible to pack them into a crystal without forming holes between individual molecules [13]. The most common method used for protein crystallization today is the hanging drop method. In this method, a drop of protein solution is brought to supersaturation by loss of water from the drop to a larger reservoir that contains salt or another dehydrating agent solution (precipitant). Once crystals appear, one must optimize growth to produce single, large crystals suitable for X-ray diffraction experiments. Some of the more common conditions to vary for optimization include precipitant/protein concentration, pH, and temperature.

Once crystals are suitable for study, X-ray diffraction data are collected using an X-ray source. X-rays can be created by a rotating anode (bombarding accelerating electrons into a metal plate), while more powerful X-rays can be produced using synchrotron radiation sources. Synchrotron radiation occurs when a charge moving at relativistic speeds (close to the speed of light) follows a curved trajectory. The particles emitted are very strong and at all wavelengths. As a historical note, the first observed synchrotron radiation, literally observed since it was visible light that was generated, was seen at the General Electric Research Laboratory in Schenectady, New York on April 24, 1947. In the 50-plus years since its discovery, synchrotron radiation in the X-ray and ultraviolet spectral regions has become a premier research tool for the study of matter in all of its varied manifestations. Facilities around the world have evolved and radiation is produced in electron storage rings (~1 mile or so in circumference). Two of the strongest

sources in the world are the Applied Photon Source (APS) at Argonne National Laboratory in the USA and the European Synchrotron Radiation Facility (ESRF) in Grenoble France, with 7 and 6 GeV energy sources respectively. Experimenters, or in these days sometimes only the crystals, travel to radiation rings around the world for data collection. For different X-ray experiments, only radiation within the suitable wavelength ranges is channeled from the storage ring to the diffraction device.

Diffraction data, which includes several hundred thousand diffraction spots, are collected on a detector. The amplitude and the phases of the diffracted rays are used to calculate an electron density map of the repeating unit cell. From this map, one can infer the positions of atoms in the protein and create an initial model of the protein. The quality of the map depends on the resolution of the diffraction data, which in turn depends on how well ordered the crystals are. The refinement process then removes errors in the initial structural model by adjusting the atomic model to improve agreement with measured diffraction data.

In the end, one is left with an atomic model of the protein. From this, one can interpret function and design experiments to test function.

1.2. Lipocalins

Lipocalins are a large and diverse group of small, mostly extracellular, proteins [14]. Lipocalins have been found predominantly in eukaryotic organisms, mostly in vertebrates, although some have been identified in other phyla [15]. Apart from

vertebrates, which are over-represented for historical reasons, the best exemplified phylum is arthropoda [15]. There have also been reports of lipocalins in plants [16,17] and prokaryotes [18]. However, lipocalins have yet to be found in the third main branch of life: the archaeobacteria [15]. The existence of prokaryotic lipocalins has potentially profound implications for understanding lipocalin evolution [18].

Lipocalins are typically small proteins (160-180 residues in length) [15]. They are characterized by the ability to bind small, principally hydrophobic, molecules and have mostly been classified as transport proteins [14]. In fact, the name lipocalin, meaning ‘calyces for lipophilic ligands’, was originally proposed in the mid-80’s by Syed Pervaiz and Keith Brew [19,20]. Together with three other distinct protein families, the fatty-acid binding proteins (FABP), avidins, and metalloproteinase inhibitors such as triabin, the lipocalin family forms part of a larger structural superfamily: the calycins [21-23]. The distinction between protein family and superfamily can appear arbitrary, but this is not simply an argument over semantics. A *protein family* demonstrates a common ancestry when sequence similarity is high enough (typically 35% or more) [14], whereas a *superfamily* is comprised of proteins with closely related three-dimensional structures and probable common ancestry that show no significant overall similarity at the sequence level [15]. The lipocalins have diversity at the primary sequence level but unity at the three-dimensional structural level. Thus, membership to the lipocalin superfamily is based on a conserved folding pattern common to all lipocalin structures determined by high resolution X-ray crystallography or NMR spectroscopy. The common structure of the lipocalin fold is well described [22,24,25]. The structure is mostly comprised of eight

anti-parallel beta strands, A-H, forming a single eight stranded beta-sheet closed back on itself to form a barrel. Typically, the barrel-shaped arrangement leads to a ligand-binding pocket preceded by an N-terminal helix and followed by a C-terminal helix and a short beta-strand [26]. The lipocalin family is also characterized by the conservation of a structural signature [15] that may act as a point that holds together the beta-barrel (See Section 1.4.4.).

1.3. Insect Feeding and the Nitrophorins

Rhodnius prolixus, a small insect prevalent in South America but also found in North America, feeds on the blood of rodents and larger mammals, including humans [27]. The insect, also more commonly known as the kissing bug, is a relatively slow feeder, and probes the tissue until a suitable internal wound is created, or a blood vessel is tapped [28]. Like other slow feeding insects, *R. prolixus* injects numerous proteins into the tissue of victims to aid in obtaining a blood meal. Many studies of *R. prolixus* are stimulated by its role in transmitting *Trypanosoma cruzi*, which causes Chagas' disease, a debilitating disease of the heart that is endemic in Central and South America [29]. Chagas' disease afflicts 16-18 million Latin Americans and there is no cure.

In *R. prolixus*, several antihemostatic proteins have been identified, including proteins that transport nitric oxide (NO), sequester histamine, interfere with blood coagulation, and hydrolyze ADP [27,30,31]. The best characterized of these are the NO carriers, called nitrophorins (NPs) (nitro = NO, phorin = carrier). In *R. prolixus*, a family

of seven NPs are known; four adult insect nitrophorins (rNP1-4) named in order of their abundances in the insect saliva [32-34] and at least three additional nitrophorins in the earlier stages of development (rNP5-7) [33,35,36]. rNP1-4 are each about 20 kD in size and on comparison of their sequences, it is clear that the family arose through gene duplications, with rNP1 and rNP4 being the most closely related (90% identical), and rNP2 and rNP3 the next most closely related (79% identical). Overall, the four nitrophorins display 38% identity [27].

rNP1-4 are stored in the adult insect saliva at low pH, with NO bound to a sequestered heme cofactor. For efficient transport and release of NO to occur, the heme iron must be stabilized in the ferric (Fe(III)) state, where NO affinity is in the micromolar range and NO release is favored. In contrast, when the iron is artificially reduced to the ferrous (Fe(II)) state (the natural state of globins and soluble guanylate cyclase (sGC)), the NO affinity is in the picomolar range and NO release is disfavored [37]. This causes nearly irreversible binding of NO ($K_d^{III}/K_d^{II} \approx 10^6$) [38]. When the protein is delivered to a potential victim, a dilution and a pH elevation in the new environment (from saliva pH ~5 to victim pH ~7.2) leads to reduced affinity for NO, which is then released. Downstream binding of the released NO by sGC results in vasodilation and platelet aggregation. Upon release of NO, the rNPs have evolved to tightly sequester histamine, which is released by the victim in response to tissue damage, ensuring complete release of NO and giving rise to an antihistamine effect that reduces inflammation while the insect feeds [39]. Additionally, rNP2 has a third activity: interfering with blood coagulation at the factor X maturation step. Together the proteins have developed a

unique way for the insect to obtain a blood meal for a prolonged time with modest knowledge from its victim.

1.4. Structural Features of Nitrophorin 4

The initial four adult *R. prolixus* nitrophorins, rNP1-4, were identified and activities determined by the fractionation of hundreds of pairs of salivary glands obtained through insect dissections [32,33,39-43]. These painstaking tasks lead to consequent cloning and expression of rNP1-4 [33,44,45]. This has allowed the four proteins to be extensively investigated both functionally, using a variety of spectroscopic techniques [37,46-53], and structurally using X-ray crystallography. The X-ray crystallographic structures of one or more ligand complexes of rNP1 [46,54], rNP2 [55] and rNP4 [38,52,53,56-58] have been determined.

The crystal structure of rNP1 [54] revealed for the first time a gas transport hemoprotein different from well-characterized globins. rNP1 has the classic eight stranded anti-parallel beta-barrel that defines the lipocalin family of proteins [24]. They also contain three short helices and two disulfide bonds (Figure 1.1.). These characteristics were also observed later in rNP2 and rNP4.

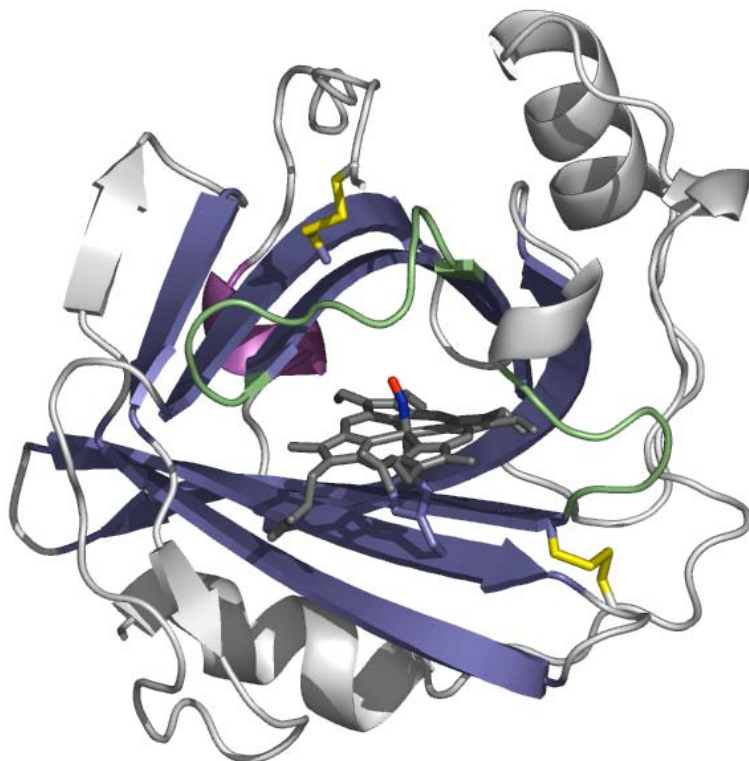


FIGURE 1.1. Overview of rNP4 Structural Features. Ribbon drawing of rNP4 highlighting the structural features that are emphasized in this dissertation. The eight-stranded beta-barrel, discussed in Section 1.4.1. and Chapter 2, is colored blue. The hydrophobic binding pocket containing heme (gray) and nitric oxide (blue/red) is discussed in Section 1.4.2. and Chapter 3. The flexible loop regions are shown in green and discussed in Section 1.4.3., 2.3.4., and Chapter 4. The N-terminal helix, discussed in Section 1.4.4. and Chapter 2, is colored purple while the disulfide bridges are in yellow and discussed in Section 1.4.5 only.

Sequence searches performed before the first rNP structure was determined failed to predict the presence of the lipocalin fold [57]. However, global similarity searches suggested there was some similarity of the rNPs to triabin, a lipocalin protease inhibitor [24]. The rNPs form a distinct group, along with tick histamine binding protein, within the lipocalins and are very distantly related to other members of the family. Indeed, their relationship to the lipocalins was first revealed by X-ray crystallography [24].

The following sections highlight the structural features of rNP4 that are emphasized in this dissertation. Explanation of the dissertation questions and their context in relation to rNP4 is also presented.

1.4.1. Eight-stranded beta-barrel and introduction to beta-barrel rigidity

The general fold of rNP4, as well as rNP1 and rNP2, is an all-beta structure dominated by a single eight-stranded anti-parallel beta-sheet forming a continuously hydrogen-bonded, beta-barrel with one ‘open-end’ and one ‘closed-end’ (Figure 1.1.). The beta-barrel encloses a ligand-binding site composed of an internal hydrophobic cavity (See Section 1.4.2.) and an external loop scaffold (See Section 1.4.3.). The barrel binds a non-polar ligand (heme) within the solvent-accessible barrel.

To date, all nitrophorin crystal structures contain the heme cofactor within the internal cavity. What happens if the heme cofactor is not present? To address this and subsequent questions concerning the role of heme in defining the rNP4 structure, I determined the structure in the absence of heme, called the apo structure. Chapter 2

presents this structure to 1.11 Å resolution. In general, the beta-barrel remains rigid independent of its heme cofactor. That is, the protein retains the general holo protein 3-D structure in the absence of its heme cofactor. Intrinsic interactions within the protein that may stabilize the beta-barrel structure are also discussed.

1.4.2. Hydrophobic molecule binding and introduction to heme distortion

Many lipocalins function through binding of a hydrophobic molecule in one end of the barrel, the ‘open-end’ [59]. This is also true of the nitrophorins. However, the nitrophorins are distinguished from most lipocalins because, in a sense, they have two hydrophobic molecules as ligands: heme, which is ‘permanent’, and nitric oxide (NO), or histamine, which bind to heme and are more ‘transient’ (Figure 1.1.). Heme is a cofactor to nitrophorin meaning that its presence is essential for its function. The barrel of rNP4 accommodates one heme molecule located in the interior with its propionate substituents at the barrel entrance. The heme is linked to the protein via a histidine-iron bond. This histidine, His59, is located in beta-strand C of the beta-barrel and is called the proximal heme ligand. The second ligand is either NO, histamine or water, which bind to the heme cofactor.

Nitric oxide binding induces a conformational change involving two flexible loops, the AB Loop and the GH Loop, at the mouth of the binding pocket and thus NO is protected from its surrounding environment during transport (See Section 1.4.3.). Upon release of NO, due to a pH change and dilution during a blood meal, histamine produced

by the host victim is sequestered by rNP4, taking the place of the NO ligand. In the absence of NO or histamine, the distal pocket is open and water is ligated to the heme and fills the cavity.

The heme of rNP4 is tightly packed into the barrel and contacts ten hydrophobic residues in addition to the proximal histidine (His 95) that forms the fifth iron ligand. Of the contact residues, distal leucines L123 and L133 form close contacts with the heme on either side of the heme iron. This packing results in a highly non-planar heme, where four pyrrole rings are rotated out of the heme plane, termed heme ruffling. Upon addition of NO, the ruffling distortion increases (Figure 1.2.).

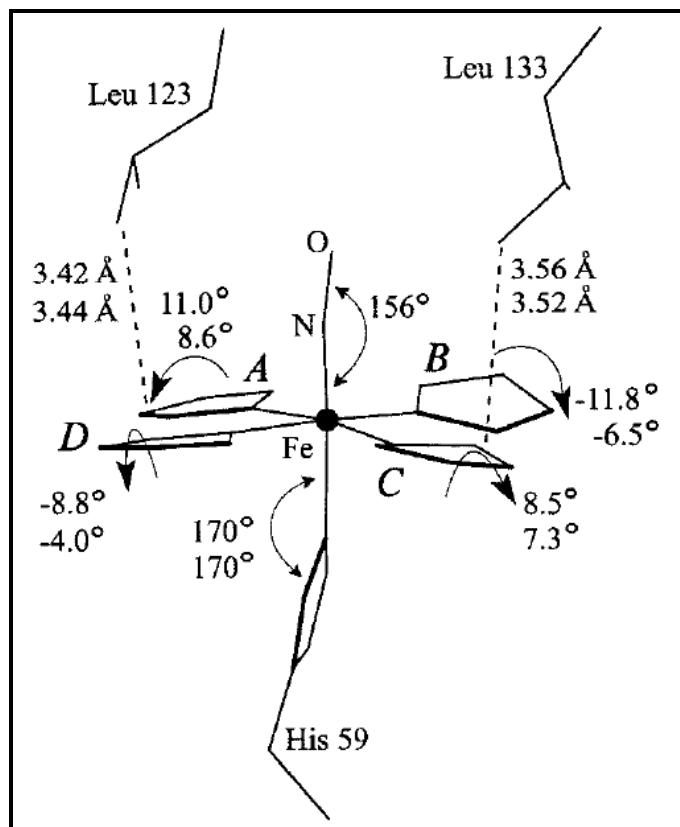


FIGURE 1.2. Heme Coordination Sphere for rNP4-NO and rNP4-NH₃. The figure displays the pyrrole ring rotations that define the heme ruffling distortion. Upper numbers and lower numbers indicate the extent of pyrrole rotation for rNP4-NO and rNP4-NH₃ respectively. Leucine side chains that may contribute to the heme distortion are also shown. (Adapted from [38]).

Figure 1.3. is a schematic representation that defines the ruffling and saddling distortions with respect to the porphyrin ring. For ruffling, opposing rings rotate in the same sense, with, in this case, rings A and C rotating clockwise (as viewed along the Np-Fe bonds) and rings B and D rotate counter clockwise. Thus, two atoms, or half, of each pyrrole ring is above and two atoms, or the other half, are below the porphyrin mean plane. In addition, alternating (or adjacent) meso carbons are above and below the porphyrin mean plane respectively. Together, this results in alternating porphyrin edges above and below the porphyrin mean plane. For saddling, two opposing pyrrole rings are above and below the porphyrin mean plane. In this case rings A and C are below and B and D are above the porphyrin mean plane.

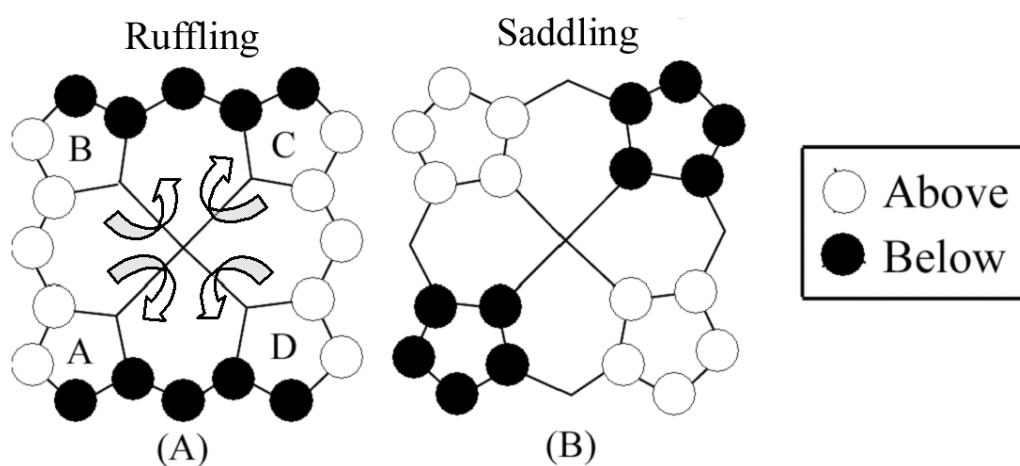


FIGURE 1.3. Schematic Representation of the Ruffling and Saddling Distortions. Pyrrole rings are labeled A-D based on heme convention. Rings A and D have propionate adducts, not shown. White and black filled circles represent atoms displaced above and below the mean porphyrin plane respectively. (A) Ruffling distortion. Curved arrows on nitrogen pyrrole-iron (Np-Fe) bonds indicate the direction of rotation for that Np-Fe. (B) Saddling distortion.

rNP4 contains one of the most highly distorted non-covalently linked hemes so far reported [60]. It provides a representative example of heme distortion in heme proteins and may act as a general example to the central question of how proteins tune hemes to fit their biological function. Non-planar distortions of macrocyclic tetrapyrroles are prevalent not only in the hemes of hemoproteins, but also in pigments of photosynthetic proteins, and in cofactor 430 of methylreductases [61]. The out-of-plane distortions observed in protein structures are ruffling, saddling, and doming. Other distortions include waving and propellering [62]. Distortions are conserved within functional classes of proteins [63] and biological properties such as redox potential, axial ligation, and UV-visible absorption may depend on the degree of non-planarity [64]. The specific functional significance (i.e. how non-planarity influences activity) is an active area of research.

The significance of the nitrophorin heme distortion, if any, is not yet known but may be linked to the setting of reduction potential. To begin understanding the significance of nitrophorin heme distortion, Chapter 3 discusses a mutagenesis study to both the protein and heme cofactor of rNP4. Here, I attempt to describe how heme distortion arises in rNP4 rather than its contributions to function, which awaits further study. In general, rNP4 has evolved a unique way to have all surrounding contacts, as well as electronic interactions between ligand and heme, contribute to distortion.

1.4.3. Flexible omega-loop and introduction to ligand protection

The eight-strands of the barrel (A-H) are linked by a succession of loop connections giving it a simple anti-parallel, meander beta-sheet topology. Seven loops (AB, BC, CD, etc.) are short beta-hairpins, except the AB Loop: this is a large mobile loop, termed the omega-loop. Together with a second mobile loop, the GH Loop (residues 125-132), the AB Loop (residues 31-37) forms a lid to partially close off the mouth of the internal ligand-binding pocket (Figure 1.1). The cavity of rNP4 can be partially open or completely closed off by the extended omega-loop.

Previous structural analyses of rNP4 revealed a substantial NO-induced conformational change [54]. In general, in the absence of NO, the distal heme pocket is 'open' with the AB Loop poorly ordered and the GH Loop located away from the heme. When rNP4 binds NO, the AB and GH Loops collapse into the binding pocket, water is expelled, and nonpolar side chains pack around the heme-ligated NO moiety (Described in more detail in Section 4.1).

NO, as a reactive radical molecule, must be protected for storage and delivery. How do the nitrophorins protect this reactive ligand against side reactions with oxygen? The NO-induced conformational change described above may be a possible answer. In Chapter 4, I discuss a mutagenesis study to the loop region of rNP4 involving residues D129 and L130, associated with GH Loop, and V36, a bulky hydrophobic residue contacting NO. Crystallographic data and kinetic measurements using stopped-flow and UV-visible spectrophotometry were obtained on a triple alanine mutant

V36A/D129A/L130A (rNP4 AAA). In general, loop closure is abolished and NO is less protected from the surrounding oxygen in the rNP4 AAA mutant. In addition, under oxygenated conditions, NO reacts with the heme iron much faster than with surrounding oxygen in both the wild type and rNP4 AAA mutant protein.

1.4.4. N-Terminal helix and a conserved interaction

As well as an overall structural similarity, rNP4 displays a distinct superimposable, non-random structural pattern characteristic of the lipocalin superfamily [25]. In particular, an arginine (rNP4 Arg 139) from the last strand of the beta-barrel (strand H) is able to form a number of hydrogen-bonds (directly or water-mediated) with the main chain carbonyls of the N-terminal, short, helix (Figure 1.1.) at the ‘closed-end’ of the barrel. In addition, Arg 139 indirectly interacts with the conserved tryptophan (rNP4 Trp 23) from the first strand (strand A) of the beta-barrel via a water molecule. Furthermore, rNP4 contains only 2 arginines and 1 tryptophan [27]. This distinct structural signature corresponds to an N-terminal sequence pattern (Gly-XXX-Trp) and a C-terminal (X-Arg/Lys-X) motif that is common to the lipocalin members [15]. Together these conserved interactions seal off the structure, and consolidate the beta-barrel by bringing the ends of strands together [24,25,65]. The possible role of this interaction in rNP4 is discussed in Chapter 2.

1.4.5. Disulfide-bridge pattern

Insect lipocalins that carry protoporphyrin IX derivatives (nitrophorins, bilin binding protein and insecticyanin) contain a disulfide pattern that differs from that in vertebrate lipocalins. The nitrophorins contain one disulfide-bridge linking the N-terminus with beta-strand G while the other couples beta-strand B with the C-terminus (Figure 1.1.). The residues that form these disulfide bonds differ in position with mammalian lipocalins such as Beta-lactoglobulin and retinal-binding protein, which commonly connect beta-strand D to the most carboxyterminal alpha-helix [57,66,67], consistent with greater divergence of the nitrophorins in the lipocalin family [57].

1.5. Dissertation Outline

In the following chapters, I explore the functional implications of the rNP4 structure. I will discuss beta-barrel rigidity in Chapter 2 using an apo structure of rNP4. Chapter 3 explores heme distortion using distal Leu (123 and 133) and heme mutants. Chapter 4 investigates ligand protection using rNP4 mutated in two loops (V36, D129, L130). Chapter 5 summarizes the experimental work in Chapters 2-4 and discusses possible future work on the system.

In addition to scientific research at the bench, teaching has been a considerable part of my graduate career. I have completed a teaching certificate for college teaching and had the honor of being part of the undergraduate Biochemistry Honors course (BIOC

462aH) for five (5) consecutive fall semesters. In Appendix D I will highlight aspects of my pedagogical advancement. These include the Teaching Certificate in College Teaching, curriculum development and instruction for Biochemistry Honors (BIOC 462aH), The Wakonse Conference on College Teaching, and the Biological Science Instructors Journal Club. I conclude this chapter, and dissertation, with my teaching philosophy.

CHAPTER 2

HIGH RESOLUTION STRUCTURE OF APO NITROPHORIN 4:
A RIGID BETA-BARREL REMAINS

2.1. Introduction

Chapter 1 introduced the nitrophorins and their structural hallmark of an eight-stranded beta-barrel topology. In this chapter, I elaborate on this hallmark and discuss barrel rigidity using an apo form of rNP4 obtained by depleting the natural holo protein of heme.

To date, all nitrophorin crystal structures obtained contain its heme cofactor within the internal beta-barrel cavity. I asked a key question, what happens if the heme cofactor is not present? Several subsequent questions follow: Is the protein disordered to the point at which it will not crystallize? Does the beta-barrel carbon backbone remain rigid (retaining the general holo protein 3-D structure in the absence of its heme cofactor) or does the binding pocket collapse? What changes, if any, occur to the heme contacting residues? Does water fill the binding pocket, even though it is hydrophobic in nature? To address these questions, I determined the structure of wild-type rNP4 absent of its heme cofactor, apo rNP4, to 1.11 Å resolution. In general, the beta-barrel remains rigid independent of its heme cofactor, with minor conformational changes in some loop regions and in residues previously in contact with heme. An intrinsic interaction that may stabilize the beta-barrel structure is discussed. This work is the subject of a paper in preparation [68].

2.2. Materials And Methods

2.2.1. Expression and purification of Apo rNP4

Expression and purification of apo rNP4 was carried out by Ms, Jacquie Brailey. Wild-type protein was expressed as inclusion bodies, denatured and refolded. The heme cofactor remained absent and protein was purified by ion-exchange chromatography followed by gel filtration as previously described [49,57,69].

2.2.2. Crystallization, data collection and processing

Detailed crystallization and preparation conditions as well as information on the beam line used for data collection are compiled in Appendix B. Initial crystallization of apo rNP4 was with the help of Ms. Abreeza Zegeer. Crystals were grown at room temperature (~25 °C) using the hanging drop technique in 2.8 M ammonium sulfate, pH 5.6. After one day of equilibration, protein drops were seeded with wild-type rNP4 crystals and large, single, apo-rNP4 crystals appeared in approximately 3 weeks. A single crystal was transferred to a cryoprotectant solution of 3.2 M ammonium sulfate, pH 5.6 and allowed to equilibrate. Following equilibration, the crystal was flash frozen in liquid nitrogen for data collection.

Data were acquired at Brookhaven National Laboratory, New York, on beam line X29 with a Q315 detector at 100 K and processed with mosflm and scala [70] to 1.11 Å

resolution by Dr. Annie Heroux. The crystal belongs to the C2 space group with cell constants typical of those found for wild-type rNP4, $a = 69.5 \text{ \AA}$, $b = 42.8 \text{ \AA}$, $c = 52.7 \text{ \AA}$, and $\beta = 94.7^\circ$ [38] (Table 2.1).

2.2.3. Structure determination

The initial apo structure was built using difference Fourier methods starting with wild-type rNP4 model 1X8O [58]. The phases were subsequently refined with anisotropic temperature factors using REFMAC from the CCP4 package [71] and model building was accomplished with the program COOT [72]. Certain residues were found to occupy more than one conformation and were built and refined as such. In such cases, the occupancies were generally set to 0.5 for each conformer and left fixed when refined. Refinement converged to R factors of 15% and 17% for R_{cryst} and R_{free} , respectively (Table 2.1).

Model quality was assessed using the program PROCHECK [73] as implemented in CCP4 [71]. All residues displayed ϕ/ψ values in the favored or allowed regions of a Ramachandran plot. Structural figures were prepared using PyMOL [74] (<http://www.pymol.org/>). Coordinates will be deposited with the Protein Data Bank.

2.3. Results and Discussion

Up to this report, all nitrophorin crystal structures contain the heme cofactor. I determined the structure of wild-type rNP4 absent of its heme cofactor, apo rNP4, to examine the stability of the beta-barrel fold. In general, the structure retains the overall wild type shape with flexibility and localized changes seen around the heme absent pocket.

2.3.1. Apo rNP4 remains ordered resulting in a high resolution structure

Apo-rNP4 crystallized but did not crystallize under the same conditions as wild-type rNP4 and previously studied mutants. Instead, ammonium sulfate, pH 5.6, was substituted for ammonium phosphate and crystals took approximately 3 weeks to emerge as compared to approximately 24 hours for wild type. The crystal structure was determined at a temperature of 100 K to a resolution of 1.11 Å and, like wild type, belongs to the C2 space group (Table 2.1.). The high resolution of this structure allowed inclusion of hydrogen atoms at calculated positions, refinement of anisotropic temperature factors, and modeling of residues in multiple conformations.

TABLE 2.1. Apo rNP4 Data Collection and Refinement Statistics

Total reflections	176,933
Unique reflections	63,130
Space group	C2
Cell dimensions	$a = 69.5 \text{ \AA}$ $b = 42.8 \text{ \AA}$ $c = 52.7 \text{ \AA}$ $\beta = 94.7^\circ$
Resolution (\AA)	50.00 - 1.11
Highest resolution shell (\AA)	1.15 - 1.11
Completeness (%) ^a	93 / 83
Multiplicity ^a	2.8 / 2.5
Average I/σ_I ^a	25.0 / 3.3
R_{merge} ^{a,b}	0.06 / 0.38
No. of protein residues ^c	184
No. of protein atoms ^c	2,340
No. of solvent molecules ^c	409
Crystallographic $R_{\text{factor}}/R_{\text{free}}$ ^d	0.15 / 0.17
RMSD bond length (\AA)	0.01
RMSD bond angle ($^\circ$)	1.67
Average B-factor (\AA^2)	13.3
Ramachandran Plot Regions	
Favored residues	155 (91.7%)
Allowed residues	14 (8.3%)
Disallowed residues	0 (0%)

^aValues in parentheses indicate the statistics for the highest resolution shell. ^b $R_{\text{merge}} = (\sum_h |I_h - \langle I \rangle|) / (\sum_h I_h)$, where $\langle I \rangle$ is the mean intensity of all symmetry-related reflections I_h . ^cPer asymmetric unit. ^d $R = (\sum |F_{\text{obs}} - F_{\text{calc}}|) / \sum F_{\text{obs}}$. Five percent of the data was reserved for calculation of R_{free} .

2.3.2. Beta-Barrel carbon backbone remains rigid and heme binding pocket is flexible

The high-resolution structure of the apo form of rNP4 determined to 1.11 Å confirms that it has a structure similar to that of holo rNP4, and that all secondary structure hydrogen bonding is intact. Minor conformational changes are observed in some loop regions and in residues previously in contact with the heme in the apo form (Figure 2.1.). Visual inspection of the apo rNP4 electron density revealed the presence of weak but significant pieces of density in the core of the beta-barrel (Figure 2.2.). The largest peaks in this region are $\sim 3.45 \sigma$ in a $F_o - F_c$ electron density map. Molecules responsible for this density in the binding cavity could not be identified, but it is likely that the unexplained density is due to the presence of water, cryoprotectant, and/or a component of the buffer used in the refolding process during protein purification. Unexplained continuous pieces of density in the internal cavity of other lipocalins, such as the apo form of human plasma retinol binding protein, have also been reported [75].

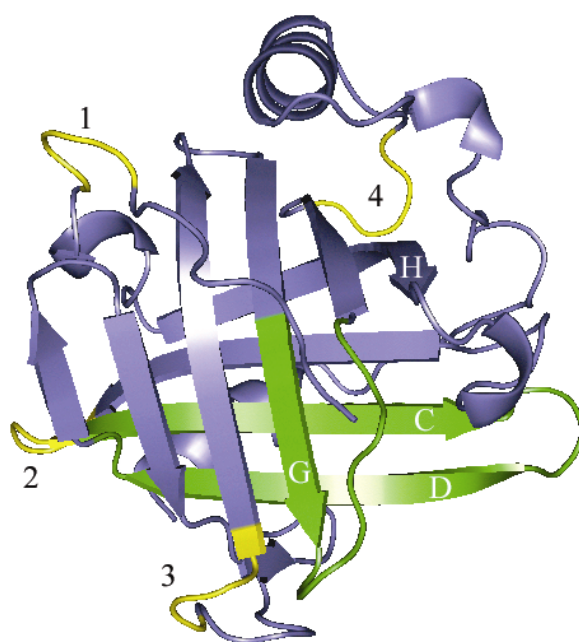


FIGURE 2.1. Ribbon Diagram of Apo rNP4. Subtle differences in the carbon-alpha backbone between apo and holo rNP4 are highlighted in yellow (turns) and green (strands). Turns 1-4 correspond to residues 9-12 between the N-terminus and helix 1, 47-53 in the BC Loop, 100-103 in the EF Loop, and 140-143 between sheet H and helix 2, respectively.

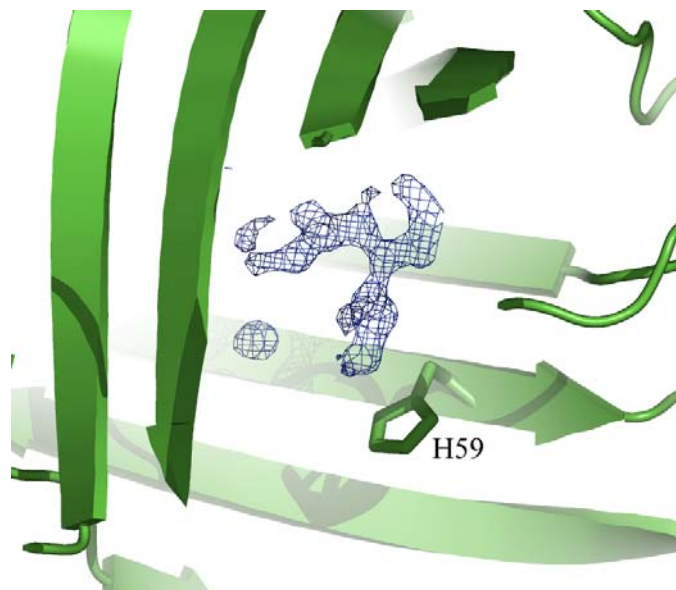


FIGURE 2.2. Electron Density in Core of Apo rNP4. The blue electron density is from the final $2|F_o| - |F_c|$ map contoured at 1.35σ . Proximal histidine 59 is labeled for orientation.

A root mean square deviation of 0.31 Å (calculated using SSM Superimpose [76]) between apo and holo rNP4 confirms that the beta-barrel remains rigid upon removal of the heme cofactor. The calculated RMSD of only the beta-barrels of apo and holo rNP4 was nearly identical to that calculated with SSM Superimpose. When examining the superimposed backbones of wild-type and apo rNP4 more carefully, a subtle flexibility is observed in two major areas. The first area is at four turns including residues 9-12 (random coil between the N-terminus and helix 1), 47-53 (BC Loop), 100-103 (EF Loop), and 140-143 (random coil between sheet H and helix 2) (Figure 2.1.). The backbones of these turns are now in two conformations and both conformations are positioned slightly more to the center of the protein. The second area affected is locally at the point of alteration, particularly residues close to the proximal side of the heme (56-79 in sheets C and D) and those near the distal of the heme (121-132 in sheet G and G-H loop). The backbone atoms of residues 56-79 now display two conformations in the apo structure. Both proximal and distal backbone residue stretches have a similar shape to that of the wild-type rNP4, but the backbone shifts into the abandoned heme pocket (Figure 2.1.).

In general, the side chains of apo rNP4 have more flexibility than wild-type rNP4. This is associated with the above-mentioned backbone motion. Overall, apo rNP4 has 69 of its 184 residues (35%) in multiple conformations, 38 more residues than wild-type rNP4 (pH 5.6). Though the side chains have more conformational freedom, they are not completely disordered, and thus modeling of the second conformation was possible.

2.3.3. Removal of cofactor slightly affects heme contacting residues

In wild-type rNP4, the heme iron is non-covalently linked *via* His 59 and is tightly packed into the lipocalin beta-barrel. The hydrophobic nature of the interior of the beta-barrel is evident from the presence of a large number of aromatic rings located within the lumen of the barrel (Figure 2.3.). Of the contact residues, six are aromatic and four of these aromatics form ring-face to heme-edge contacts. Upon removal of the heme cofactor, the overall integrity of the area surrounding the heme is maintained. However, all residue side chains, except Leu 133, are slightly affected. Tyr 28, Leu 57, Tyr 105, Phe 107, Ile 119 and Leu 123 now display 2 conformations. The second conformation of Leu 57 and Ile 119 and both conformations of Tyr 105 and Leu 123 slightly collapse into the pocket. The second conformation of Tyr 28 remains in the same plane but translated. Tyr 40, which is proximal to the heme, remains in one conformation but collapses into the heme pocket. Proximal His 59, which coordinates to the heme iron in wild-type rNP4, remains in one conformation but is bent over due to the lack of interaction between His 59 N ϵ 2 and Fe of the heme. The new position of His 59 occupies the space normally taken up by Phe 68, thus the ring of Phe 68 occupies a new position away from the pocket. Though the ring of proximal His 59 is in a new conformation, atom ND1 remains hydrogen bonded to Asp 70 via a structural water (2.36 Å) (not shown), as seen in wild type [57].

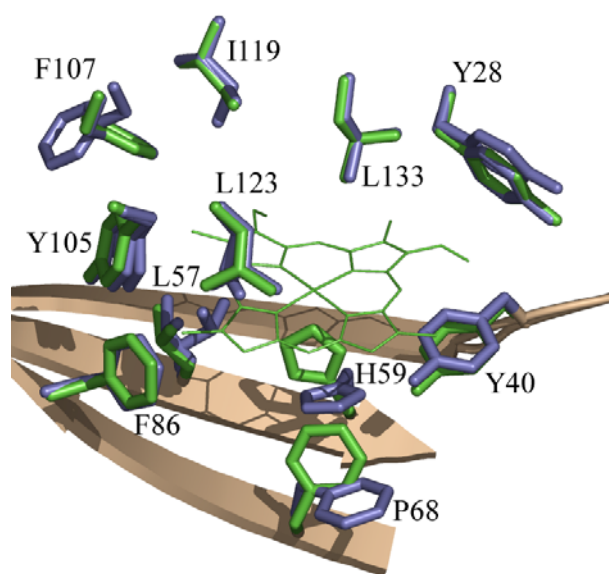


FIGURE 2.3. Heme Contacting Residues in Apo and Holo rNP4. Proximal backbone atoms have been omitted for clarity. Apo and wild-type rNP4 residues are in blue and green respectively. Heme of wild-type rNP4 is in green and represented as skinny lines with heme propionates omitted for clarity. See text for details.

In addition to these residues, several other residue side chains are greatly affected by removal of the heme. Val 36, within the AB Loop, collapses into the heme pocket due to absence of the vinyl substituent (Figure 2.4.). Along with their change in backbone conformation mentioned above in the last section, the side chains of turn 47-53 (BC Loop) and proximal stretch 58-68 (sheet C and CD Loop), which contains the coordinating histidine, are now in two conformations, with the second conformation differing greatly from the first (not shown).

The slight effects on heme contacting residues mentioned in this section along with the backbone rigidity and flexibility of the heme binding pocket discussed in Section 2.3.2. implies that the size of the binding cavity in the apo structure is nearly the same as that of the wild-type structure. Simple minimization showed that the binding pocket is capable of accommodating a flat, rigid heme. Though a flat heme could fit, a distorted heme, as seen in wild type, may fit even better and side chains within the binding pocket move to accommodate binding. In addition, the barrel may need to be rigid for this distortion to occur.

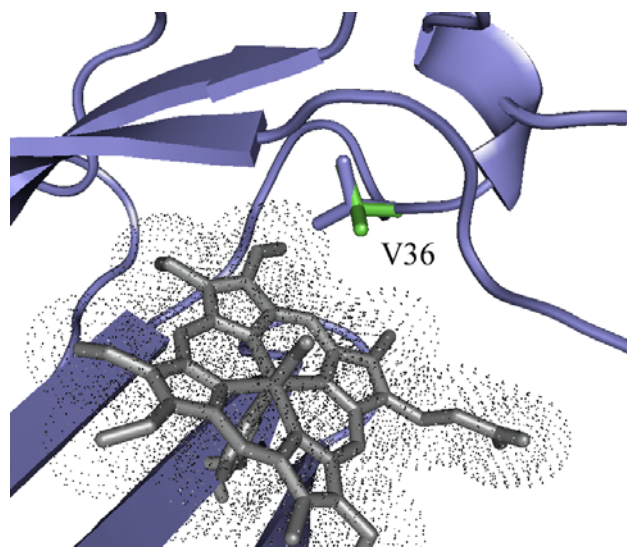


FIGURE 2.4. Collapse of Val 36. V36 of apo rNP4 (blue) collapses into the space previously occupied by the holo rNP4 vinyl substituent of the heme (gray). The position of V36 in holo rNP4 is shown in green. Van der Waals radii of the heme atoms are displayed by dots. Note that heme in rNP4 displays a static disorder such that ~50% of the molecule is “right-side-up” and ~50% of the molecule is “up-side-down” leading to the appearance of four vinyl positions rather than two [38].

2.3.4. AB and GH loops closed at low pH

Characteristic loop dynamics of wild-type rNP4 are also observed in the apo rNP4 structure. This low pH (pH 5.6) structure displays the previously described closed conformation at low pH [52,56]. Both open and closed conformations of the GH Loop (residues 125-133) are present but the closed conformation predominates. In the closed conformation, Asp 30, Asp 129, and Leu 130 make up an extensive hydrogen bonding network where the 130-131 peptide bond flips to form new hydrogen bonds to Asp 30 and Asp 129 and L130 packs across the opening to the binding cavity. The AB Loop (residues 31-37) has good electron density, is very well ordered, and thus could be correctly modeled. It has been previously noted that NO binding and low pH contributes to this extensive conformational change in the protein [38,52,56,58]. However, apo rNP4 is unable to bind NO but still displays the closed conformation associated with low pH, thus low pH rather than ligand binding is the driving force behind loop closure in this particular system.

2.3.5. Apo lipocalins retain general holo protein structure

The hydrophobic beta-barrel structure of apo rNP4 is very similar to those previously reported in rNP4 holo structures [38,57,58]. The apo rNP4 structure shows that the absence of a ligand (heme) does not cause a collapse of the beta-barrel. In searching the crystallographic literature, structural rigidity of the beta barrel seems to be a general trend among lipocalins. That is, other lipocalins absent of their ligand or cofactor

retain the general 3-D structure of their holo protein. The structures of several other apo forms of lipocalins obtained by depleting the natural holo protein of its ligand, such as beta-lactoglobulin [12], retinol binding protein [75], and cellular retinoic acid binding protein [77-79], among others, confirm this suggestion (Table 2.2.). Thus, this appears to be a general feature of the fold even where permanent cofactor binding occurs, as in the nitrophorins.

TABLE 2.2. Actual Comparison of Apo and Holo Lipocalins in Current Literature

Protein ^a	Citation	PDB	Apo/ Holo	Ligand ^b	Res ^c	Source	RMSD/ SID ^d
CRAPB II	[77]	1XCA	Apo ^e	retinoic acid	2.3	<i>human</i>	
	[78]	1CBS	Holo		1.8		0.85/99
	[79]	1BLR	Apo	n/a			
CRBP II	[80]	1OPA	Apo	retinol	1.9	<i>rat</i>	
	[80]	1OPB	Holo		1.9		0.63/100
	[81]	1B4M	Apo	n/a			
	[82]	1EII	Holo	n/a	n/a		
PRBP	[75]	1HBQ	Apo	retinol	1.7	<i>bovine</i>	
	[75]	1HBP	Holo		1.9		0.31/99
	[83]	1BRQ	Apo	2.5	<i>human</i>		
	[83]	1BRP	Holo	2.5	0.31/92 ^f		
FABP ^g	[84]	1IFB	Apo	palmitate	1.9	<i>rat</i>	
	[85]	2IFB	Holo		2.0		0.37/100
A2U	[86]	2A2U	Apo	odorants	2.5	<i>rat</i>	0.29/100
		2A2G	Holo		2.9		
E-RABP	[59]	1EPA	Apo	retinoic acid	2.0	<i>rat</i>	0.55/100
		1EPB	Holo		2.2		
THBP	[87]	1QFT	Apo		1.25	<i>tick^h</i>	0.09/100
		1QFV	Holo		1.4		
Blg	[12]	1BEB	Apo	fatty acids	1.8	<i>bovine</i>	n/a

^aCRAPB II, Cellular Retinoic Acid Binding Protein II; CRBP II, Cellular Retinol Binding Protein II; PRBP, Plasma Retinol Binding Protein; FABP, Fatty Acid Binding Protein; A2U, Alpha-2u-Globulin (Rodent Urinary Proteins); E-RABP, Epididymal Retinoic Acid Binding Protein; THBP, Tick Histamine Binding Protein; Blg, B-lactoglobulin. ^bEndogenous ligand. ^cCrystal structure resolutions are in angstroms; NMR solution structures are non-applicable (n/a). ^dRMSD and SID are the root mean square deviation of all alpha carbon atoms and sequence identity respectively as determined by the SSM superimpose program in Coot. Only crystallographic coordinates were subjected to analysis. ^eMutant form. ^fRMSD and SID between the human and bovine holo-protein. ^g10 stranded beta-barrel calycins structural superfamily. ^h*Rhipicephalus appendiculatus*.

2.3.6. Interaction may act to hold rNP4 beta-barrel intact

The folding mechanism of beta-sheet proteins in general, and beta-barrel proteins in particular, are less well understood than those of other structural classes [88]. The conversion of an unstructured polypeptide to form an open barrel would require major structural reorganization after hydrophobic collapse [89]. Since the apo form of rNP4 displays minimal changes in the beta-barrel with respect to its holo form, there may be some intrinsic interaction that stabilizes the beta-barrel structure. As described in the introduction, rNP4 shares a distinct structural pattern among lipocalins despite its low level of global sequence identity with other lipocalins. This structural pattern involves an arginine (or sometimes lysine), which is able to form a number of potential hydrogen bonds with the main chain carbonyls of a short N-terminal helix, that packs across a conserved tryptophan in a structurally superimposable, non-random manner (Figure 2.5.). This region maybe a key structural element of rNP4. Furthermore, rNP2, rNP3, and rNP7, closer relatives to rNP4, contain a His rather than an Arg at this position that forms ring stacking interactions with the tryptophan. But what role does this keepsake Arg-Trp structural motif play? Might it stabilize the overall protein structure and act to ‘pin’ together the two ends of the beta-barrel in order to help maintain the beta-barrel fold? Or, might it be a key interaction in the folding pathway that guides the formation of the beta-barrel? In the absence of further data, for example a mutation study, this remains an open question for rNP4.

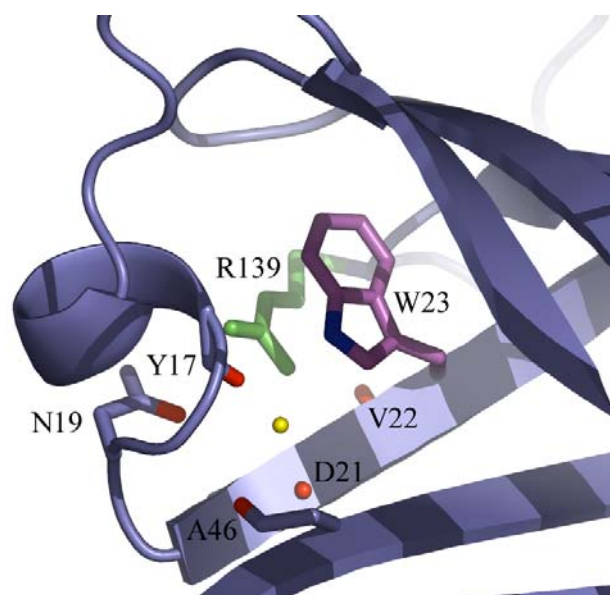


FIGURE 2.5. Tryptophan-Arginine Interaction in rNP4. This lipocalin interaction is also seen in apo rNP4. Tryptophan 23 and arginine 139 are in purple and green respectively. Carbonyl oxygens in direct or water-mediated interaction (yellow sphere) with arginine 139 are in red. See text for details.

CHAPTER 3

HEME DISTORTION IN NITROPHORIN 4: HIGH RESOLUTION STRUCTURES OF HEME ALTERED, and L123V and L133V MUTANT PROTEINS

3.1. Introduction

Chapter 1 introduced the nitrophorins, its hallmark hydrophobic binding cavity and heme distortion in general. In this chapter, I elaborate on the cavity and how heme distortion may arise in rNP4.

As mentioned, heme distortions are conserved within functional classes of heme-binding proteins [60] and heme biological properties, such as the setting of heme iron reduction potentials, are thought to depend in part on the degree of heme non-planarity [64]. However, the underlying principles that govern heme distortion are still not clear and remain to be uncovered. This chapter contributes to this area of research using the *Rhodnius* nitrophorins as a model system. Of the rNPs, rNP4 is best suited for in-depth structural analyses by X-ray crystallography. Wild-type rNP4 crystals diffract beyond 0.8 Å resolution [58] and previously analyzed rNP4 mutant structures have been determined to atomic resolution at 1.0 – 1.2 Å [52]. This high resolution allows accurate modeling of individual atoms and precise placement of the heme coordination sphere, allowing for reliable calculations of heme distortion, bond lengths and bond angles. In contrast, rNP4 is not well suited for NMR solution studies because of a tendency to aggregate at high concentrations [90].

The heme molecule of rNP4 is tightly packed into a lipocalin beta-barrel in which 2 distal leucines, L123 and L133, as well as 9 other hydrophobic amino acids, contact the heme edge. High resolution crystal structures of wild-type rNP4 and rNP2 revealed one of the most distorted non-covalently linked heme geometries of any known protein [38,58]. Upon addition of NO, as well as other π -acceptor ligands, the ruffling distortion increases (π -acceptor distortion), while π -donating ligands such as imidazole reduce ruffling [38] (distortions are defined in Section 1.4.2.). Thus, both steric and electronic factors seem to play a role. A series of questions arise from these results: (1) Is steric interaction the main cause of distortion of rNP hemes? Or is there some as-yet unknown electronic factor? (2) How do π -acceptor ligands such as NO and CN⁻ increase ruffling (π -acceptor distortion), while π -donating ligands reduce ruffling? (3) Is heme distortion linked to biological function? More over, what factors stabilize the ferric oxidation state in rNP? Heme distortion? Electrostatic interactions? Proximal Ligand?

This chapter focuses mainly on the cause of distortion in rNP4. The π -acceptor distortion and possible biological relevance of distortion are discussed. However, they remain to be experimentally explored by a future investigator. We hypothesized [38] that steric interaction is the main cause of distortion for rNP hemes. To begin understanding how protein influences geometry, heme distortion was probed using mutagenesis to both the protein and heme cofactor (Figure 3.1).

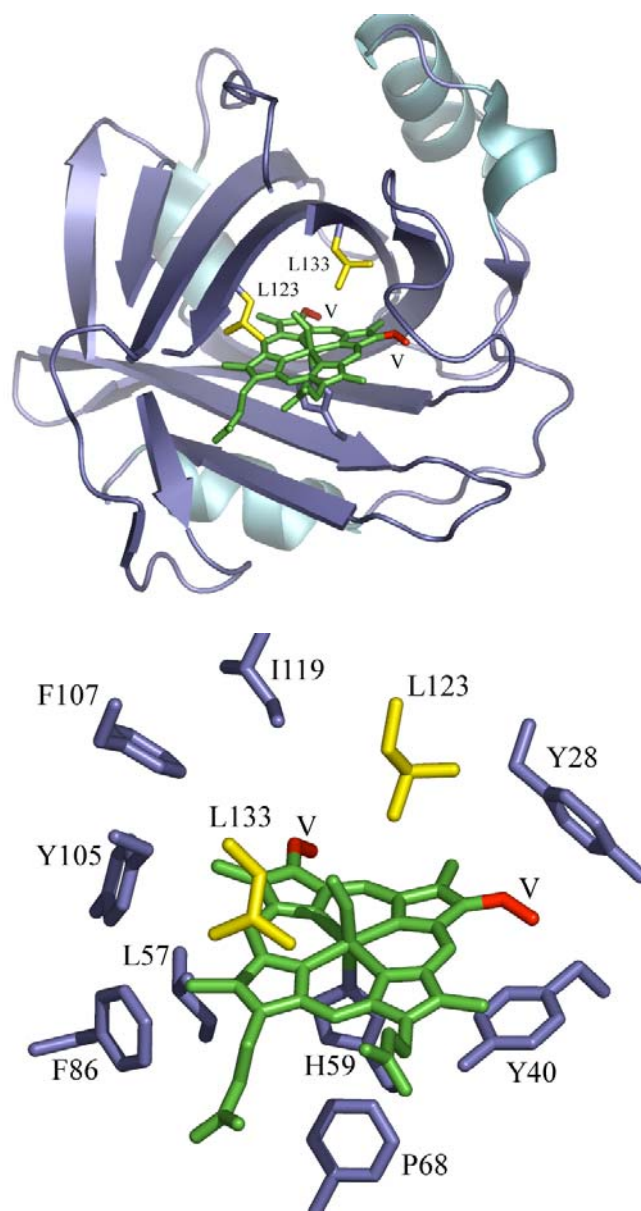


FIGURE 3.1. Protein and Heme Alterations in rNP4. (Top) Ribbon drawing of wild-type rNP4 (blue) containing heme. Positions L123 and L133, which were mutated, are in yellow and heme vinyl substituents, which were replaced with hydrogen or methyl groups, are in red. (Bottom) Hydrophobic residues surrounding the heme in the binding cavity. The same color scheme is used as above. Note that the heme in rNP4 displays a static disorder described in FIGURE 2.4. but only one orientation is displayed here.

Protoporphyrin IX (heme) is inserted into the hydrophobic lipocalin beta-barrel and non-covalently linked through proximal His59. Leucines at distal positions 123 and 133 are positioned above the points of highest distortion seen in the heme cofactor [38] and were mutated to valines in order to relieve steric contact between the protein and the heme. The closest contacts between the heme cofactor and the protein were calculated at the vinyl substituent positions. Wild-type rNP4, unlike for example, the bedbug nitrophorin, displays a highly ordered and highly constrained heme with close van der Waals contacts between the heme vinyls and the protein. Despite this, the heme shows a static disorder with ~50% of the molecules “right-side-up” in the heme pocket and ~50% “up-side-down”, which serves to alter the vinyl positions but has no apparent additional effect on heme position. Vinyl steric clashes can lead to ruffling [91,92]. To explore this, a heme analog with vinyl substituents replaced with hydrogen or methyl groups was inserted into wild-type rNP4 to relieve steric contact between the heme cofactor and the protein.

The results of eight crystallographically refined structures with either modification to the protein or to the cofactor are presented. These include two distal-pocket mutations, rNP4 L123V and rNP4 L133V, and two heme analogs. One heme analog, analog 1, incorporates Fe(III) deuteroporphyrin IX that has vinyl to hydrogen substitutions, and the other heme analog, analog 2, incorporates Fe(III) 2,4 dimethyl deuteroporphyrin IX with vinyl groups replaced with methyl groups. Heme distortion in these structures is in terms of porphyrin normal modes (NSD) [64], rotation of the pyrrole ring that is at the heart of the ruffling distortion, and atomic deviations from planarity

represented by formal core diagrams. Comparison of altered protein pockets and heme distortion calculations to that of wild-type rNP4 allows for the deduction of where and how distortion arises in rNP4. In general, rNP4 has evolved to have numerous van der Waals contacts as well as electronic interactions that contribute to heme distortion. This work is the subject of a paper in preparation [93].

3.2. Materials and Methods

3.2.1. Mutagenesis of proteins

rNP4 mutants L123V, L133V and L123V/L133V were constructed using PCR and Stratagene's QuickChange™ Site-Directed Mutagenesis Kit by Ms. Carrie Plumer. The following oligonucleotides purchased from Midland Certified Reagent Co. (Midland, TX) were used as PCR primers to create cloning plasmids containing the mutation(s) of interest: 5'-CCACACATGTGTGCATAAAGGA-3' (rNP4 L123V); 5'-CTTATCCACACATGTTTGCATAAAGGAAACAAGGACTTGGGAGATGTTTACGCTGTATTAAATCGC-3' (rNP4 L133V). After confirmation of mutation by DNA sequencing (Arizona Research Laboratories, University of Arizona), the gene encoding fragments were inserted into a modified pET17b expression vector (pShep225) in which the *NdeI* restriction site was inserted at the beginning of the coding sequence for the rNP4 gene, as described previously [57]. The resulting expression plasmids named pCBP10, pCBP12, and pCBP43, carrying the rNP4 L123V, L133V, and L123V/L133V mutations,

respectively, were moved into competent *Escherichia coli* BL21(DE3) cells by transformation for protein expression.

3.2.2. Expression, purification, and activity of mutant and analog proteins

Expression, purification, and activity conformation of mutant and analog proteins was carried out by Ms. Carrie Plumer (mutants) and Ms. Jacquie Brailey (analogs). Wild type and mutant proteins were expressed as inclusion bodies, denatured and refolded. At this point protoporphyrin IX (rNP4 L133V and rNP4 L123V/L133V), Fe(III) deuteroporphyrin IX or Fe(III) 2,4 dimethyl deuteroporphyrin IX (rNP4 wild type) (synthesized by Frontier Scientific) were titrated into the protein until a Soret ($\sim A_{420}$) to protein ($\sim A_{280}$) ratio of 3:1 was observed by UV-Visible spectroscopy. The wild-type protein containing Fe(III) deuteroporphyrin IX or Fe(III) 2,4 dimethyl deuteroporphyrin IX are referred to as heme analog 1 and heme analog 2, respectively, throughout this dissertation. Following cofactor addition, all proteins were purified by ion-exchange chromatography followed by gel filtration as previously described [49,57,69].

UV-visible absorption spectrum of rNP4 mutants (L123V, L133V, L123V/L133V), heme analogs 1 and 2, and their NO complexes were recorded on a Cary 50 to confirm the presence of heme, Fe(III) deuteroporphyrin IX chloride or Fe(III) 2,4 dimethyl deuteroporphyrin IX chloride and to confirm NO binding activity.

3.2.3. Crystallization, data collection and processing

Detailed crystallization and preparation conditions as well as information on the beam line used for data collection are compiled in Appendix B. All crystals were grown at room temperature ($\sim 25^{\circ}\text{C}$) using the hanging drop technique with some help from Ms. Abreeza Zegeer. Mutant and analog proteins gave rise to crystals in 2.65 – 3.5 M ammonium phosphate, pH 7.0-7.5. Spontaneous growth occurred at 2.8 M and above, thus drops at a lower concentration were seeded. Single mutant rNP4 L123V could not be crystallized under any attempted condition. rNP4 L123V/L133V required co-crystallization with 20 mM imidazole to obtain crystal growth. Single crystals were transferred to a cryoprotectant solution of 3.2 – 3.95 M ammonium phosphate at either pH 7.5 or 5.6 and allowed to equilibrate for 1-2 hours. If the crystal was to be complexed with NO, the cryoprotectant was saturated with argon prior to crystal transfer. Following equilibration in argon saturated solution, the crystal was either transferred and soaked for 30 minutes in an identical cryoprotectant solution saturated with NO gas as previously described (heme analog 1 and 2), or a final concentration of 1 mM diethylamine NONOate (DEA/NO) (yields ~ 2 mM NO) was added to the crystal-containing argon saturated solution for 10 minutes (rNP4 L133V). The generation of NO by DEA/NO was observed by the presence of bubbles and a change in crystal color from brown to red in the crystal, consistent with nitrosylation, under all soaking conditions. Crystals were flash frozen in liquid nitrogen for data collection with the help of Dr. Andrzej Weichsel.

All X-ray diffraction data were collected at 100 K. Data were acquired at one of two places by Dr. Andrzej Weichsel, Dr. Estelle Maes, and/or myself: Stanford Synchrotron Radiation Laboratory, Palo Alto, CA on beam line 9-1 with a Mar345 imaging plate (rNP4 L123V/L133V) and remotely at beam line 9-2 with a Mar325 CCD detector (rNP4 L133V-NO); the Advanced Photon Source (Argonne National Laboratory, Argonne, IL) on beam line 14BM-C with a Quantum-4 CCD detector (heme analog 1) or Q315 detector (heme analog 2) and beam line 14BM-D with a Quantum-4 CCD detector (rNP4 L133V-NH3).

All data were processed with d*TREK [94], with the exceptions of rNP4 L133V-NO and apo-rNP4, which were processed with MOSFLM and SCALA [70]. All crystals belong to the C2 space group with cell constants typical of those found for wild-type rNP4, $a = 70.2 \text{ \AA}$, $b = 42.4 \text{ \AA}$, $c = 52.9 \text{ \AA}$, and $\beta = 94.2^\circ$ [38], and range from 0.96 \AA to 1.22 \AA resolution. Additional relevant crystallographic data and refinement statistics for the rNP4 altered structures can be found in the results section (Tables 3.2. and 3.6.).

3.2.4. Structure determinations

The initial mutant, and analog structures were built using difference Fourier methods starting with wild-type rNP4 models 1X8O, 1X8P, 1X8Q [58] or 1YWB [53]. The phases were subsequently refined with anisotropic temperature factors using REFMAC from the CCP4 package [71] and model building was accomplished with the software O [95] or COOT [72]. Due to the ultra-high resolution of the structures, the

weighting term between the X-ray and geometric part of the refinement residual was set between 2.0-4.0, which allows for loose model restraints. Certain residues were found to occupy more than one conformation and were built and refined as such. In such cases, the occupancies were generally set to 0.5 for each conformer and left fixed when refined. Refinements converged to R factors ranging from 12 – 17% and 15 – 19% for R_{cryst} and R_{free} , respectively.

After refinement completion, one cycle of full-matrix refinement using SHELXL [96] was applied to the mutant and analog structures to obtain an estimate of the standard deviations of the bond distances and angles for the heme/heme analog coordination sphere. The heme/heme analog, proximal ligand (His 59), and axial ligand (NO, NH₃, water, or imidazole) were left completely unrestrained while all other atoms remained fixed.

Model quality was assessed using the program PROCHECK [73] as implemented in CCP4 [71]. All residues for all nine structures displayed ϕ/ψ values in the favored or allowed regions of a Ramachandran plot (not shown). Structural figures were prepared using PyMOL [74] (<http://www.pymol.org/>) or MOLSCRIPT [97] and RASTER3D [98].

Coordinates for the all structures reported have been deposited with the Protein Data Bank (PDB entries 2ASZ, 2AT0, 2AT3, 2AT4, 2AT5, 2AT6, 2AT7, 2AT8).

3.2.5. Quantifying heme distortion and orientation of imidazole ligand

To determine the overall degree of heme distortion in each structure, deformation calculations were performed using the normal coordinate structural decomposition (NSD) program, developed by Shelnutz and coworkers [64]. Using the NSD method, we report the mean out-of-plane displacement of the heme atoms (\AA) for distortions associated with ruffling (B_{1u}) and saddling (B_{2u}).

More local changes in heme distortion were analyzed by calculating the rotation angle of each pyrrole ring relative to the mean plane containing the nitrogen heme atoms using MOLEMAN2 [99] from the Uppsala Software Factory. The orientation of the imidazole ligand was also calculated using this program. We also report the angle between the planes of the imidazole ligand and imidazole side chain of the proximal histidine (Φ_{imid}).

Specific deviations (units of 0.01 \AA) of each heme atom from the mean plane of the heme ring were calculated using the program `pdbTransform` (<http://www.shokhirev.com/nikolai/programs/prgsciedu.html>), created by Dr. Nikolai V. Shokhirev at the University of Arizona, and are reported as formal core diagrams (FCD) constructed using ChemDraw (CambridgeSoft).

In all cases, the altered structures were compared to the respective wild type structure, 1X8O, 1X8P, 1X8Q [58], 1YWB [53] or 1IKJ [38].

3.3. Results

As noted previously [38] and central to the work performed in this study, the rNP4 heme is severely distorted from planarity. Wild-type rNP4 shows two distortions: ruffling and saddling. Several factors can contribute to distortion, including direct van der Waals contacts and electronic interactions. In the current study we focused on steric contributions to heme distortion through mutation of the protein or of the heme cofactor. We focused on steric contacts above the heme that correspond with the highest points of distortion [38] by mutating positions L123 and L133 to valines and on contacts with the vinyl heme substituents by incorporating heme analogs (See Materials and Methods). All proteins were produced and their structures determined to high resolution with several ligands to examine the role of protein induced heme distortion.

3.3.1. Mutations of distal positions L123 and L133

Mutant proteins rNP4 L123V, L133V, and L123V/L133V were examined for their role in heme distortion, since they contact heme at the positions of greatest distortion (Figure 3.1.). The purified proteins displayed absorption spectra similar to those for ferric wild type: unligated protein exhibited a maximum for the Soret band at 402-4 nm, and NO derivatives displayed maxima for the Soret, α and β bands at 418-20, 565-7, and 530-33 nm, respectively (Table 3.1.).

TABLE 3.1. UV-Visible Absorption Maxima (nm) for rNP4 and rNP4 Altered Structures at pH 8.0

	-NO		
	Soret	α	β
wild-type rNP4 (ferric) ^a	403	-	-
wild-type rNP4 (ferrous)	426	-	557
L123V	404	-	-
L133V	403	-	-
L123V/L133V	402	-	-
Heme Analog 1 ^b	392	-	-
Heme Analog 2 ^c	395	-	-
	+NO		
	Soret	α	β
wild-type rNP4 (ferric)	419	568	534
wild-type rNP4 (ferrous)	416	571	549
L123V	420	567	533
L133V	418	566	533
L123V/L133V	418	565	530
Heme Analog 1 ^b	411	557	525
Heme Analog 2 ^c	413	559	529

^aAdditional bands at 625 nm and 496 nm. ^bContains Fe(III) Deuteroporphyrin IX. ^cContains Fe(III) 2,4 Dimethyl Deuteroporphyrin IX.

Structures were obtained for the complexes rNP4 L133V-NH₃ (pH 7.5), rNP4 L133V-NO (pH 5.6), and rNP4 L123V/L133V-imidazole (pH 5.6) to 1.07 Å, 1.0 Å, and 1.0 Å resolution respectively (Table 3.2.). Crystals could not be obtained for single mutant L123V under any attempted condition. Double mutant rNP4 L123V/L133V was unable to crystallize without the presence of imidazole in the crystallization buffer. Imidazole binds to rNP4 in the same manner as histamine, a natural ligand of rNP4, and induces loop closure.

Initial model building and refinement proceeded with heme restraints. The high resolution also allowed us, as a final step, to perform unconstrained full matrix refinement of the entire coordination sphere including heme, distal ligand, and proximal histidine (see Section 3.2.4.). The final structures yielded excellent models (Table 3.2.).

TABLE 3.2. Crystallographic Data and Refinement Statistics for rNP4 Mutant Structures

	L133V- NH3	L133V- NO	L123V/L133V- imidazole
PDB accession	2ASZ	2AT0	2AT3
pH	7.5	5.6	5.6
wavelength (Å)	0.90	0.98	0.75
resolution (Å)	1.07	1.0	1.00
total no. of reflns	484,613	341,858	266,648
no. of unique reflns	67,479	83,901	81,947
completeness (%) ^a	98 / 98	100 / 99	97 / 88
mean I/σ_I ^a	15.4 / 4.0	13.9 / 5.3	20.8 / 2.6
R_{sym} ^{a,b}	0.06 / 0.30	0.08 / 0.18	0.04 / 0.25
R_{cryst}/R_{free} ^{a,c}	0.14 / 0.17	0.14 / 0.16	0.14 / 0.17
Rmsd ^d			
distances	0.02 (0.02)	0.01 (0.02)	0.01 (0.02)
angles	1.74 (2.00)	1.50 (2.00)	1.66 (2.00)
DPI ^e	0.03	0.03	0.03
no. of multiple conformations	34	42	46
comment	Open	Closed NO shifts Heme shifts	Closed Imidazole shifts Heme shifts

^aOverall/ outermost shell. ^b $R_{sym} = (\sum_h |I_h - \langle I \rangle|) / (\sum_h I_h)$, where $\langle I \rangle$ is the mean intensity of all symmetry-related reflections I_h . ^c $R_{cryst} = (\sum |F_{obs} - F_{calc}|) / \sum F_{obs}$. R_{free} as for R_{cryst} , using a random subset of the data (5%) not included in the refinement. ^dRmsd distances and angles are in angstroms and degrees respectively. Target values are in parentheses. ^eCruickshank Dispersion Precision Indicator [100].

Ligand geometry. Perhaps the most striking change in the mutant proteins was a change in NO and imidazole geometry. NO and imidazole rotate in a way that all atoms lie just beyond the NB-Fe-ND axis, rather than in the plane of His 59 (axis CHB-Fe-CHD), as seen in wild type (Figures 3.2., 3.3.a,b). This new axis is $\sim 48^\circ$ from the His 59 plane and bisects the heme through pyrrole ring B and C. The electron density for imidazole (Figure 3.2.) and NO (data not shown) are consistent with single conformations.

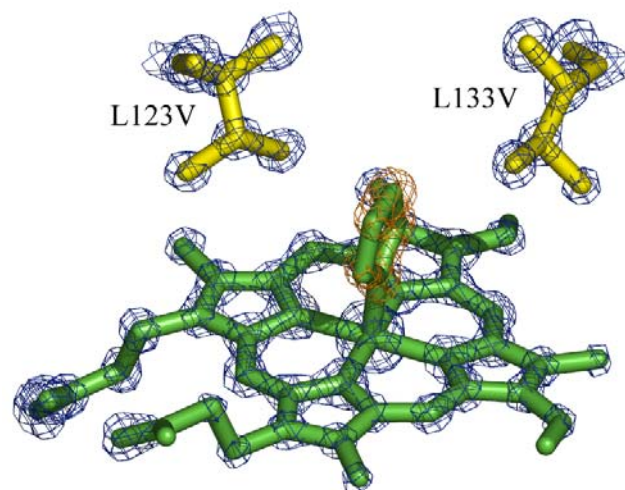


FIGURE 3.2. Electron Density for the rNP4 L123V/L133V Coordination Sphere. The blue and orange (imidazole) electron density is from the final $2|F_o| - |F_c|$ map contoured at 2.0σ . Distal mutations rNP4 L123V and rNP4 L133V are in yellow.

Heme geometry. The entire heme of rNP4 L123V/L133V-imidazole shifts into the distal pocket by, on average, 0.18 Å, with greatest movement seen at the meso carbons (average of 0.20 Å) and pyrrole ring A (average of 0.28 Å). In contrast, only heme atoms at or near the point of mutation move into the distal pocket for the rNP4 L133V-NO complex. The greatest shift is seen at meso carbon C (0.33 Å) and 2 atoms of pyrrole ring C (C1C (0.33 Å) and C2C (0.47 Å)).

The thermal ellipsoid plots for coordination sphere atoms of rNP4-NO (1.01 Å) and rNP4 L133V-NO (1.0 Å) are in Figure 3.3.a. and b. respectively. The ellipsoids are created based on anisotropic temperature factors and thus indicate the positional variability for each atom in the crystal, which, in turn, is related to atomic motion at low (100°C) temperature. The ellipsoids for heme atoms of wild-type rNP4-NO are small and spherical indicating a well ordered system. The ellipsoids for heme atoms of rNP4 L133V-NO remain spherical but display larger radii, indicating more motion. The figure also illustrates the anisotropy (or motion) of NO has changed. In wild type, the NO oxygen is bending in the same plane as the Fe-N-O atoms (CHB-Fe-CHD axis). In the mutant rNP4 L133V-NO, the NO oxygen is bending more perpendicular to the plane in which the atoms lie. The space created in the L133V mutant leads to increased anisotropy in the direction of Val 133, out of the Fe-N-O plane.

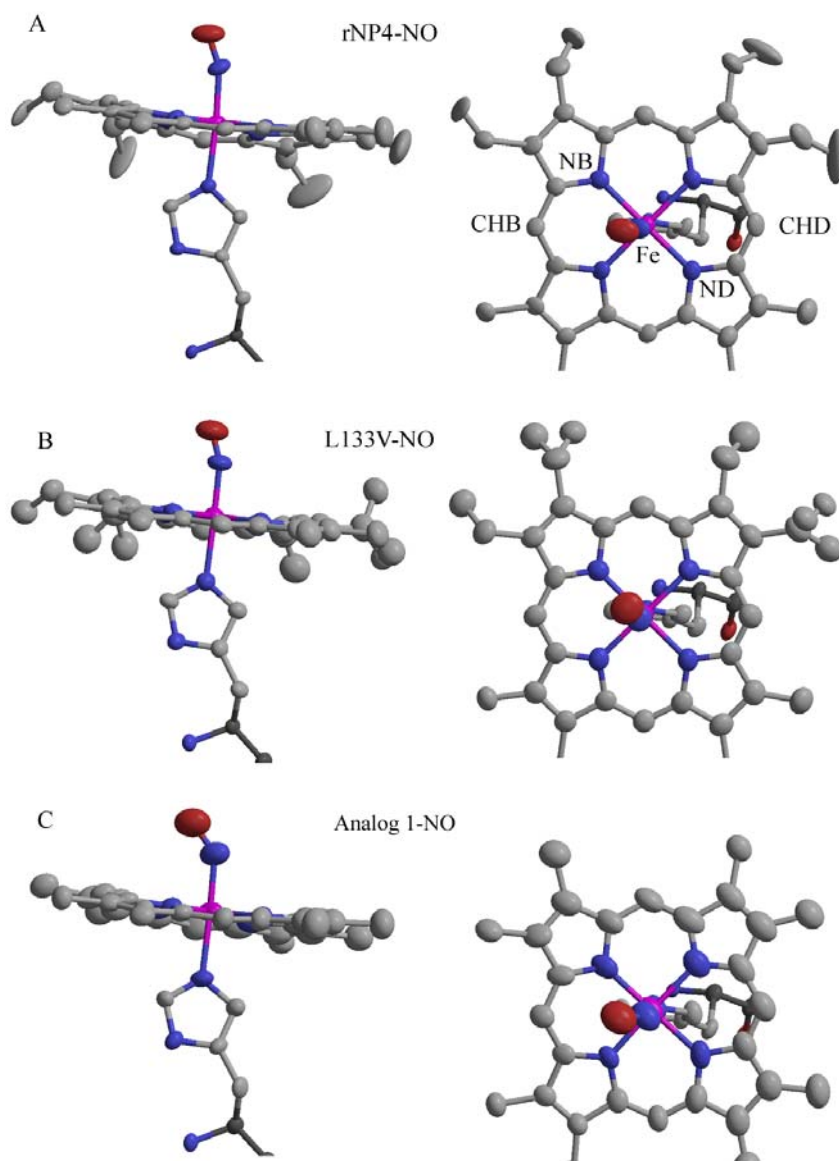


FIGURE 3.3. Thermal Ellipsoid Plots. Thermal Ellipsoids (contoured at 30% probability) illustrating anisotropic temperature factors for the iron coordination sphere in the rNP4-NO (A), rNP4 L133V-NO (B), and analog 1-NO (C) complexes. Heme carboxylate groups have been removed for clarity. (left) Side views emphasizing the consistency of proximal histidine position. (right) Views down the ON-Fe bond emphasizing the position and motion of the NO oxygen atom (in red) and heme atoms (in grey). The CHB-Fe-CHD and NB-Fe-ND axes are labeled for direction orientation.

Heme coordination. The oxidation state of the iron can be determined due to the geometry of the Fe-N-O. An Fe(III)-N-O tends to be linear [101] while an Fe(II)-N-O tends to be 140°, with a longer proximal bond (by 0.1 Å), due to greater trans effect. Bond distances and angles for the iron coordination sphere in the mutant proteins are similar to those for the wild type protein (Table 3.3.), with the exception of rNP4 L133V-NO. As compared to wild-type rNP4-NO (Fe (III)) complex [58], rNP4 L133V-NO shows an increase of the His-Fe bond by 0.08 Å and a decrease in the Fe-N-O angle by 3.4°. This His-Fe bond length is more characteristic of the rNP4-NO (Fe(II)) complex. However, the Fe-N-O angle is characteristic of the rNP4-NO (Fe(III)) complex. Thus, though we assigned the rNP4 L133V-NO complex in the ferric (Fe(III)) oxidation state based on the Fe-N-O angle, the protein complex may be in a mixed ferric and ferrous oxidation state.

TABLE 3.3. Coordination Sphere Geometrical Parameters for rNP4 and rNP Altered Structures

Structure	Oxi state ^a	Fe-NA ^b	Fe-NB	Fe-NC	Fe-ND	Fe-His	Fe-Lig	Fe-N-O	N-O
L133V-NH ₃	+3	1.98(2)	2.00(2)	2.01(3)	2.00(3)	2.00(2)	2.04(2)	n/a ^f	n/a
-NO	+3	1.99(1)	2.00(1)	2.03(1)	2.00(1)	2.09(1)	1.70(1)	152.9(2)	1.13(2)
DM-Im ^c	+3	1.98(2)	2.00(2)	2.00(2)	2.01(2)	2.00(2)	1.98(2)	n/a	n/a
Analog 1 ^d -NH ₃	+3	1.99(2)	1.97(2)	2.00(2)	2.00(2)	2.00(2)	2.00(2)	n/a	n/a
-NO	+2	1.98(2)	1.96(3)	1.99(3)	2.04(3)	2.10(2)	1.77(3)	139.8(3)	1.17(2)
-H ₂ O	+3	2.01(3)	1.90(4)	2.01(5)	2.01(3)	2.02(3)	2.01(3)	n/a	n/a
Analog 2 ^e -NH ₃	+3	1.96(1)	1.98(1)	2.00(1)	2.03(1)	1.97(1)	1.99(1)	n/a	n/a
-NO	+2	1.92(1)	1.96(2)	1.99(1)	1.96(2)	2.07(1)	1.72(1)	136.5(2)	1.20(2)

^a Assigned based on Fe-N-O geometry. ^b Distances in angstroms, angles in degrees. Final distances and estimated standard deviations (numbers in parentheses) determined after unrestrained full-matrix refinement of the heme (see Materials and Methods). ^c L123V/L133V-Imidazole. ^d Contains Fe(III) deuteroporphyrin IX. ^e Contains Fe(III) 2,4 dimethyl deuteroporphyrin IX. ^f Not available.

Loop geometry. rNP4 L133V-NO and rNP4 L123V/L133V-imidazole are low pH (pH 5.6) structures and show loop closure consistent with that of wild type low pH structures. For rNP4 L133V-NO, faint density for the AB Loop and both conformations of the GH Loop were seen and approximate positions determined. rNP4 L123V/L133V-imidazole displays hardly any density for the AB Loop. However, both conformations of the GH Loop were present with the closed conformation predominating.

Heme distortion. As highlighted by Roberts et al. [38], and central to the work performed in this study, the rNP4 heme is severely distorted from planarity with dominant and minor distortions of ruffling and saddling, respectively (distortions defined in Section 1.4.2.). The high resolution of the structural data collected allowed us, as a final step, to perform unconstrained full matrix refinement of the entire coordination sphere including heme, distal ligand, and proximal histidine (see Section 3.2.4.). Unconstrained refinement allowed us to remove model bias from the iron coordination sphere, accurately calculate estimated standard deviations for individual bond distances and angles, and reliably calculate heme distortions and atomic deviations from planarity.

Heme distortion was analyzed on three levels, each increasing in specificity. The most general analysis was performed using the Normal Coordinate Structural Decomposition (NSD) program developed by Shelnutz and coworkers [64]. This analysis measures heme conformation in terms of the lowest energy out-of-plane distortions. Table 3.4. provides representative heme distortions in the altered proteins. The mean out-of-plane displacement of the heme atoms as well as the difference from the respective

wild type structures is reported. The mutant complexes are clearly less distorted (significant deviation above 0.1 Å), by up to 0.25 Å in both ruffling and saddling, than any of the analog complexes and the saddling distortion is affected more than ruffling. The saddling distortion in the rNP4 L133V mutant complexes decreases by about half and is almost eliminated in rNP4 L123V/L133V-imidazole compared to its wild type value [38,58]. Interestingly, the ruffling distortion of rNP4 L123V/133V-imidazole increases by a significant amount. A plausible mechanism for how this increase in ruffling while the elimination of saddling occurs is described in the discussion.

TABLE 3.4. Representative Heme Distortions in rNP4 Altered Structures

<i>Structure</i>	<i>Ruffling</i> ^a	Δ ^b	<i>Saddling</i>	Δ
rNP4-NH ₃ ^c	-0.64	-	0.33	-
rNP4-NO (pH 5.6) ^c	-0.81	-	0.37	-
rNP4-NO (pH 7.4) ^c	-0.76	-	0.30	-
rNP4-H ₂ O ^c	-0.56	-	0.29	-
rNP4-Imidazole ^d	-0.42	-	0.31	-
rNP4-NO (Fe ⁺² pH 5.6) ^e	-0.69	-	0.36	-
L133V-NH ₃	-0.46	-0.18	0.15	-0.18
-NO	-0.61	-0.20	0.13	-0.24
L123V/L133V-Imidazole	-0.53	+0.11	0.07	-0.24
Analog 1 ^f -NH ₃	-0.54	-0.10	0.40	+0.07
-NO	-0.67	-0.02	0.36	0.00
-H ₂ O	-0.49	-0.07	0.37	+0.08
Analog 2 ^g -NH ₃	-0.66	+0.02	0.30	-0.03
-NO	-0.76	+0.07	0.33	-0.03

^aTotal deviation along heme normal modes in angstroms for ruffling (B_{1u}) and saddling (B_{2u}) distortions, using NSD [64] and defined in [38].

^bDifference from wild type of equivalent conditions 1X8O, 1X8P, 1X8Q [58], 1YWB [53] or 1IKJ [38]. A positive difference indicates an increase in distortion; negative indicates a decrease. ^cPublished in [58], 0.85-1.08 Å.

^dPublished in [38], 1.27 Å. ^ePublished in [53], 0.97 Å. ^fContains Fe(III) deuteroporphyrin IX. ^gContains Fe(III) 2,4 dimethyl deuteroporphyrin IX.

At the heart of ruffling is the rotation of the pyrrole rings about the Fe-N bonds. Thus, the rotation angle (degrees) of the pyrrole ring relative to the mean plane containing the nitrogen heme atom was calculated for a more specific analysis of distortion (Table 3.5). The rNP4 L133V mutant complexes show a decrease in rotation of all pyrrole rings, consistent with a decrease in ruffling calculated through NSD. However, the double mutant rNP4 L123V/L133V shows an increase in rotation about pyrrole rings A, B and D, consistent with an increase in ruffling calculated through NSD.

TABLE 3.5. Pyrrole Ring Rotation in rNP4 and rNP4 Altered Structures

Structure	Φ_A^a	$\Delta^b \Phi_A$	Φ_B	$\Delta \Phi_B$	Φ_C	$\Delta \Phi_C$	Φ_D	$\Delta \Phi_D$	$ \Phi ^c$	$\Delta \Phi $
rNP4-NH ₃	9.56	-	-6.80	-	8.05	-	-6.32	-	7.68	-
rNP4-NO (pH 5.6)	10.93	-	-10.27	-	9.32	-	-7.97	-	9.62	-
rNP4-NO (pH 7.4)	10.38	-	-10.00	-	8.86	-	-7.16	-	9.10	-
rNP4-H ₂ O	9.19	-	-6.13	-	7.38	-	-5.62	-	7.08	-
rNP4-Imidazole ^d	7.12	-	-5.14	-	7.27	-	-3.93	-	5.87	-
rNP4-NO (Fe ⁺² pH 5.6)	10.33	-	-8.79	-	8.41	-	-7.42	-	8.74	-
L133V-NH ₃	8.22	-1.34	-5.32	-1.48	5.01	-3.04	-4.28	-2.04	5.71	-1.97
-NO	9.75	-1.18	-6.23	-4.04	6.21	-3.11	-6.71	-1.26	7.23	-2.39
L123V/L133V-Im ^e	7.19	+0.07	-5.55	+0.41	5.36	-1.91	-4.98	+1.05	5.77	-0.10
Analog 1 ^f -NH ₃	10.14	+0.58	-5.73	-1.07	5.57	-2.48	-5.37	-0.95	6.70	-0.98
-NO	10.81	+0.48	-7.76	-1.03	6.27	-2.14	-7.03	-0.39	7.97	-0.77
-H ₂ O	9.81	+0.62	-5.28	-0.85	5.38	-2.00	-5.41	-0.21	6.47	-0.61
Analog 2 ^g -NH ₃	10.96	+1.40	-6.00	-0.80	7.75	-0.30	-7.81	+1.49	8.13	+0.45
-NO	10.28	-0.05	-8.10	-0.69	8.50	+0.09	-7.99	+0.57	8.72	-0.02

^a Rotation angle (deg) of pyrrole ring relative to the mean plane containing the nitrogen heme atoms. A positive rotation is defined as clockwise when looking down the nitrogen-iron bond. ^b Difference from wild type of equivalent conditions. A positive difference indicates an increase in rotation; negative indicates a decrease. ^c Average rotation of pyrrole rings from planarity. ^d Published in [38]. ^e Imidazole. ^f Contains Fe(III) Deuteroporphyrin IX. ^g Contains Fe(III) 2,4 Dimethyl Deuteroporphyrin IX.

Formal core diagrams (FCD) illustrate the deviations of each macrocycle atom from the mean plan of the macrocycle ring and is the most specific measurement of the three analyses performed for macrocycle distortion. Figure 3.4 contain FCD's for the mutant structures as well as the change of each atom's position relative to wild type (units 0.01 Å). The mutant complexes show greater deviations in atom positions overall than either heme analog (Figure C.1. and Figure C.2.) as expected from NSD and pyrrole ring rotation calculations. Significant deviations (above 0.07 Å) are localized near the point of mutation or directly adjacent to the meso carbons. In the rNP4 L133V mutant complexes, the macrocyclic carbon atoms with the largest change from wild type are correlated with atoms at the mutation site in rNP4 L133V. For the rNP4 L123V/L133V mutant, the largest changes are correlated to atoms at mutation site rNP4 L123V and rNP4 L133V.

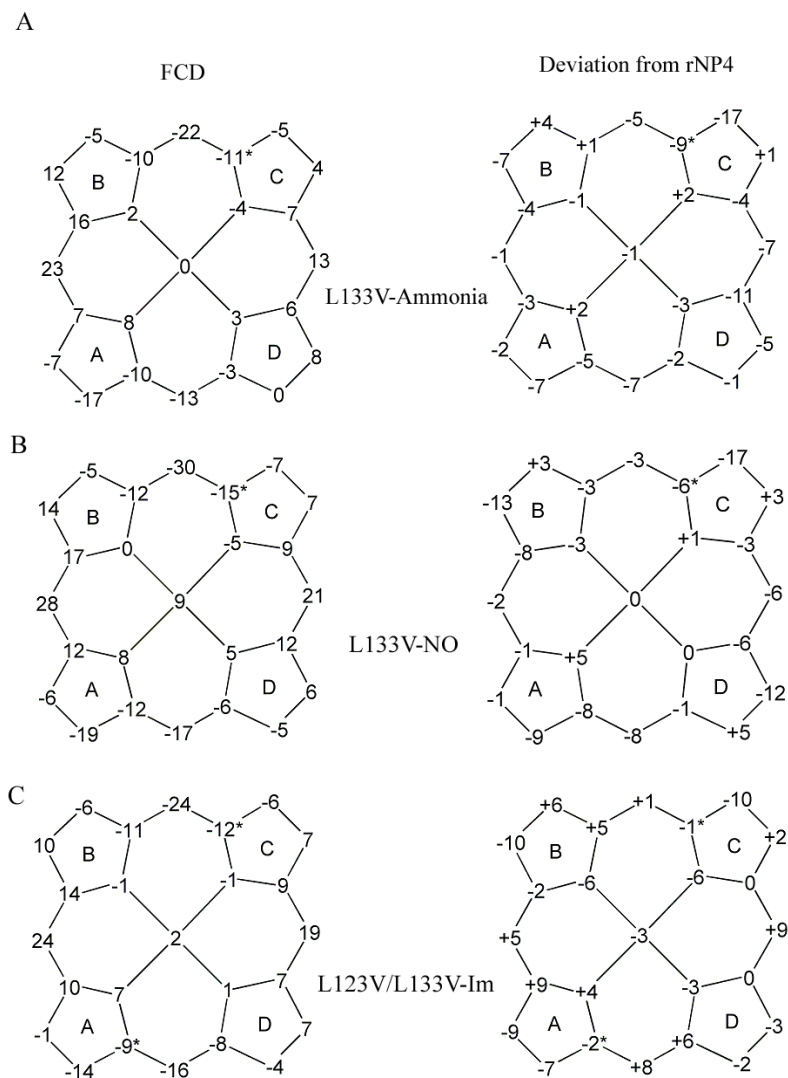


FIGURE 3.4. Atomic Deviations From Planarity for Mutant Complexes. rNP4 L133V-ammonia (A), rNP4 L133V-NO (B), and rNP4 L123V/L133V-imidazole (C) mutant complexes are shown. The starred atoms are those at closest contact to L123V and/or L133V. (left) Formal core diagrams for rNP4 altered structures. Positive values indicate deviations into the distal pocket, negative values into the proximal pocket. (right) Difference between respective wild type and rNP4 altered structures. Positive values indicate a shift away from planarity relative to wild type, negative values toward planarity.

3.3.2. Alteration to heme at vinyl positions

Just as protein residue side chains contact the core macrocycle of heme, close contacts of the heme substituents to the protein may lead to heme deformation. Upon examining the wild-type rNP4-NO and ammonia complexes, the closest contacts between the protein and the heme were found to be at the vinyl substituents. Thus, two heme analogs were obtained from Frontier Scientific in which vinyl groups were replaced with either hydrogen or methyl substituents. The analogs were inserted into wild-type rNP4 and UV-visible spectrum were obtained (Figure 3.5, Table 3.1.). Spectrum of the unligated heme analogs were similar to each other but exhibited Soret band shifts of 8-11 nm with respect to unmodified heme. Upon binding NO, the intensity of the α - and β -bands increased and the 620 nm band receded, a typical behavior of ferric nitrosyl systems. Soret maxima also exhibited a blue-shift with respect to wild type again 6-11 nm in all cases (Table 3.1., Figure 3.5.). The spectral blue shift of ~8-11 nm of the heme analogs compared to wild-type rNP4 is due to the electron withdraw by the vinyl substituent [102]. Also noteworthy is that the intensities of the α - and β - bands (Figure 3.5. inset) is opposite of that seen in wild-type rNP4 [53], with β (525 nm) now showing the larger extinction coefficient.

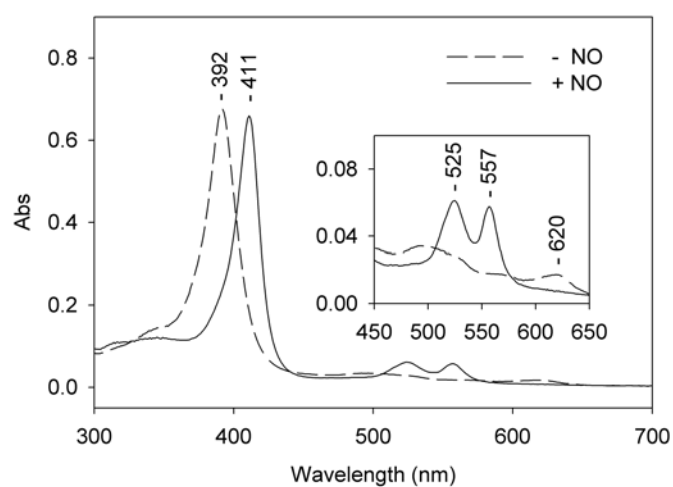


FIGURE 3.5. UV-Visible Spectrum of Heme Analog 1. Wild-type rNP4 was reconstituted with Fe(III) deuteroporphyrin IX chloride and solution spectrum recorded at room temperature (pH 8.0). Soret maximum is indicated. Dashed and solid lines represent unligated and the NO complex, respectively. Inset: expanded view of Q-band region. Heme analog 2 has a similar spectrum.

We determined structures of the ammonia and NO complexes of both heme analogs as well as a low pH aqua complex of analog 1 to resolutions ranging from 0.96 Å to 1.22 Å (Table 3.6.). The NO complexes were photo-reduced by the X-ray source to the ferrous state during data collection (Table 3.3.), as indicated by the severe Fe-N-O angles of 139° and 137° [53]. We were able to refine all structures in the same manner as the mutant complexes, including anisotropic thermal parameters and performing full-matrix refinement as a final step.

TABLE 3.6. Crystallographic Data and Refinement Statistics for rNP4 Heme Altered Structures

	Analog 1 ^a			Analog 2 ^b	
	NH ₃	NO	aqua	NH ₃	NO
PDB accession	2AT4	2AT5	2AT6	2AT7	2AT8
pH	7.5	5.6	5.6	7.5	5.6
wavelength (Å)	0.90	0.90	0.90	0.90	0.90
resolution (Å)	1.08	1.22	1.22	0.98	0.96
total no. of reflns	439,356	269,086	278,663	378,953	289,896
no. of unique reflns	65,307	44,702	44,684	75,395	81,981
completeness (%) ^c	95 / 91	96 / 96	96 / 94	86 / 72	86 / 89
mean I/σ_1^c	16.1 / 3.6	24.3 / 10.6	15.3 / 3.4	30.3 / 4.3	22.6 / 2.9
$R_{sym}^{c,d}$	0.06 / 0.18	0.06 / 0.18	0.07 / 0.31	0.08 / 0.40	0.08 / 0.41
$R_{cryst}/R_{free}^{c,e}$	0.14 / 0.16	0.12 / 0.15	0.13 / 0.17	0.17 / 0.19	0.16 / 0.19
Rmsd ^f					
distances	0.02 (0.02)	0.02 (0.02)	0.02 (0.02)	0.02 (0.02)	0.02 (0.02)
angles	1.73 (2.00)	1.68 (2.00)	1.76 (2.00)	2.55 (2.00)	1.75 (2.00)
DPI ^g	0.03	0.04	0.05	0.04	0.04
no. of multiple conformations	31	39	45	37	40
comment	Open	Closed	Closed	Open	Closed
^h heme pivot (°)	9.4	9.5	n/m	4.6	4.7

^aContains Fe(III) deuteroporphyrin IX. ^bContains Fe(III) 2,4 dimethyl deuteroporphyrin IX. ^cOverall/ outermost shell. ^d $R_{sym} = (\sum_h |I_h - \langle I \rangle|) / (\sum_h I_h)$, where $\langle I \rangle$ is the mean intensity of all symmetry-related reflections I_h . ^e $R_{cryst} = (\sum |F_{obs} - F_{calc}|) / \sum F_{obs}$. R_{free} as for R_{cryst} , using a random subset of the data (5%) not included in the refinement. ^fRmsd distances and angles are in angstroms and degrees respectively. Target values are in parentheses. ^gCruickshank Dispersion Precision Indicator [100]. ^hAngle between atom NC_{wild type}-Fe_{wild type}-NC_{analog}.

The overall protein structure is similar to wild type. Surprisingly, the analog macrocycles remain in the same plane as wild type, but are pivoted counter clockwise about pyrrole ring A when viewed down the ligand-Fe-proximal histidine axis (Figure 3.6.). Coupled to this pivoting is the pivoting of the proximal histidine, iron and ligand. As compared to wild type, analog 1 and analog 2 pivot $\sim 9.5^\circ$ (0.4 Å) and $\sim 4.7^\circ$ (0.2 Å) respectively at the nitrogen of pyrrole ring C (Table 3.6., Figure 3.6.). The degree of pivoting is independent of ligand.

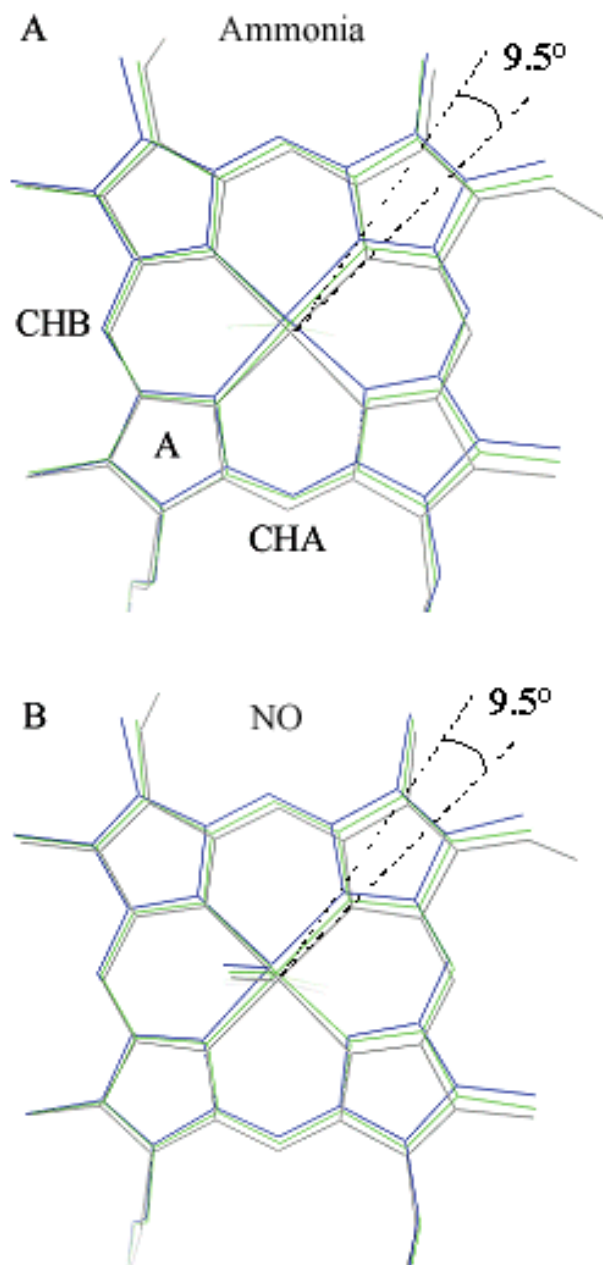


FIGURE 3.6. Coordination Sphere Superimposition of Analog Complexes and Wild-Type rNP4. Shown are heme positions in the NH_3 complexes (A) and NO complexes (B) for analog 1 (blue), analog 2 (green) and wild type (black) proteins, after superimposition. Angle between atom $\text{NC}_{\text{wild type}}\text{-Fe}_{\text{wild type}}\text{-NC}_{\text{analog 1}}$ is labeled.

Since the structures were refined with anisotropic (3-dimensional) temperature factors, anisotropic movements of the macrocycle could be examined (Figure 3.3.c., pg. 70). The NO complex of analog 1 illustrates additional disorder in the macrocycle atoms. All atoms of the macrocycle ring, with the exception of pyrrole A, are drastically non-spherical and elongated, with greatest anisotropy indicated in pyrrole ring C. This result also indicates that the macrocycle is pivoting back and forth and is less rigidly held in the binding pocket, displaying greater disorder over the ensemble of molecules in the crystal. The motion of NO has also changed. Similar to wild type (Figure 3.3.a) the NO oxygen lies in the CHB-Fe-CHD axis. However, similar to rNP4 L133V-NO, the NO oxygen is now revolving more perpendicular to this plane rather than parallel. Analog 2-NO behaves in the same manner. Additionally, the degree of anisotropy of each atom in analog 2 is similar to analog 1 even though analog 2 pivots by half the amount of analog 1.

Heme distortion. The general geometry for heme distortion that was described for the mutant structures also applied to the analog complexes. The analog complexes display heme distortions that are nearly identical to those for the wild type protein. Nonetheless, there are small changes worth noting. The analog complexes displayed less change in distortion than the mutant proteins, but the differences are in opposite direction (Table 3.4.). That is, all complexes of analog 1 decrease in ruffling and increase in saddling while complexes of analog 2 have the opposite differences. This may or may not have significance due to the fact that the absolute value of the difference are small.

Similar to wild type, addition of NO to the rNP4 L133V mutant, analog 1 and analog 2 increases the ruffling distortion by 0.15 Å, 0.13 Å, and 0.10 Å respectively.

Analog 1 complexes and the ammonia complex of analog 2 display an increase in rotation of pyrrole ring A (Table 3.5.), which seem to be involved with the pivoting of the analog macrocycle. Analog 2 shows mixed results. In each complex, two pyrrole rings increase, while two decrease in rotation. Though the increase/decrease of the pyrrole ring's rotation is not the same for the NO and ammonia complexes, the equality is consistent and may contribute to the increase in ruffling and decrease in saddling observed by NSD (see discussion).

3.4. Discussion

An overview of highlighted structural features to be discussed for the eight complexes studied is presented in Table 3.7.

TABLE 3.7. Highlighted Structural Features for rNP4 Altered Proteins

Structure	Resolution (Å)/pH	Highlighted Structural Features ^d
L133V-NH ₃	1.07 / 7.5	• open, ferric
-NO	1.00 / 5.6	• closed, ferric • heme moves at point of mutation • NO ligand rotates (Figure 3.3.) • anisotropy of NO has changed (Figure 3.3.) • π -acceptor distortion remains (Table 3.4.)
L123V/L133V-Im ^a	1.00 / 5.6	• Closed, ferric • Entire heme moves • imidazole ligand rotates (Figure 3.2.) • increase ruffling/decrease saddling (Table 3.4.)
Analog 1 ^b -NH ₃	1.08 / 7.5	• Open, ferric • macrocycle pivots (Figure 3.6.)
-NO	1.22 / 5.6	• Closed, ferrous • anisotropy of NO has changed (Figure 3.3.) • macrocycle pivots (Figure 3.6.) • π -acceptor distortion remains (Table 3.4.)
-H ₂ O	1.22 / 5.6	• Closed, ferric • Similar to analog 1-NH ₃
Analog 2 ^c -NH ₃	0.98 / 7.5	• Similar to analog 1-NH ₃
-NO	0.96 / 5.6	• Similar to analog 1-NO

^aImidazole. ^bContains Fe(III) Deuteroporphyrin IX. ^cContains Fe(III) 2,4 Dimethyl Deuteroporphyrin IX. ^dFigures and/or tables relevant to the highlighted structural feature are in parentheses.

3.4.1. NO binding induces increased ruffling in altered proteins

Binding of NO and other π -acceptor ligands to both ferric and ferrous forms of rNP4 induces increased heme ruffling [38]. Here, we show that this trend extends to mutated proteins and to proteins with modified hemes. All of the proteins examined retained ruffled hemes in the absence of NO, and in all cases this ruffling increased on binding NO from 0.10-0.15 Å (Table 3.4.), as compared to 0.17 Å for ferric wild type and 0.32 Å for ferrous wild type [53]. The underlying cause of this increased distortion remains to be determined but may arise by the short pyrrole nitrogen-Fe (N_p -Fe) distances (Table 3.3.), causing steric strain.

3.4.2. Distal ligand orientation and NO anisotropy changed in altered proteins

The alterations to the protein or heme have caused a change in ligand orientation in rNP4 mutants L133V and L123V/L133V (Figures 3.2.,3.3.) and/or a change in NO anisotropy in rNP4 L133V and analog complexes (Figure 3.3.). In the mutated proteins, Val 133 settles into a new conformation that removes a binding pocket obstacle. This causes the heme pocket to open up and allows the NO ligand of rNP4 L133V or imidazole ligand of rNP4 L123V/L133V to rotate $\sim 48^\circ$ to just beyond the NB-Fe-ND axis (Figure 3.2.). Thus, regardless of its electronic properties, the ligand is allowed to rotate freely, settling into a new position. Additionally, the imidazole ligand of rNP2 L122V/L132V also rotates in the same manner (A. Weichsel & W.R. Montfort, in

preparation). However, the imidazole ligand in rNP2 L122V/L132V rotates $\sim 69^\circ$ (Figure 3.7.). This new conformation of rNP4 L133V may interfere with ligand induced conformational change as indicated by a faster capture and release of NO (E.M. Maes & W.R. Montfort, unpublished).

In addition to the NO in the rNP4 L133V-NO complex rotating to a new axis, the motion (anisotropy) of the NO oxygen has changed from revolving in the plane of Fe-N-O (wild type motion) to revolving more perpendicular to the plane (Figure 3.3.). This could also be because the pocket has more room, allowing for more freedom for NO motion.

Though the NO oxygen in the analog-NO complexes do not rotate to a new axis, the motion has changed to revolve more perpendicular to the Fe-N-O plane, similar to that seen in rNP4 L133V-NO (Figure 3.3.). This new motion may be a result of the macrocycle pivoting.

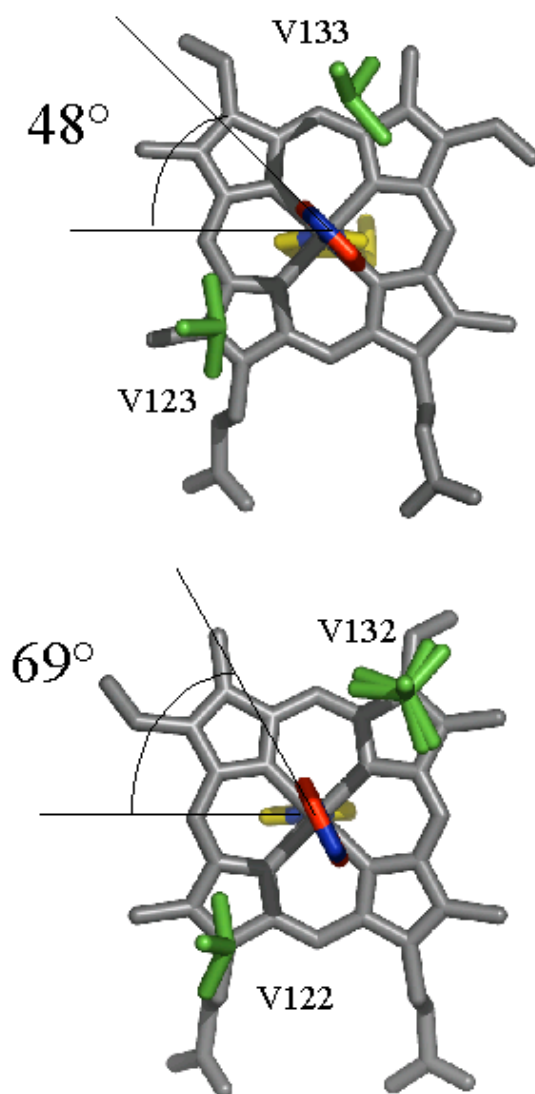


FIGURE 3.7. Imidazole Rotation. The angle of rotation for the imidazole ligand in rNP4 L123V/L133V (top) and rNP2 L122V/L132V (bottom) are labeled for comparison. Distal leucines are in green and labeled; imidazole is in red and blue.

3.4.3. Macrocycle pivots in heme analog structures

To investigate the role of the vinyl groups in distortion, we produced proteins with vinyl exchanged for hydrogen (analog 1) or methyl (analog 2) and determined their structures with ammonia, H₂O, and NO.

In general, with respect to the wild-type protein, the analog structures show little change in overall protein structure and, in contrast to the mutant structures, show little change in heme deformation (Tables 3.4.,3.5.), (Figures C.1., C.2.). However, they display a new pivoting of the macrocycle (Figure 3.6) and increased anisotropy (Figure 3.3.c). Pyrrole ring rotation calculations (Table 3.5.) show pyrrole ring A has a more positive rotation in all complexes. This causes meso carbon atoms CHB and CHA to move up and down respectively (Figures C.1., C.2.) and the macrocycle pivots counter-clock wise about pyrrole ring A to alleviate new steric contacts of atom CHB with ligand. Analog 2 pivots less than analog 1 due to a bulkier substituent (methyl versus hydrogen) at the 2,4-substituent position. Interestingly the “up/down” disorder in analog 1 is retained. For analog 2, the “up/down” orientations are irrelevant since it is a symmetrical macrocycle.

3.4.4. Increase in ruffling and elimination of saddling in double mutant gives insight into general distortion mechanism in rNP4 heme

Though an ammonia or a NO complex of double mutant rNP4 L123V/L133V could not be obtained, the rNP4 L123V/L133V imidazole complex has proven exceedingly valuable to this study. It was predicted that by removing steric contacts of L123 and L133, the ruffling and saddling deformations would decrease. However, contrary to intuition, the double mutation causes a slight increase in ruffling (0.1 Å) and an elimination of saddling (Table 3.4.). Keeping in mind the distortion definitions described in Section 1.4.2 and Figure 1.3., a detailed explanation of how this may occur is described.

Increase in ruffling. A possible atomic explanation for the increase in ruffling distortion in rNP4 L123V/L133V is outlined in Figure 3.8.. In wild-type rNP4, distal leucines 123 and 133 contact atoms CHA/C1A/C2A and CHC/C1C/C2C, respectively (Figure 3.8.a.), causing the original deformation to be predominantly classic ruffling and saddling. In addition, in the wild-type rNP4-imidazole complex [38], the distal imidazole ligand and the imidazole of the proximal histidine are relatively parallel to each other and lie in the meso CHB-Fe-CHD plane (Figure 3.8.a.). The relative position of the distal imidazole ligand may be due to steric conflicts with distal leucines 123 and 133. Due to steric interactions above and below by the two imidazoles, meso carbon atoms CHB and CHD are locked into place.

When L123 and L133 are replaced with valines, two major consequences result (Figure 3.8.b,c.): (1) atoms in direct contact with positions 123 and 133 become more planar, as noted by FCD calculations (Figure 3.4.c.) and (2) the imidazole ligand rotates $\sim 48^\circ$ to a new axis (NB-Be-ND), as clearly indicated by the electron density (Figure 3.2.).

As shown by pyrrole ring rotation calculations in Table 3.5., release of local steric interaction causes pyrrole C to rotate counter clockwise and thus become more planar as expected (Figure 3.8.b.).

In contrast, the latter consequence, rotation of the distal imidazole ligand, causes pyrrole rings A, B, and D to become more nonplanar (Figure 3.8.c.) and can partly account for the observed increase in ruffling. Rotation of the distal imidazole removes steric interactions above meso carbon atoms CHB and CHD. This results in these two atoms moving more above the porphyrin mean plane and, as a counter effect, meso carbon atoms CHA and CHC move more below the mean plane. The upward movement of meso carbon CHB causes pyrrole rings A and B to rotate more clockwise and more counter clockwise, respectively. Similarly, the upward movement of meso carbon CHD causes pyrrole ring D to rotate more counterclockwise.

The orientation of distal imidazole with respect to proximal imidazole has been proposed to be correlated to the ruffling distortion [103,104]. With no outside influence, the distal and proximal imidazoles prefer to be 90° apart from one another. The type of deformation that predominates (ruffling or saddling) depends on which axes the axial pair lies. In the case of the ruffled conformation, the axial ligands are 90° apart bisecting the

Np-Fe-Np axes, causing two adjacent pyrrole rings to be twisted clockwise and counterclockwise and bringing the meso carbons above and below the porphyrin mean plane. Thus, with the rotation of 48° by the distal imidazole in respect to the proximal imidazole, the angle between the pair approaches 90° , and because the axial pair becomes closer to bisecting the Np-Fe-Np axis, there is an observed increase in ruffling (Table 3.4.). The rotation of distal imidazole ligand and increase in ruffling is also observed in the rNP2 L122V/L132V-imidazole complex (A. Weichsel & W.R. Montfort, in preparation).

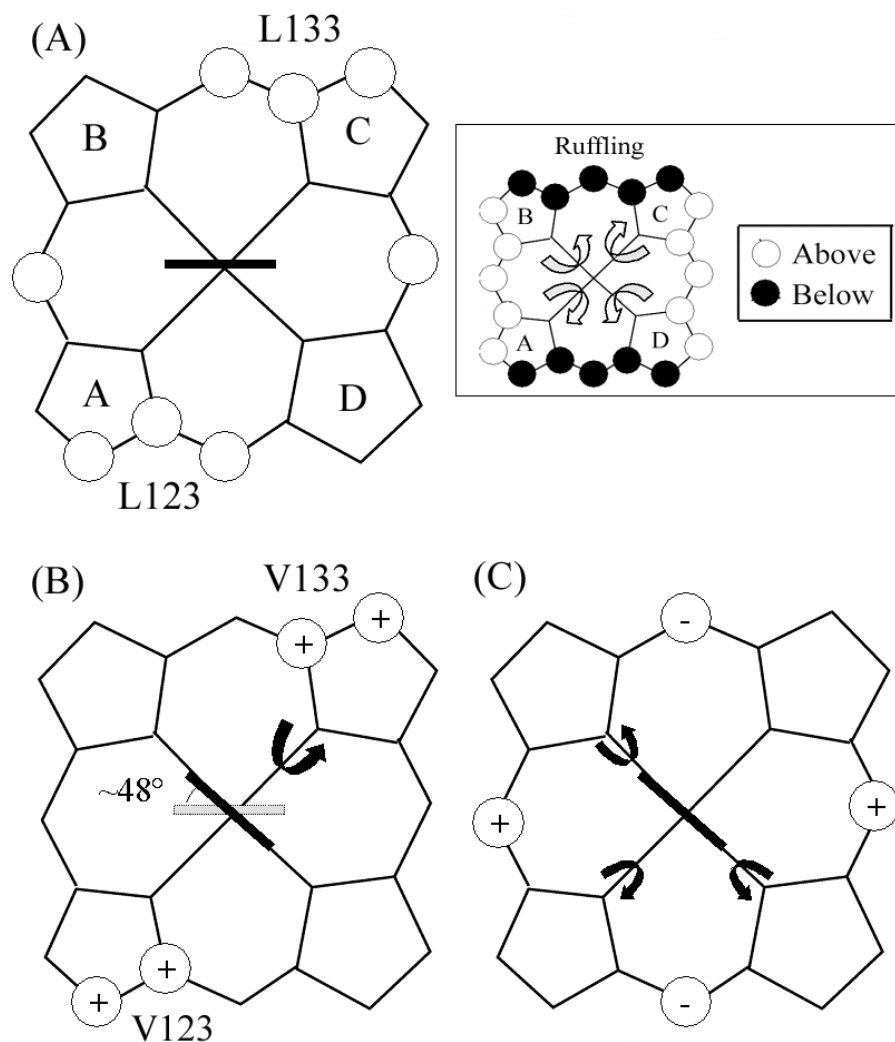


FIGURE 3.8. Increased Ruffling in rNP4 L123V/L133V. (A) Wild-type rNP4. Pyrrole rings are labeled A-D based on heme convention. Positions of L123 and L133 are noted and atoms of interest for each step are circled. Position of imidazole ligand is represented by a black solid bar. (B) Shift due to 133 and 123 contact. (C) Shift due to imidazole rotation. Plus (+) and minus (-) signs within a circle indicate movement up or down of the atom relative to wild type based on FCD calculations (Figure 3.4.c.). Curved arrows on nitrogen-iron bonds indicate the direction of rotation for that Np-Fe bond based on pyrrole ring rotation calculations (Table 3.5.). See text for details. Inset: Ruffling definition from Section 1.4.2., Figure 1.3..

Near elimination of saddling. As mentioned above, the saddling deformation of rNP4 L123V/L133V-imidazole is nearly eliminated with respect to wild type [38] (Table 3.4.). In the classic definition of saddling, two pyrrole rings are fully above while two are fully below the porphyrin mean plane. Since our heme is predominately ruffled, by definition, half of each pyrrole ring is above while the other half is below the porphyrin mean plane. Taking both definitions and translating them to our system, an elimination in saddling would occur if (1) each individual atom of each ring moved in the same direction (regardless of becoming more planar or non planar) and (2) each alternating ring as a whole moved in the opposite direction. These two criteria are indeed observed in the double mutant system (Figure 3.9.). With the distal imidazole lying just beyond the NB-Fe-ND axis all atoms of pyrrole rings B and D move down while, as a counter effect, pyrrole rings A and C move up (Figure 3.4.c) and thus saddling is eliminated.

Furthermore, though not eliminated, the saddling deformation in the rNP4 L133V-NO complex decreases by the same magnitude (-0.24 Å) as that of the rNP4 L123V/L133V-imidazole complex (Table 3.4.). This may be correlated to the fact that both the distal ligands lie just beyond the NB-Fe-ND axis.

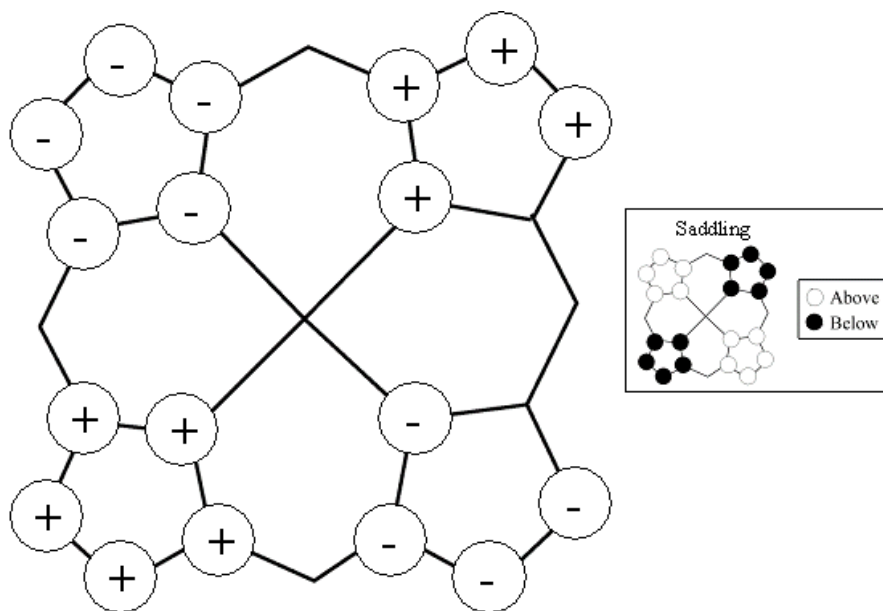


FIGURE 3.9. Elimination of Saddling in rNP4 L123V/L133V. Pyrrole rings are in the same orientation as Figure 3.8.. Plus (+) and minus (-) signs within a circle indicate movement up or down of the atom respectively relative to wild type based on FCD calculations (Figure 3.4.c). Pyrrole ring atoms with no signs indicate the atom is in the same position as wild type. See text for details. Inset: Saddling definition from Section 1.4.2, Figure 1.3..

3.4.5. Proximal histidine orientation may contribute to ruffling in rNP4

A possible contribution to ruffling is that the rNP4 protein has placed its proximal histidine in an orientation that causes maximum ruffling due to steric contacts of the residue hydrogens.

In rNP4, the proximal histidine is hydrogen bonded to Asp 70 and locked into place by the well ordered Phe 68; thus the hydrogens of His 59 are positioned toward the meso carbons B and D. This contact is close enough (3.73 Å and 3.83 Å respectively) to cause a steric effect and thus these atoms will pucker above the plane. In addition, the distal leucines at positions 123 and 133 are pushing down on meso carbons A and C causing these positions to be below the plane. These two factors together illustrate the classic definition of ruffling: 2 opposite meso carbons are above the plane while the other two are below the plane (or adjacent meso carbons are above and below the plane in an alternating fashion) (Figure 1.3.).

As a comparison, we examined the proximal coordinating histidine-heme orientation in a recently collected 0.95 Å myoglobin-NO complex [105]. The histidine is oriented in such a way that the hydrogens are positioned directly in the center of pyrrole rings A and C. This positioning does not cause a steric effect by the hydrogens. Thus, by visual inspection as well as through NSD calculation (data not shown), the heme remains flat.

Further investigation to determine if the proximal histidine contributes to ruffling would consist of future mutational studies in rNP4 at residues His 59, Phe 68 and Asp 70.

Goodin *et al* have deposited into the PDB a H60C mutant of rNP1 complexed with histamine (1U18) (unpublished structure). Histamine is a natural ligand of rNP4 and binds in the distal pocket after NO is released into the victim's tissue. This structure is to 1.96 Å at pH 7.5 and has a P2₁ space group, different from the rNP4 C2 space group. A water molecule occupies the space of the proximal histidine and the structural water that hydrogen bonds the proximal histidine to Asp 70 in wild type is missing in the mutant. The distal histamine is oriented so that the ring hydrogens are positioned directly in the center of pyrrole rings B and C, similar to that seen in wild-type rNP4-histamine (1IKE) [38]. This positioning cannot cause a steric effect from the distal side. Thus, although the structure is to modest resolution, it appears the heme is less ruffled and less distorted in general.

3.4.6. Tuning heme properties to proper biological function

Heme proteins in general have evolved with cofactor properties tuned to perform specific biological functions. The rNPs must resist autoreduction and stabilize heme iron in the ferric oxidation state to efficiently bind and release NO [37]. There are several ways in which this stabilization might be accomplished. The first may be heme distortion. It is accepted that nonplanar porphyrins are easier to oxidize and more difficult to reduce than planar porphyrins in certain model complexes [38,60,106,107]. Several studies have directly linked heme distortion to stabilizing the ferric oxidation state of the heme iron. For example, a correlation between ruffling and reduction

potential for ferricytochromes c_3 has been noted [108]. The reason for this may be for heme π and iron orbital mixing, partially filling the unoccupied d orbital used for reduction of Fe(III) to Fe(II). More recently, Shokhireva et al. (2003) investigated leucine to valine distal pocket mutations of rNP2 and their NO complexes by spectroelectrochemistry. The leucine to valine mutations in rNP2, L122V and L132V, are structurally positioned in the same manner as L123V and L133V in rNP4. NO complexes of the rNP2 mutants, with the exception of L122V, exhibit more positive reduction potential shifts than does the wild-type protein, which indicates stabilization of the Fe(II)-NO state [47]. Although these measurements have yet to be made for rNP4, the more positive reduction potential is consistent with the current work in that smaller valine residues allow the heme to regain the planarity seen for rNP2 L122V/L132V. Electrochemical measurements on rNP4 were attempted but proved not straightforward to analyze.

Second, the anisotropy change of the NO oxygen (Figure 3.3.) seen in the rNP4 L133V mutant and analog complexes may be linked to reduction potential. Theoretical vibrational frequency ($\nu_{\text{Fe-NO}}$ vs ν_{NO}) and bond length ($R_{\text{Fe-NO}}$ vs R_{NO}) correlation calculations for five-coordinate $[\text{Fe}(\text{Porph})\text{NO}]^+$ complexes [109] show direct correlations and may be the basis for both redox stability and NO lability of rNP4-NO. Recent computational studies revealed a correlation between the sensitivities of Fe-NO and N-O bond strengths to electronic and environmental factors [110]. As more experimental data become available for imidazole-bound 5-coordinate complexes, it will

be interesting to learn whether Fe-NO bond length and k_{off} or K_d actually track inversely with Fe-N-O angle [109].

CHAPTER 4

LIGAND PROTECTION AND NITRIC OXIDE INTERACTIONS WITH HEME IN
NITROPHORIN 4: KINETIC AND STRUCTURAL ANALYSES
OF A LOOP MUTANT

4.1. Introduction

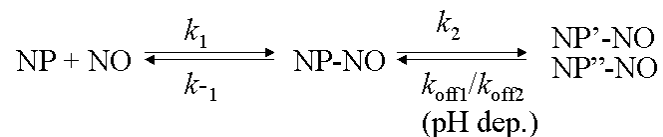
Chapter 1 introduced the nitrophorins, the lipocalin fold and flexible loop region, and ligand protection in general. In this chapter, I explore the role of flexible loops in ligand protection in rNP4.

Reactive radical molecules, such as nitric oxide, require protection to avoid side reactions with the environment. A central question in NO biology involves understanding how this protection occurs as well as the chemistry involved in side reactions with oxygen and other physiological compounds.

The primary function of the nitrophorins is to store, transport, and release NO. How do these proteins protect their reactive ligand against side reactions with oxygen? Previous structural analyses of rNP4 revealed a substantial NO-induced conformational change in which two poorly ordered loops collapse into the binding pocket, expel water, and pack nonpolar side chains around the heme-ligated NO moiety. In the absence of NO, the distal heme pocket is 'open' with the AB Loop (residues 31-37) poorly ordered and the GH Loop (residues 125-133) located away from the heme. Residues Glu 32 and Asp 35 are extremely mobile in this open complex. Asp 129 is weakly associated with the N-terminus and the 130-131 peptide bond is flipped open and weakly associated with solvent. When rNP4 binds NO, the AB and GH Loops collapse into the binding pocket.

Residues Asp 30, Asp 129 and Leu 130 are involved in an extensive hydrogen bond network stabilizing the closed conformer, which includes flipping of the 130-131 peptide bond and new hydrogen bonds to Asp 30 and Asp 129. In addition, the L130 side chain packs directly against the NO ligand.

Previous kinetic analyses revealed a slow, biphasic, and pH-dependent NO release, which was proposed to be associated with loop movements (Scheme 4.1.) [37,52]. There is an initial binding phase (k_1) representing nitrosyl complex formation. This is followed by a lagging phase (k_2) that is suggested to involve protein conformational change. NO release begins with a biphasic, pH sensitive step (k_{off1} and k_{off2}), again suggested to involve the protein conformational change, followed by a faster phase (k_{-1}) that was suggested to represent release from the completely open conformation.



(SCHEME 4.1.)

Charged and hydrophobic groups surrounding the cavity sense pH (D129, D35, D30) and NO (T121, L130, V36) respectively, leading to a pH dependent hydrophobic trap. In recent studies, every residue mentioned above, with the exception of D35, has been mutated and each mutant studied both structurally and kinetically [52]. Of particular interest to this project are residues D129 and L130, associated with the GH

Loop, and V36, a hydrophobic residue at the entrance to the internal cavity (Figure 4.1.). For the double mutant, D129A/L130A, the NO-induced conformational change is largely abolished and kinetic analyses using stopped-flow spectroscopy revealed the pH dependence for NO release is eliminated [52]. However, the multi-phasic kinetic behavior was retained.

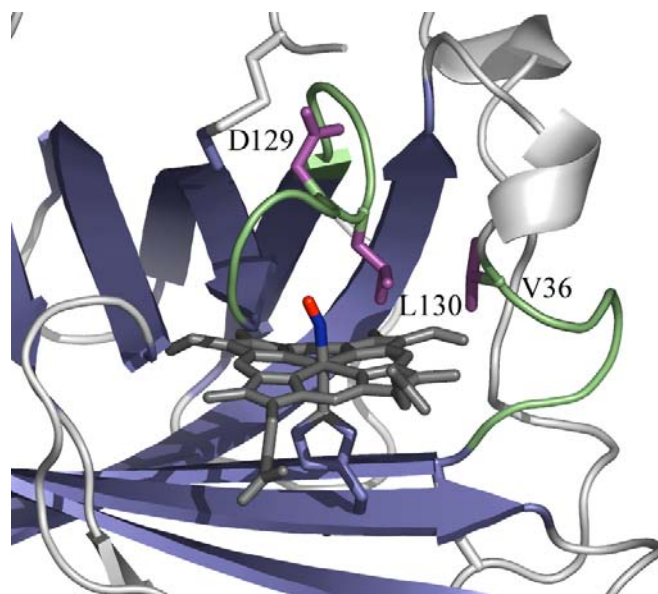


FIGURE 4.1. Loop Mutations in rNP4. Flexible loop regions (green) containing the three mutated residues (purple). D129 and L130 are associated with loop closure while V36 blocks the entrance to the beta-barrel.

In the current study, we created a triple alanine mutant (rNP4 AAA) of the rNP4 loop region (V36A/D129A/L130A) to investigate the effects of loop closure and protection of NO from oxygen. By eliminating the hydrophobic group of valine (V36A) at the entrance to the cavity in a mutant that already contains a dysfunctional GH Loop (D129A/L130A) [52], movement of NO in and out of the internal cavity appears to be unhindered. Crystallographic data and kinetic measurements using stopped-flow and UV-visible spectrophotometry were obtained. To date, all experiments involving rNP4 and NO have been done under deoxygenated (anaerobic) conditions to minimize side reactions between oxygen and NO. Thus, I investigated NO binding and NO-protein complex decay in rNP4 and the rNP4 AAA mutant in the presence and absence of oxygen at pH 8 and pH 5. Our results indicate that loop closure is now completely eliminated, but biphasic binding is retained. Interestingly, the oxygen reaction with NO is much slower than heme NO binding, leading to extensive protection. This work is the subject of a paper in preparation [111].

4.2. Materials and Methods

4.2.1. Mutagenesis

rNP4 mutant V36A/D129A/L130A (rNP4 AAA) was constructed in two stages using PCR and Stratagene's QuikChange™ Site-Directed Mutagenesis Kit by Ms. Jacquie Brailey. The construction of double mutant D129A/L130A (pCBP11) was described

previously [52]. The following oligonucleotide purchased from Midland Certified Reagent Co. (Midland, TX) was designed by Lauren Murata and Jacquie Brailey and used as a PCR primer to create a DNA sequence containing the V36A mutation:

5'- TTGGAACCTGACGACGCTCCAAAAAGATACTGCG-3'. This sequence was then combined with the previous plasmid (pCBP11) to produce the resulting triple mutant plasmid, pCBPV36A. After confirmation by DNA sequencing (Arizona Research Laboratories, University of Arizona), pCBPV36A, carrying the V36A/D129A/L130A mutations were transformed into competent *Escherichia coli* BL21(DE3) cells for expression.

4.2.2. Expression and purification

Expression and purification of wild type and mutant proteins was carried out by Ms. Jacquie Brailey. Wild type and mutant proteins were expressed as inclusion bodies, denatured, and refolded. Protoporphyrin IX was titrated into the protein until a Soret/protein ratio of 3.7:1 was observed by UV-Visible spectroscopy. The proteins were purified by ion-exchange chromatography followed by gel filtration as previously described [49,57,69]. UV-visible absorption spectra recorded on a Cary 50 confirmed the presence of heme and NO binding activity.

4.2.3. rNP4 AAA crystallization, data collection and processing

Detailed crystallization, preparation conditions, and information on the beam-line used for data collection are in Appendix B and summarized here. Crystals were grown at room temperature ($\sim 25^{\circ}\text{C}$) in 2.2 M ammonium phosphate, pH 7.5, using the hanging drop technique by Dr. Andrzej Weichsel and Mr. Chris Roessler during a rotation through the laboratory. A single crystal was transferred to an argon saturated cryoprotectant solution (3.2 M ammonium phosphate, pH 5.6) and allowed to equilibrate. Following equilibration, the crystal was transferred and soaked in an identical cryoprotectant solution saturated with NO gas as previously described. Crystals were frozen in liquid nitrogen for data collection. Diffraction data to 1.0 Å was collected at the Advanced Photon Source (Argonne National Laboratory, Argonne, IL) on beam line 14-BMD with a Quantum-4 CCD detector (100 K) and processed with HKL2000 by Dr. Andrzej Weichsel. The crystal belongs to the C2 space group with cell constants $a = 70.22$ Å, $b = 42.64$ Å, $c = 52.91$ Å, $\beta = 94.07^{\circ}$, typical of the wild type structure.

4.2.4. Structure determination

The rNP4 AAA mutant model was built using difference Fourier methods starting with the published D129A/L130A structure (1SXX) [52]. The phases were subsequently refined with anisotropic temperature factors using REFMAC from the CCP4 package [71] and model building was accomplished with COOT [72]. Due to the ultra high

resolution of the structures, the weighting term between the X-ray and geometric part of the refinement residual was set between 2.0-4.0, which allows for loose model restraints. Residues found to occupy more than one conformation were modeled as such, generally with occupancies set to 0.5 for each conformer. Refinement converged to $R_{\text{cryst}} = 0.22$ and $R_{\text{free}} = 0.25$, somewhat higher than typically found for rNP4 crystals, but still high quality. Model quality was assessed using the program PROCHECK [73] as implemented in CCP4 [71] and structural figures were prepared using PyMOL [74] (<http://www.pymol.org/>). Coordinates will be deposited with the Protein Data Bank.

4.2.5. Kinetics

NO association rates for the mutant and wild type complexes were obtained as previously described [52] and modifications summarized here. Data were acquired under aerobic or anaerobic conditions at 25 °C using rapid stopped-flow spectrophotometry on an OLIS RSM-1000 apparatus (OLIS Inc.), which allows measurements of full absorption spectra every millisecond. For anaerobic experiments, protein solutions (~10 μM), in either 40 mM Tris-HCL (pH 8.0) or sodium citrate (pH 5.0), were deoxygenated with a stream of oxygen-free argon gas before rapid mixing. NO solutions for both aerobic and anaerobic experiments were prepared as follows. Diethylamine NONOate (DEA/NO) was used as the NO donor source. Septum capped test tubes were filled with 5 mL of deoxygenated pH 8.0 or pH 5.0 buffer and DEA/NO was injected with a gastight syringe while keeping a steady argon flow entering to achieve the desired NO

concentrations (2.5-60.0 μM). Desired DEA/NO concentrations were calculated based on the concentration of a stock solution as determined by UV-visible spectroscopy. It was assumed that 1 mole DEA/NO yields 2 moles of NO. The final solution was immediately withdrawn into a 2.5 mL gas tight syringe to avoid NO escape into excess headspace and attached to the OLIS port for 20 min (pH 8) or 10 min (pH 5) to allow for full release of NO from the donor compound before starting the experiment. The data were analyzed using a singular value decomposition (SVD) approach and the Global fitting software provided by OLIS [112], leading to greater accuracy. Association (k_1) and dissociation (k_{-1}) rates, along with estimated errors were calculated as previously described [37,52]. Briefly, rate constants k_1 and k_{-1} were obtained through fitting to eq 1 using SigmaPlot (SPSS, Inc. , Chicago, IL), where k_{obs} was the average of four to eight shots in the stopped-flow instrument:

$$k_{\text{obs}} = k_1[\text{NO}] + k_{-1} \quad (1)$$

Estimated errors for k_1 and k_{-1} were obtained through averaging of multiple experiments. Surprisingly, the mutant protein illustrated good agreement with a biphasic model. However, a larger uncertainty was obtained by fitting the second phase (Scheme 1) because of its small ligand dependence. In practice, measurement of k_2 is difficult since it is similar in value to $k_1[\text{NO}]$, and relatively large, thus k_2 rate constants are not reported.

NO-protein complex decay was monitored under aerobic and anaerobic conditions using a Cary 300-Bio UV-Visible Spectrophotometer supplied by Dr. Gordon Tollin. The NO donor, DEA/NO was used as the NO source and acquired from Dr. Katrina Miranda. For experiments without glutathione (-GSH), 20 μM NO was added to 10 μM protein (pH 8 or pH 5) in either a cuvette exposed to air or one that was argon deaerated and capped with a septum, and spectra were collected over ~ 4 hours to allow binding saturation and release of NO. For experiments in the presence of GSH (+GSH), 10 μM NO was added to 10 μM protein (pH 8 or pH 5) in either a cuvette exposed to air or one that was argon deaerated and capped with a septum, and the NO-protein complex was allowed to saturate. Once saturation occurred, 1 mM GSH was added to the NO-protein complex and spectra were collected over ~ 1 hour. In both experiments (-GSH and +GSH), disappearance of the 420 nm Soret peak, characteristic of the NO-protein complex, and appearance of the 404 nm Soret peak, characteristic of the unligated protein, was monitored. Spectral fitting was to determine $t_{1/2}$. Aerobic conditions allowed the NO-protein complex to decay beyond its half-bound state. The calculated spectrum for the half-bound, half-unbound species ($\text{Half Bound}_{\text{calc}}$) was obtained by adding together the fully ligated (+NO) and fully unligated (-NO) protein spectrum and dividing by two. An approximate $t_{1/2}$ was estimated by matching an experimental spectrum ($\text{Half Bound}_{\text{exp}}$) to $\text{Half Bound}_{\text{calc}}$. If conditions did not allow the NO-protein complex to reach $\text{Half Bound}_{\text{calc}}$, an approximate percent recovery of the unligated protein was estimated by fitting the spectrum at 120 min to a percentage of the fully unligated spectrum (-NO).

4.3. Results and Discussion

In wild-type rNP4-NO, D129 and L130 are involved in a hydrogen bonding network that stabilizes the closed conformation. In addition, L130 contacts NO in the closed conformation, while V36 is a hydrophobic residue at the entrance to the binding cavity and contacts L130. This loop closure and cavity blockage may help protect NO from a surrounding oxygen-rich environment. To test the role of the rNP4 AB and GH Loops, including V36, in NO protection, we created a triple alanine mutant, V36A/D129A/L130A (rNP4 AAA), in order to eliminate loop closure and block NO from escaping from the binding pocket. In what follows, I report the structural and kinetic consequences of this triple mutation. In general, the mutations lead to a constant open conformation, NO reacts with the heme iron before surrounding oxygen under aerobic conditions, and rNP4 AAA-NO complex decay is faster than in wild type.

4.3.1. rNP4 AAA (V36A/D129A/L130A) at 1.0 Å

The structure of the rNP4 AAA-NO complex, pH 5.6, 100 K, was determined to 1.0 Å resolution (Table 4.1.). (see Materials and Methods).

 TABLE 4.1. rNP4 AAA Mutant Data Collection and Refinement Statistics

pH	5.6
wavelength (Å)	0.90
resolution (Å)	1.00
total no.of reflns	882,416
no. of unique reflns	79.668
completeness (%) ^a	94.1 / 90.1
mean I/σ_I ^a	37.0 / 5.33
R_{sym} ^{a,b}	0.10 / 0.39
R_{cryst}/R_{free} ^{a,c}	0.22 / 0.25
Rmsd ^d	
distances	0.01 (0.02)
angles	1.414 (2.00)
DPI ^e	0.04
no. of multiple conformations	
comment	Open conformation

^aOverall/ outermost shell. ^b $R_{sym} = (\sum_h |I_h - \langle I \rangle|) / (\sum_h I_h)$, where $\langle I \rangle$ is the mean intensity of all symmetry-related reflections I_h . ^c $R_{cryst} = (\sum |F_{obs} - F_{calc}|) / \sum F_{obs}$. R_{free} as for R_{cryst} , using a random subset of the data (5%) not included in the refinement. ^dRmsd distances and angles are in angstroms and degrees respectively. Target values are in parentheses. ^eCruickshank Dispersion Precision Indicator [100].

The electron density is consistent with a single NO conformation. As with wild type, the Fe-NO bond is bent such that all three atoms lie in the plane of His 59, the proximal trans ligand. The iron-nitrogen bond distance (1.8 Å), iron histidine bond distance (2.05 Å), and iron-nitrogen-oxygen bond angle (~140 °) indicate that the heme has been photoreduced to the ferrous state (Fe(II)) during data collection.

The rNP4 AAA-NO structure is similar to that for the wild type protein except for the AB and GH loops, which display the open conformation. The structure is entirely in an open conformation. The 130-131 peptide remains unflipped and hydrogen bonded to the N-terminus, preventing formation of strong hydrogen bonds with Asp 30 and Asp 129 (Figure 4.2.). This loss of the ability to hydrogen bond disrupts the hydrogen bonding network needed to stabilize the closed conformation. The backbone arrangement of residue 36 and surrounding residues is almost identical to that of wild-type rNP4-NO at pH 5.6. However, by removing the branched valine side chain, van der Waals contacts between residue 36 and Asp 30 are eliminated.

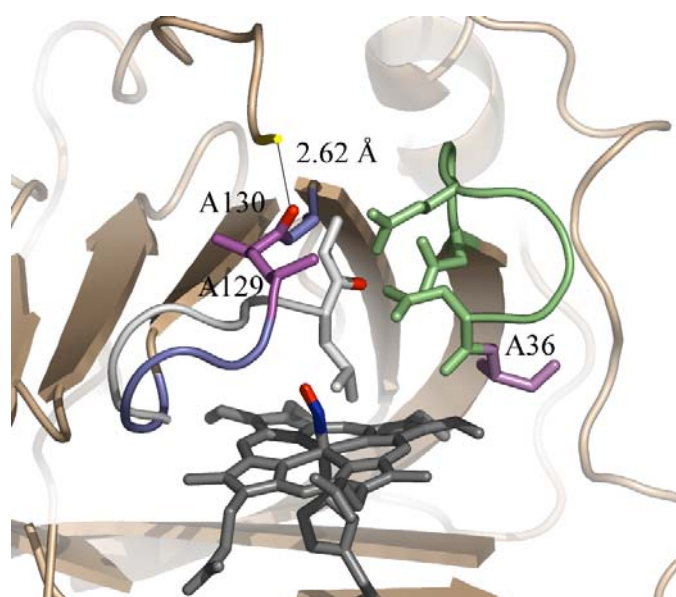


FIGURE 4.2 Open Conformation in rNP4 AAA Mutant. The AB and GH Loops that surround the heme (gray) and NO (blue/red) are in green and blue respectively. The mutated residues with associated loops are in purple. The N-terminus involved in the open conformation is in yellow. The 130-131 peptide bond that characterizes the open or closed conformation is in red. For comparison, the closed conformation of the GH Loop is in white.

Evident from the 1.0 Å structure of rNP4 AAA-NO pH 5.6 presented here, a constant, open conformation in rNP4 minimizes side chain obstruction of NO binding and release from the heme. This allows free movement of NO into and out of the binding pocket and the potential for NO to react with surrounding environmental molecules, such as oxygen. This potential reaction can occur either free in solution, or through direct reaction on the heme [113].

4.3.2. Fast phase kinetics

To test whether NO reacts with heme iron before it reacts with environmental oxygen, we used stopped-flow spectroscopy to measure NO binding to wild type and AAA mutant rNP4 proteins in the presence and absence of oxygen. Binding rates were obtained through mixing of rNP4 or rNP4 AAA with NO (produced by the NO donor DEA/NO) at defined concentrations and monitoring spectral changes. Full spectra (365-595) were recorded every millisecond using a stopped-flow device (dead time ~2 ms) attached to a rapid-scanning spectrophotometer, and kinetic rate constants (k_{obs}) were obtained by simultaneously fitting spectra through a singular value decomposition (SVD) approach as previously described [52]. The absorption spectra for all apparent species in the reaction are extracted in the SVD approach, which aids in the choice of kinetic mechanism. Both single and double exponential fits were examined. The residual errors for the fit illustrated agreement with a biphasic model in all cases. First phase kinetic rates, k_1 and k_{-1} (Figure 4.3.), were extracted using eq 1.

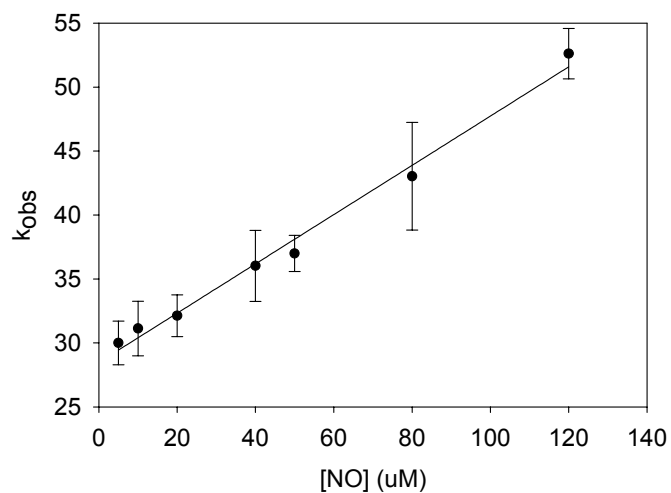


FIGURE 4.3. Extraction of First Phase Kinetic Rates. Shown is the NO concentration dependence of k_{obs} . The average and standard deviations for three measurements of k_{obs} at each NO concentration are displayed. Data for the first phase were fitted to eq 1, yielding k_1 and k_{-1} .

Table 4.2. summarizes the fast phase NO rate constants at 25 °C for wild type and AAA mutant rNP4 proteins in the presence and absence of oxygen at pH 5.0 and 8.0. As previously found, the wild-type protein displays a pH independent biphasic NO association in the absence of oxygen. The biphasic and pH independent behavior remains in the presence of oxygen. The rates for the rNP4 AAA mutant are very similar and are also pH independent. Thus, rates for both wild type and AAA mutant rNP4 proteins are unaffected by the presence of oxygen.

TABLE 4.2. Fast Phase NO Rate Constants at 25°C

	pH 5.0		pH 8.0	
	k_1^a	k_{-1}^b	k_1	k_{-1}
rNP4 (anaerobic) ^{c,d}	2.5 ± 0.6	21 ± 4	2.5 ± 0.4	15 ± 7
rNP4 (anaerobic) ^c	0.37 ± 0.06	28.6 ± 1.7	0.26 ± 0.04	24.6 ± 0.9
rNP4 (aerobic)	0.39 ± 0.02	28.5 ± 0.5	0.27 ± 0.03	23.5 ± 0.8
AAA (anaerobic) ^c	0.32 ± 0.03	30.1 ± 0.9	0.35 ± 0.07	34.1 ± 1.9
AAA (aerobic)	0.37 ± 0.04	25.0 ± 1.3	0.21 ± 0.03	34.2 ± 0.8

^aRate constant for NO association ($k_1, \mu\text{M}^{-1} \text{s}^{-1}$). Slope of association data. ^bRate constant for NO dissociation (s^{-1}). Intercept from association data. The linear kinetic fit of the rate for the fast association phase gave parameters whose standard deviations did not exceed 10 % of their values. ^cTwo replicate measurements were performed and the relative standard deviation for the rate constants was less than 10 %. ^dPublished previously [52].

The dissociation rates (k_{-1}) measured herein using DEA/NO are in agreement with previously published values. However, the association rates (k_1) from this study are internally consistent but on average five times smaller than those previously published [52]. Several reasons could account for this difference in NO association rates (k_1). (1) An error in the value for NO concentration in the previous and/or present experiments would alter estimates for k_1 . To account for the discrepancy, either the amount of NO in the previous experiment would have to be greater than reported, or the amount generated in the present experiment must be less. However, if anything, the NO gas experiment concentrations are overestimated due to chemistry involved in the NO gas tank. (2) A decomposition product of DEA/NO possibly may be inhibiting complex formation. In the absence of further data, this remains open to further investigation.

In summary, the aerobic stopped-flow data show that NO reacts with the heme iron before it reacts with the surrounding oxygen in both rNP4 and its AAA mutant. This suggests that the affinity of NO for the heme is higher than that with oxygen and that NO prefers to bind in the hydrophobic packing environment of the protein.

4.3.3. NO decay from NO-protein complex

In previous studies, NO release from the NO-protein complex was measured under anaerobic conditions using stopped-flow spectroscopy in the presence of excess histamine, which prevents the rebinding of NO to the heme [37,52]. In the current study, we examined NO-protein complex decay in the presence and absence of oxygen while allowing NO to rebind to the heme. In addition, the effects of the presence of GSH on the rate of NO-protein complex decay were examined (Figure 4.4.).

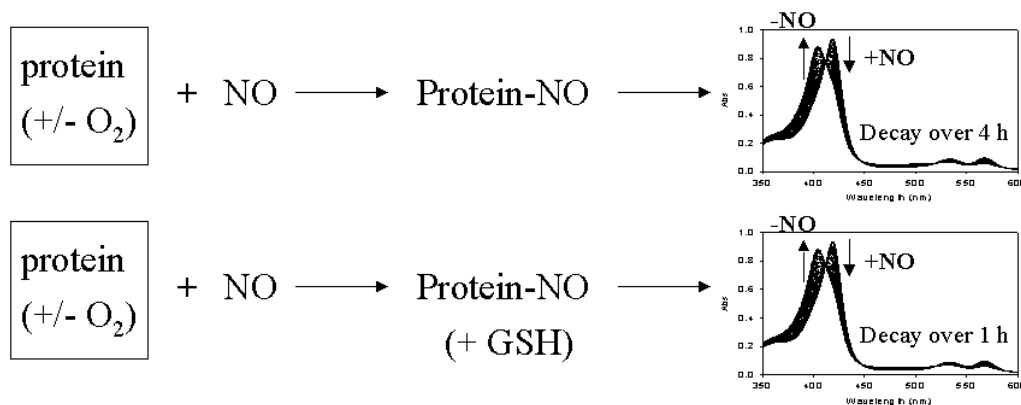


FIGURE 4.4. NO-Protein Complex Decay Experimental Design. (top) -GSH. NO produced from DEA/NO was added to aerobic or anaerobic protein. The saturated protein-NO complex (1:2) was allowed to form, and spectra were collected over a period of ~4 hours. (bottom) +GSH. The saturated protein-NO complex (1:1) was allowed to form as above followed by the addition of 1 mM GSH. Spectra were collected over a period of ~1 hour. In both experiments (-GSH and +GSH), disappearance of the 420 nm Soret peak, characteristic of the NO-protein complex, and appearance of the 404 nm Soret peak, characteristic of the unligated protein, was monitored.

NO-protein complex in the absence of GSH (-GSH). Figure 4.5 and Figure 4.6 display the UV-visible spectra monitoring the disappearance of the Soret band at 420 nm (Fe-NO) and appearance of the Soret band at 404 nm (Fe-H₂O), under aerobic and anaerobic conditions, respectively.

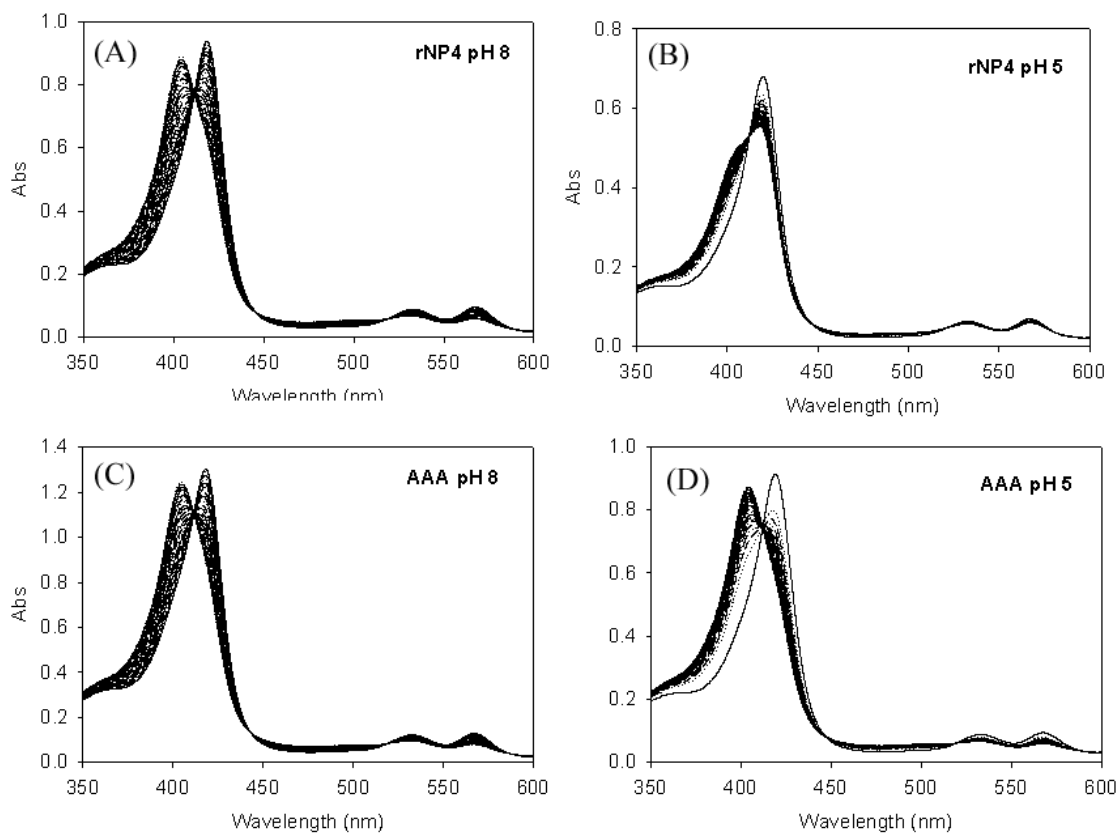


FIGURE 4.5. NO-Protein Decay Under Aerobic Conditions. UV-Visible spectra illustrating the disappearance of the Soret 420 nm band and appearance of the Soret 404 nm band for rNP4 (A-B) and rNP4 AAA (C-D). Each spectrum represents an interval of 10 minutes for 4 hours. pH is indicated on each set of spectra.

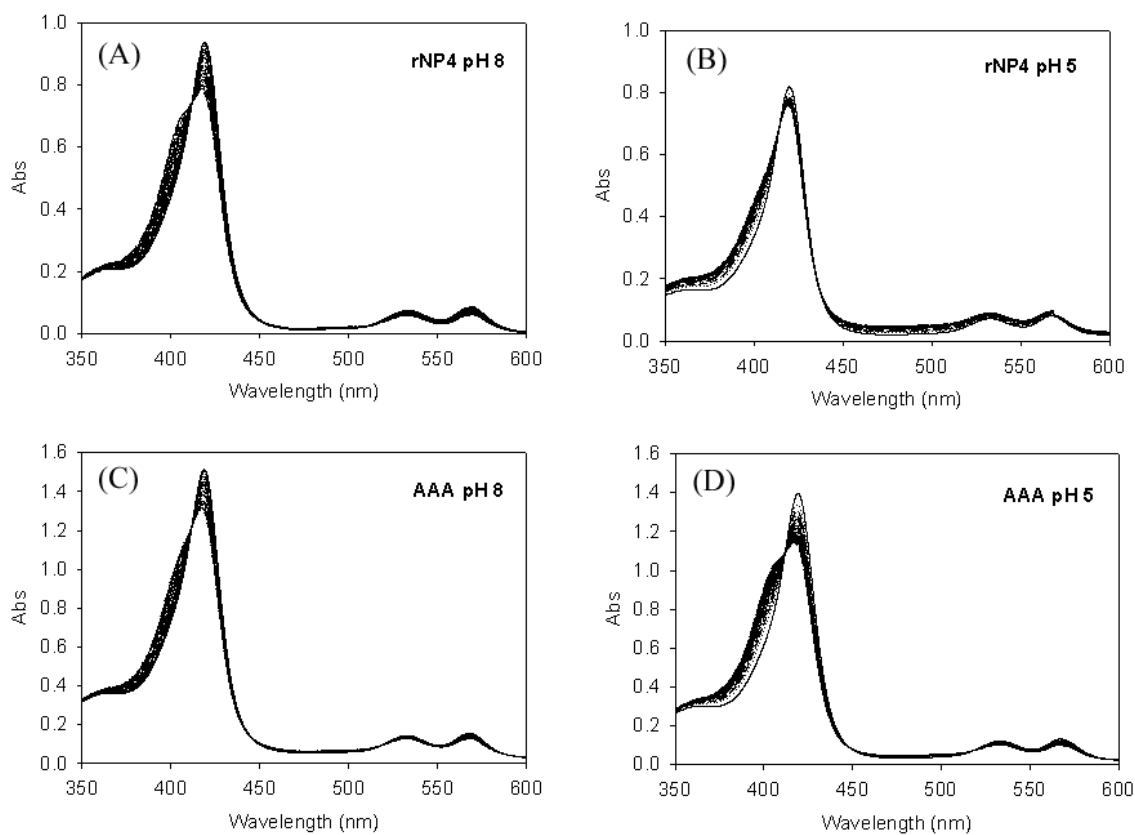


FIGURE 4.6. NO-Protein Decay Under Anaerobic Conditions. UV-Visible spectra illustrating the disappearance of the Soret 420 nm band and appearance of the Soret 404 nm band for rNP4 (A-B) and rNP4 AAA (C-D). Each spectrum represents an interval of 10 minutes over 4 hours. pH is indicated on each set of spectra.

When fit to a single exponential decay function, the solution was unstable, indicating multiple processes were occurring. Thus, an approximate half-life ($t_{1/2}$) of the NO-protein complex was obtained through spectral matching. In the case where $t_{1/2}$ was beyond the time course of the experiment, an approximate percent recovery of unligated protein at 120 minutes was obtained through spectral matching (See Materials and Methods). Table 4.3. summarizes the $t_{1/2}$ and percent recovery for rNP4 and rNP4 AAA.

The presence of oxygen accelerates decay in both rNP4 (Figure 4.5.a,b. and Figure 4.6.a,b.) and rNP4 AAA (Figure 4.5.c,d. and Figure 4.6.c,d.) regardless of pH as noted by $t_{1/2}$ and % recovery (Table 4.3.). The pH dependence of NO-protein complex decay remains for wild-type rNP4 but is abolished for the rNP4 AAA mutant in both the presence and absence of oxygen (Table 4.3.).

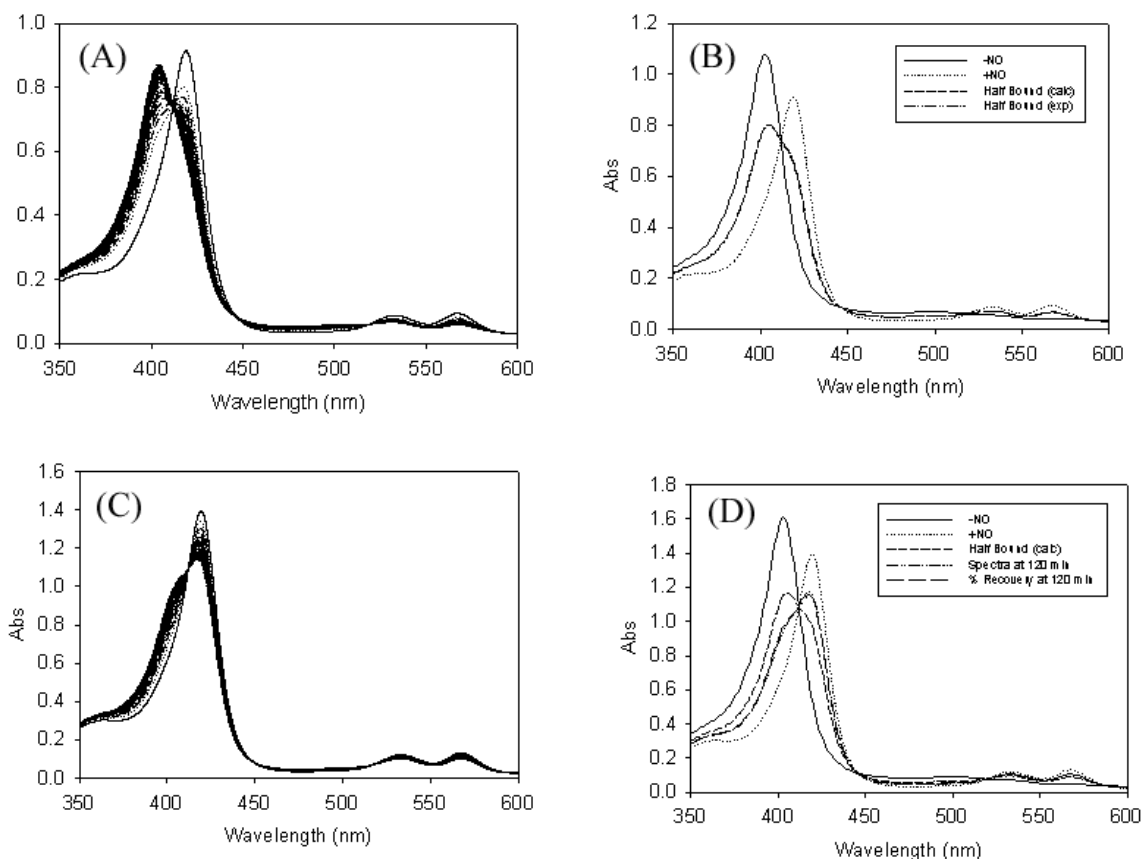


FIGURE 4.7. Spectral Matching for rNP4 AAA at pH 5. (A) Aerobic conditions allowed the NO-protein complex to decay beyond its half-bound state. (B) Calculated spectrum for the half-bound, half-unbound species (Half Bound_{calc}) was obtained by adding together the fully ligated (+NO) and fully unligated (-NO) protein spectrum and dividing by two. An approximate $t_{1/2}$ was estimated by matching an experimental spectrum (Half Bound_{exp}) to Half Bound_{calc}. (C) Anaerobic conditions did not allow the NO-protein complex to reach Half Bound_{calc}. (D) An approximate percent recovery of the unligated protein was estimated by fitting the spectrum at 120 min to a percentage of the fully unligated spectrum (-NO). In this case, ~30% recovery of the unligated protein has occurred by 120 min.

 TABLE 4.3. NO-Protein Complex Decay

	$t_{1/2}$ (% recovery) ^a	
	+O ₂	-O ₂
<hr/>		
-GSH		
rNP4 pH 8	202	>200 (~20%)
AAA pH 8	98	>200 (~20%)
rNP4 pH 5	>200 (~30%)	>200 (~10%)
AAA pH 5	90	>200 (~30%)
<hr/>		
+GSH		
rNP4 pH 8	31	>60 (~40%)
AAA pH 8	33	30 (~50%)
rNP4 pH 5	>60 (~30%)	>60 (~20%)
AAA pH 5	44	>60 (~40%)

^aApproximate half life (min). An approximate percent recovery of unligated protein at 120 minutes (-GSH) and 30 minutes (+GSH) is reported in the case where $t_{1/2}$ was beyond the time course of the experiment.

NO-protein complex in the presence of GSH (+GSH). Glutathione is a thiol-containing tripeptide (γ -Glu-Cys-Gly) that is naturally present in all cells as well as blood plasma of the victim at concentrations from \sim 1-10 mM. Reactions between glutathione and NO have been the subject of many recent studies [114] and have been suggested to speed decay of the soluble guanylate cyclase Fe-NO complex [115]. To test the effect of GSH on NO-protein complex decay, 1 mM GSH was added to a saturated NO-protein complex and disappearance of the 420 Soret and appearance of the 404 Soret was monitored for \sim 1 hour (Figure 4.4.). Figure 4.8 and Figure 4.9 display the UV-visible spectra that monitor the disappearance of the Soret peak at 420 nm and the appearance of the Soret peak at 404 nm under aerobic and anaerobic conditions respectively. Like the experiments in the absence of GSH, the fit of the data to a single exponential decay function was unstable. Thus, $t_{1/2}$ and percent recovery at 30 minutes was obtained (Table 4.3.) through spectral matching (Figure 4.7.).

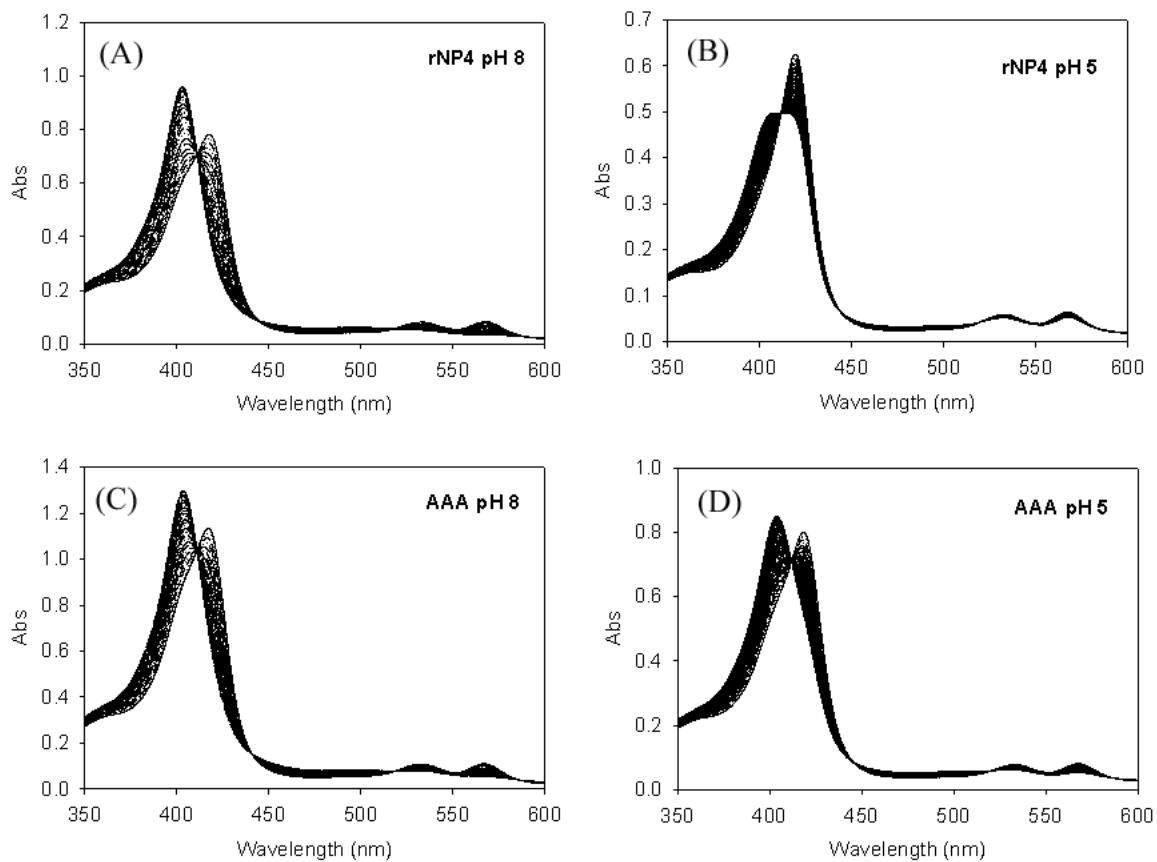


FIGURE 4.8. NO-Protein Decay Under Aerobic Conditions (+GSH). UV-Visible spectra illustrating the disappearance of the Soret 420 nm band and appearance of the Soret 404 nm band for rNP4 (A-B) and rNP4 AAA (C-D). Each spectrum represents an interval of 1 minute for 1 hour. pH is indicated on each set of spectra.

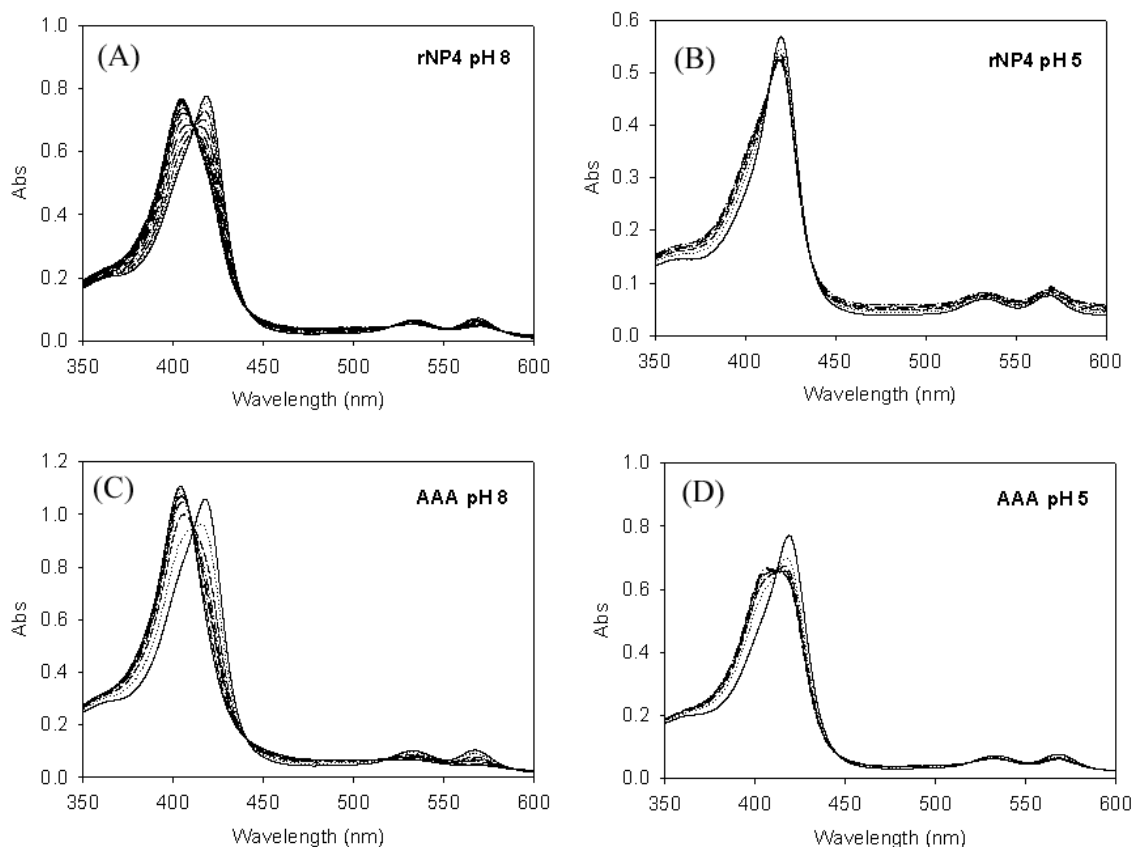
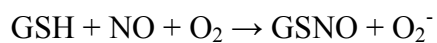


FIGURE 4.9. NO-Protein Decay Under Anaerobic Conditions (+GSH). UV-Visible spectra illustrating the disappearance of the Soret 420 nm band and appearance of the Soret 404 nm band for rNP4 (A-B) and rNP4 AAA (C-D). pH is indicated on each set of spectra. In B and D each spectrum represents an interval of 10 min. In A, each spectrum represents an interval of 2 min. In C, the first ten minutes of the experiment are represented in 2 minutes intervals while the rest of the experiment is in intervals of 10 minutes.

The NO-protein complex decay is accelerated by the presence of GSH in all cases as compared to the absence of GSH. In addition, the decay rates are faster in the presence of oxygen. This suggests that the destroyed loops are allowing GSH to somehow react with NO and that the presence of oxygen may also contribute to GSH-accelerated decay. Under aerobic conditions, GSH and NO can possibly form GSNO or another product. One possible mechanism for this is that when NO is released from the protein it can react with GSH to form GSNO, which is then further oxidized by oxygen yielding O₂, or by GSSG, yielding [GSSG]. A second mechanism is that GSH directly interacts with NO while bound to the ferric rNP4 heme iron. This would result in a reduction of the iron to the ferrous state and GSNO formation. GSNO may then react with another GSH to form GSSG and HNO. There has been no reported evidence that GSH directly reacts with NO while bound to heme under biological conditions (Dr. Katrina Miranda, personal communication [116]).

Allowing NO to rebind to heme stabilizes NO-protein complex against decay. Previous NO dissociation experiments prevented the rebinding of NO to the heme by displacing NO with histamine [37,52]. Under these conditions, the approximate half-life for the NO-protein complex is 0.007 min and 0.3 min for wild-type rNP4 at pH 8 and pH 5.6, respectively. In contrast, when NO is allowed to rebind to the heme, NO-protein complex decay is hundreds of times slower. This suggests that the closed-loop conformation protects NO from other reactions, since NO consumption is faster in the mutant protein at all pH values, and in the wild type at pH 8.

The most likely mechanism for rNP4-NO decay is that on NO release from the protein, the free NO molecule reacts with oxygen, GSH, or escapes from the cuvette. One possible mechanism for this would be



but many other possible mechanisms exist. Alternatively, it is possible that oxygen or GSH could react directly with Fe-NO, leading to GSNO or some other oxidation product and reduced heme. However, no evidence was seen for ferrous nitrophorin in the experiment.

CHAPTER 5

RESEARCH SUMMARY AND FUTURE DIRECTIONS

This dissertation explored the functional implications of the rNP4 structure. I experimentally tested and discussed beta-barrel rigidity using an apo structure of rNP4, explored heme distortion using distal pocket (Leu 123 and Leu 133) and heme mutants, and investigated ligand protection using a loop (V36, D129, L130) mutant of rNP4. This final chapter summarizes the experimental work presented and discusses possible future work on the system.

5.1. Barrel rigidity

Chapter 2 discussed beta-barrel rigidity using an apo structure of rNP4. In summary, the beta-barrel of rNP4 remains a rigid structure in the absence of its heme cofactor and is similar to that of holo rNP4. Other apo proteins retain similar structure to their respective holo protein supporting this result as a general feature of lipocalins. Apo rNP4 retains a conserved tryptophan-arginine interaction located at the “closed-end” of the beta-barrel. A mutational study involving Trp 23 and/or Arg 139 in rNP4 would be of interest to examine whether this interaction is crucial for maintaining a stable beta-barrel in the absence of heme. The initial experimental studies examining the role of the conserved Trp and Arg in structure and stability was described by Keith Brew’s laboratory using human serum retinol-binding protein [88]. In this model for the

lipocalin superfamily, substitutions of three different amino acids for Trp 24 or replacement of Arg 139, the conserved residue that interacts with Trp 24, lead to large losses in stability (thermal and chemical-induced equilibrium unfolding) and lower yields of native protein generated by *in vitro* folding (circular dichroism). The results support the idea that conserved residues in functionally divergent lipocalin homologs have roles in stabilizing the native relative to misfolded or unfolded structures. Brew and Greene have also suggested this region to play a pivotal role in folding [117,118]. rNP4 also contains two disulfide bonds that may contribute to the stability of the barrel. Studies involving rNP4 with reduced or mutated disulfides bonds would be of interest in this regard.

In addition, it was found that the pH dependence for loop closure is an inherent feature of the protein itself. The findings reported for the apo structure of rNP4 will act as a cornerstone to developing rNP4 into an NO sensor molecule that can be used in the detection of NO in a system.

5.2. Heme distortion

Heme distortion in rNP4 was explored using alterations to both protein and heme cofactor in Chapter 3 of this dissertation. In summary, the heme cofactor is more easily distorted from planarity than we expected at the onset of this work. In all altered proteins, local changes to the heme are seen at the point of alteration and are evident from anisotropy plots of heme atoms as well as detailed deformation calculations represented

by formal core diagrams. Classical normal mode distortions involving multiple atoms change to a lesser degree, highlighting the softness of the macrocycle. Mutations to the protein create additional room in the heme cavity allowing NO to rotate to a new axis and the revolving motion of the NO oxygen to differ from that of wild type. Alterations to the macrocycle leads to a pivoting of the macrocycle to alleviate new steric contacts, and in the case of the NO complex, changed the revolving motion of NO. The rNP4 protein has evolved a unique way to have surrounding contacts, as well as electronic interactions between ligand and heme, contribute to distortion. The combined local contributions may prove important for tuning heme to biological function.

In this study we have changed distortion in rNP4 hemes, but have the properties of the heme changed? Because this study focused on how heme distortion arises, further studies investigating kinetic properties of NO binding and release, ligand affinity, and redox potential are in order to connect change in distortion to biological function. Furthermore, studies involving different metal porphyrins, for example zinc, may give additional insight into porphyrin distortion.

5.3. Ligand protection and nitric oxide interactions with heme

The mechanism in which rNP4 protects its reactive ligand, NO, was investigated in Chapter 4 of this dissertation. In summary, the NO ligand in rNP4 is protected by flexible loops and the barrel cavity. A loop mutant that was unable to collapse, as well as wild-type protein, showed that the oxygen reaction with NO is much slower than heme

NO binding, leading to extensive protection. NO-protein complex decay was accelerated by the presence of oxygen and/or GSH suggesting that NO, oxygen and GSH are interacting in some yet-to-be determined way. In addition, when NO is allowed to rebind to the heme, NO-protein complex decay is hundreds of times slower than when NO is not allowed to rebind. All together, these data suggest that NO binds to the heme iron and then dissociates and associates hundreds of times before reacting with any surrounding compound.

APPENDIX A
ABBREVIATIONS

AB Loop – loops connecting beta-strand A and B, etc. Also known as the omega loop.

Analog 1 – Fe(III) deuteroporphyrin IX; vinyl groups to hydrogen's

Analog 2 – Fe(III) Fe(III) 2,4 dimethyl deuteroporphyrin IX; vinyl groups to methyl's

Apo rNP4 – rNP4 absent of heme cofactor

APS – Advanced Photon Source at Argonne National Laboratory

β lg – beta-lactoglobulin

DEA/NO – diethylamine NONOate

ESRF – European Synchrotron Radiation Facility

FABP – Fatty acid binding protein

FCD- Formal Core Diagrams

GSH – Glutathione, reduced

Holo rNP4 – rNP4 containing heme cofactor

NH₃ – ammonia

NMR – Nuclear Magnetic Resonance Spectroscopy

NO – nitric oxide

Np-Fe – nitrogen-iron bond in heme

NPs – nitroporins

NSD – Normal Coordinate Structural Decomposition

PDB – Protein Data Bank

RBP – retinol binding protein

RMSD – root mean square deviation

rNP1-7 – *Rhodnius prolixus* nitrophorin 1-7

rNP4 AAA – mutant of rNP4 V36A/D129A/L130A

APPENDIX B

CRYSTAL GROWTH AND PREPARATION; BEAMLINER INFORMATION

PDB	Crystal Growth ^a				Crystal Preparation ^b	
	Precipitant	pH	Ratio ^c	Seed ^d	Cryoprotectant ^f	NO Treatment ^g
Apo	2.80 M AS 100 mM sodium citrate	5.6	2:2	yes ^e	3.20 M AS, pH 5.6	N/A
2ASZ	3.5 M AP	7.5	2:2	no	N/A	N/A
2AT0	2.65 M AP 100 mM sodium citrate	7.5	7:7	yes	3.95 M AP, pH 5.6 100 mM sodium citrate	2
2AT3	2.80 M AP 100 mM cacodylate 20 mM imidazole	7.0	1:2	no	3.2 M AP, pH 5.6	N/A
2AT4	2.8 M AP	7.3	2:2	no	3.2 M AP, pH 7.5	N/A
2AT5	2.8 M AP	7.3	2:2	no	3.2 M AP, pH 5.6	1
2AT6	2.8 M AP	7.3	2:2	no	3.2 M AP, pH 5.6	N/A
2AT7	2.6 M AP	7.5	4:4	yes	3.5 M AP, pH 7.5	N/A
2AT8	2.8 M AP	7.5	2:2	no	3.2 M AP, pH 5.6	1
AAA	2.2 M AP 100 mM tris	7.5	2:2	yes	3.2 M AP, pH 5.6	1

^aAll crystals were grown at room temperature (~25 °C) using the hanging drop method. AP and AS are ammonium phosphate and ammonium sulfate respectively. ^bAll crystals were flash frozen in liquid nitrogen for data collection. ^cProtein to precipitant ratio in drop. ^dProtein drop seeded with previously existing crystals. ^eFor the apo protein only, drop seeded at ~24 hours and crystals appeared in ~3 weeks. ^fCrystals transferred and equilibrated for 15min-2hr. ^gNO complexes obtained by equilibration (15min-2hr) of a single crystal in cryoprotectant solution saturated with argon followed by: (1) transferring and soaking for 30 minutes in an identical cryoprotectant solution saturated with gaseous NO or (2) addition of 1 mM DEA/NO (yields 2 mM NO) and allowing to sit for 10 min. The generation of NO by DEA/NO was observed by the presence of bubbles and a change in color from brown to red, consistent with nitrosylation, was observed under all soaking conditions. ^hStructure to be deposited in PDB.

TABLE B.2. Beam Line Information

PDB	X-Ray Source ^a	Beam line	λ (Å)	Detector	Date
Apo ^c	BNL	X29	0.80	ADSC Quantum 315	11/05
2ASZ	APS	14-BMD	0.90	Quantum 4 CCD	04/02
2AT0	SSRL-R ^b	9-2	0.98	Mar 325 CCD	07/05
2AT3	SSRL	9-1	0.75	Mar 345	02/02
2AT4	APS	14-BMC	0.90	Quantum 4 CCD	07/03
2AT5	APS	14-BMC	0.90	Quantum 4 CCD	07/03
2AT6	APS	14-BMC	0.90	Quantum 4 CCD	07/03
2AT7	APS	14-BMC	0.90	Q315	02/05
2AT8	APS	14-BMC	0.90	Q315	02/05
AAA ^c	APS	14-BMD	0.90	Quantum 4 CCD	02/05

^aBNL Brookhaven National Laboratory (Upton, New York); APS Advanced Photon Source at Argonne National Laboratory (Argonne, Illinois); SSRL Stanford Synchrotron Radiation Laboratory (Palo Alto, California). ^bData collected remotely; SSRL beam line controlled at University of Arizona (Tucson, Arizona). ^cStructure to be deposited in PDB.

APPENDIX C

FORMAL CORE DIAGRAMS FOR HEME ANALOG STRUCTURES

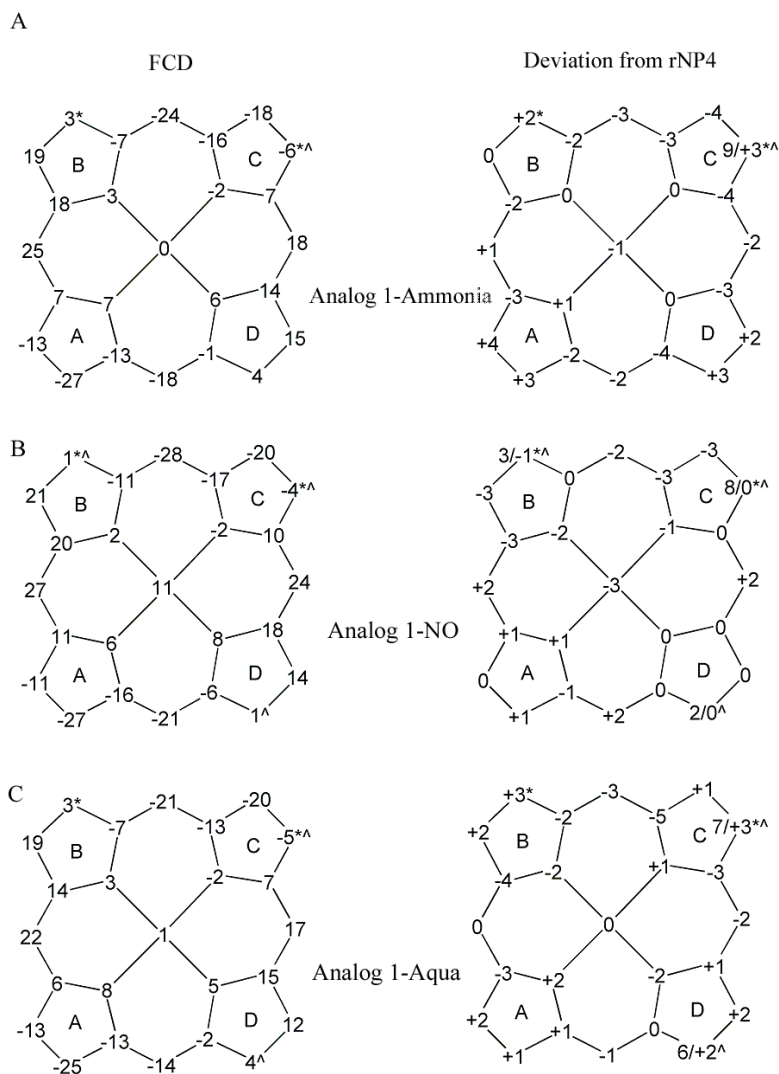


FIGURE C.1. Atomic Deviations from Planarity for Analog 1 Complexes. Ammonia (A), NO (B), and aqua (C) complexes are shown. See Figure 3.4. for definitions. The starred atoms are those at the vinyl substituent alteration. For atoms that have switched signs relative to wild type (indicated by a carrot), two values are indicated in the right diagram. The first number indicates the total absolute shift while the second number indicates the shift in planarity as defined in Figure 3.4..

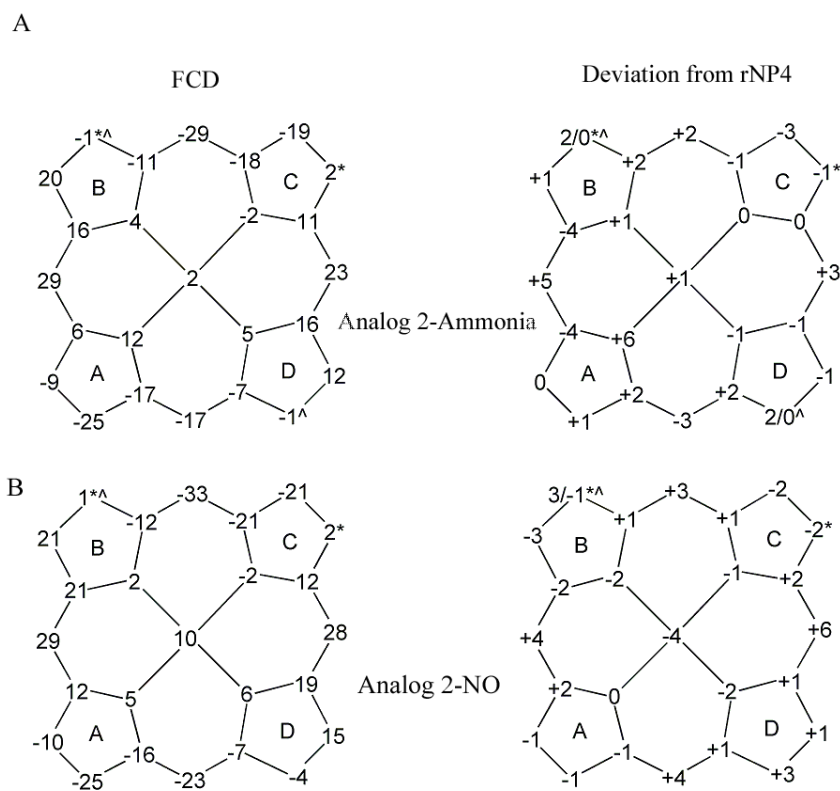


FIGURE C.2. Atomic Deviations from Planarity for Analog 2 Complexes. Ammonia (A) and NO (B) complexes are shown. See Figure 3.4. and Figure C.1. for definitions.

APPENDIX D

TEACHING AT THE COLLEGE LEVEL: A SIDE DISH

D.1. Introduction

In addition to scientific research at the bench, teaching has been a considerable part of my graduate career. I have completed a teaching certificate for college teaching and had the honor of being part of the undergraduate Biochemistry Honors course (BIOC 462aH) for five (5) consecutive fall semesters. In this chapter, I will highlight my teaching experiences which will include the Certificate in College Teaching, the Wakonse Conference on College Teaching, curriculum development for BIOC 462aH, and my teaching philosophy.

D.2. Pedagogical Advancements

D.2.1. Certificate in college teaching

The Certificate in College Teaching Program was designed by the Graduate College and the University teaching Center at the University of Arizona to give interested graduate students the preparation needed to become outstanding teachers. The program consists of a structured series of courses that provide foundational information and encourages development of skills necessary to teach at the college level. To earn the

certificate I partook in one course from each of the following categories in consecutive order:

- A. College-level Teaching
- B. Ethics and Professional Development
- C. Practicum in College Level Teaching

For category A, a course entitled ‘Workshop of Teaching at the College Level’ was taken with Dr. James Knight. This course dealt with the practical application of teaching/learning theories at the college level as they relate to instructional methodologies, strategies and planning. Such things included instructional objectives, content organization, and assessment of learning experiences. The workshop also involved the exchange of ideas and focused on practical methods, skills, and principles.

For category B, a course entitled ‘Survival Skills and Ethics’ with Dr. Cindy Rankin and Dr. Jenny Hoit was completed. The course was a combination of lecture presentations, class and panel discussions, and a variety of in-class activities. Topics discussed were those such as the art and science of teaching, mentoring, research integrity, effective speaking and writing, grants and grantspersonship, career options, among others. Discussion of ethical issues and resources was integrated across topics.

The third and final category involved supervised teaching at the college level. To fulfill the practicum component, a molecular modeling and web design section of an upper division honors biochemistry course consisting of approximately 25 students was developed and taught in the Department of Biochemistry and Molecular Biophysics at the

University of Arizona. This is to be discussed in Section D.2.2. My teaching mentor from the University Teaching Center was Randi Lydum.

The Certificate in College Teaching Program was beneficial to my graduate career as well as for the future. I was provided the opportunity to strengthen my teaching tactics as well as given direction on things one must do beyond the interactions with students. For instance, writing a syllabus or learning objectives was covered. Though tasks like these may seem simple, many professors have not had any formal training and thus tasks as such may be daunting. I do believe that ‘learning how to teach’ comes from ‘teaching itself’. However, it was beneficial to learn instructional methodologies, strategies and planning.

D.2.2. Molecular graphics curriculum development and instruction in Biochemistry Honors 462aH

I have had the honor of being part of the undergraduate Biochemistry Honors course (BIOC 462aH) for five (5) consecutive falls semesters (2002-2006). Over the years I have had the pleasure to work with Drs. Megan McEvoy, Carol Dieckmann, Vahe Bandarian, Matt Cordes, and most recently Nancy Horton. The course enrolls approximately 25 junior/senior students a year and covers material on equilibrium, thermodynamics, kinetics, protein composition, structure and function, and nucleic acids. Beyond the roll and responsibilities of a teaching assistant, I re-designed and developed the class website into a much more user-friendly format. To fulfill the practicum

component for the Certificate in College Teaching, the Fall of 2003 consisted of curriculum development and instruction of the molecular graphics component of the course. I have continued with this instruction for the Fall 2004 and Fall 2006 semesters. Dr. Matt Cordes instructed the section for the Fall 2005 semester modifying the curriculum for improvement.

The distinguishing feature between regular and honors Biochemistry 462a is that one of the five course hours is devoted to molecular graphics and other computer-aided exercises. Students participate in weekly computer session in order to develop tools for an end-of-semester project using primary biochemical literature and molecular graphics programs such as RasMol or Swiss PDB Viewer. The goal of the project was three fold: (1) to integrate existing knowledge about the structure and function of a protein or nucleic acid in sufficient detail to be able to design theoretical experiments that will further reveal how the molecule works; (2) to develop a scholarly paper and (3) to develop a presentation to be given orally at the end of the semester that included an annotated molecular graphics script designed in RasMol.

For the Certificate I taught (5) lectures during the Fall 2003 semester. All were set up as tutorials, but I lead students through the lessons using the computer and projector in the computer lab. The tutorial format was useful for students so that they could re-work through the lesson on their own later if needed/desired. Two lessons were given on the graphics program RasMol. One lesson was an introduction while the second lesson was on more advanced aspects of this program. A third session was dedicated to an in-class practical assignment that encompassed the skills learned in the first two

lessons. This assignment involved the making of novel RasMol scripts. Next, two lessons on the use of the Swiss PDB Viewer molecular graphics program Deep View were given. The first was an introduction and the second incorporated a mini lecture on molecular symmetry, ligand binding, and introducing mutation. The fifth lesson was on how to use the program Dreamweaver to make a simple web page. Each student was required to make a simple web page about his or her individual projects. I also implemented a lesson developed by Dr. Carol Dieckmann using the kinetic simulator program KinTek Sim that correlated with the in-class kinetic enzyme lectures.

In the subsequent semesters I taught the section, I modified and implemented lessons on PubMed and the Protein Data Bank as well as developed a series on bioinformatics. In the current semester, Fall 2006, I gave an introduction to the concepts of the lesson and then allowed the students to work through the tutorials at their own pace while I was available to answer their questions. I found this technique more efficient as I could individualize my efforts to each student.

In addition to the graphics component of the course, I gave an in-class lecture on solving structures by X-ray crystallography. This lecture covered methods and theory from purifying proteins on through refining and publishing structures.

I have thoroughly enjoyed my experience teaching as well as working as a team to evaluate and assess students.

D.2.3. The Wakonse Conference on college teaching

The Wakonse Conference on College Teaching brings together faculty and teaching/ learning professionals from Arizona's postsecondary institutions who recognize and are devoted to the inspirational aspect of the teaching and learning process. Wakonse is an organization of individuals dedicated to promoting and sharing with colleagues the excitement and satisfaction of teaching in higher education. The purpose is to take everyone away from campus, from their phones, from their offices and professional obligations, and engage in scholarly exchange. The conference consisted of four days of workshop activities exploring teaching through highly interactive large and small group presentations as well as discussion groups and hands-on experiential sessions. There were many informal opportunities for support and networking to occur as participants became acquainted with each other and shared their talents and experiences. In addition, Wakonse Fellows themselves hosted sessions beyond the scope of the classroom in an area of their extracurricular expertise or choice. For example, I lead a morning yoga class each of the four mornings of the conference.

The conference is like no other conference I have ever been to, including other teaching conferences. It was held in Payson, Arizona and similar to the BMCB Retreat, we stayed in cabins. However, the difference was that there was less structure and more freedom to choose what activities you wanted to do to enhance your teaching experiences. I enjoyed the conference and would gladly sponsor a fellow colleague for a future conference.

D.2.4. Biological science instructors journal club

The Biological Sciences Instructor's Journal club was implemented in 2005 by current graduate students with an interest in teaching at the undergraduate or graduate level. We believed that the venue needed to be created in order to accomplish the following three objectives:

1. exchange scholarly literature
2. discuss contemporary issues for college-level biology instructors and/or TAs
3. develop ideas for practical and effective teaching methodologies

Meetings are held approximately every other week and rotate through these three themes, with some general issues. The journal club has been beneficial because I have been exposed to teaching literature that was novel to my library. The exposure to this literature, as well as the literature with which I am already familiar, will guide me in my future endeavors.

D.3. My Teaching Philosophy

What time is it? When is this class over? What do I have to do next? Where do I have to go? O' my, is that assignment already due tomorrow? Can't sleep...as I lay there my mind races about the next day, week, month...am I going to make it? There's my morning alarm to wake...What time is it?...

I've been there; all teachers/professors have been there. 'There' is called a student. Answering three questions can sum up my philosophy of teaching:

1. What is it like to be a student?
2. How do I want to be taught?
3. What do I want to learn?

Fortunately, these questions are easy for me to answer and they stem from the word that cornerstones my philosophy: EMPATHY.

E. Enthusiasm (& Motivation): This is a large component of my teaching as well as what has inspired me by current colleagues and past professors. Without enthusiasm and creativity on a topic you cannot capture your student's attention and thus stimulate their own internal enthusiasm and creativity. I quickly learned that being able to captivate your audience was imperative if you wanted them to learn. I believe students can learn if I can motivate them to do so and enthusiasm is a way of motivation.

M. Mentor: Teaching in general has evolved from being primarily teacher-centered to being primarily student-centered. Here students take greater responsibility for their own learning and my role in the classroom moves from 'sage on the stage' to 'guide on the side' and thus allows students to take ownership of their learning. The following figure sums up my concept of a mentor and is described below (Figure D.1).

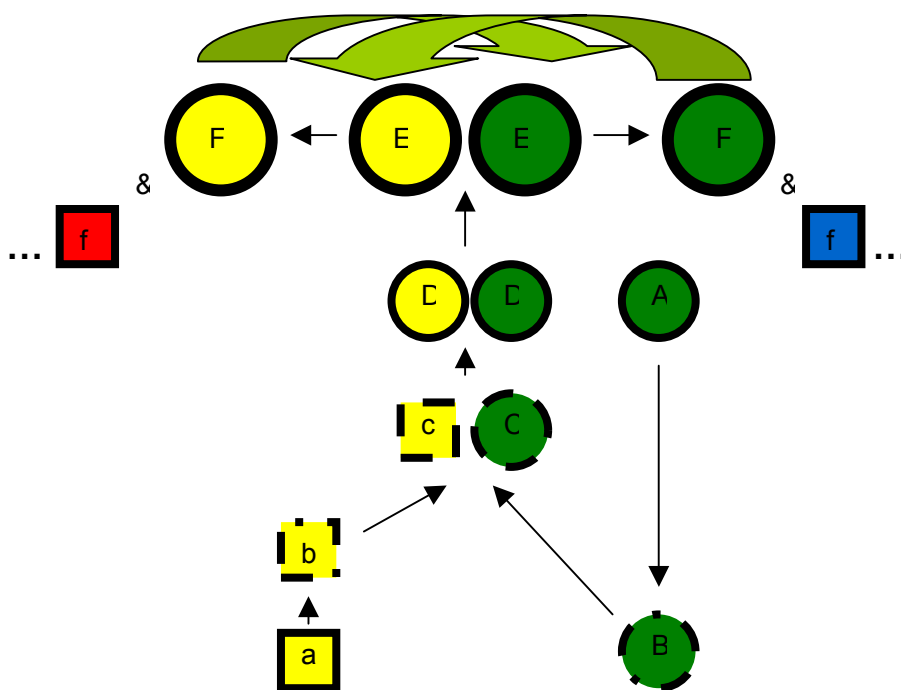


FIGURE D.1. Concept of A Mentor. See text for details.

A teacher (green) is the foundation of a student's (yellow) learning and acts as a corner stone to build a student's interest, knowledge and skill. The 'Job of the Teacher' is to *guide* not to command and the 'Job of the Teacher & Student' together is to learn something everyday.

The model begins at point 'A' and 'a' for the teacher and student respectively. Here the teacher is portrayed as a pliable circle with a rigid black border signifying what they solidly know to this point. (Note that the Teacher begins at a level higher than the student.) The student is portrayed as a rigid square also with a rigid black border signifying what they solidly know to this point. The teacher transitions to point 'B' where they open their boundaries (denoted by a highly dashed line) and begin to understand their student's current and potential knowledge and skill level. Some ways one can do this is to reword vocabulary to bring your student to the desired level, accommodate your student's learning style and adapt to your student's needs. At the same time, the student is also transitioning to point 'b' where they are breaking down their barriers and becoming open and aware of new ideas. Together, they reach point 'C' and 'c' respectively. This is an important point in the journey. It is here that the student and teacher reach a common level and their boundaries begin to close again. During the transition to point 'D' the student is transformed into a circle and is now labeled with a capital letter. This signifies the student transitioning into a person that will soon become an independent mentor. Together they will continue to grow together (point 'E') until finally the student is ready to take on their own student (point 'yellow F' and 'red f'), the mentor takes on another beginning student (point 'green F' and 'blue f') and the process

begins once again. During this new mentorship journey, the original student and original mentor are in constant contact with each other to exchange scholarly information and advice (light-green arrows). Learning never ends by either the student or the teacher and constant reflection and reiteration are needed for improvement.

Two things are to note in this model: (1) Although the student is ultimately transitioning into a mentor (represented by the transition from a square to a circle), they keep their own identity throughout the entire process (denoted by the yellow color). (2) At first glance the circles and squares up to point 'C' and 'c' respectively look to be the same size. If you were to superimpose the two shapes, you would find that indeed the four points of the square would intersect with the boundary of the circle and thus they are the 'same size'. However, the circle would be slightly larger in respect to surface area due to the extra area that is formed by the arc between two corners of the square. This extra surface area represents anticipation of a student's questions, mistakes, etc. In other words, up to this point the teacher may be 'in the trenches' learning right along with the students, but they are still always that one-step ahead.

P. Passion: One may say that this is the same as enthusiasm. However, I will beg to differ. Passion is an internal drive that is conveyed to the surface when speaking/writing on a topic which you love and/or admire. Yes, one can still be enthusiastic while being passionate but one can be enthusiastic without passion on a topic they care little about or know little of.

A. Articulate: When I talk of articulation it can be drawn back to clarity: clarity in respect to expectations, both of myself as a teacher and of my students, to what I want from them. This refers to both speaking and writing and also encompasses consistency. For example, when writing handouts or speaking of information on a topic that has connected lessons, one must stick to the same nomenclature or make it clear that ‘X’ can also be known as ‘Y’. This tends to become a major place of confusion for young learning scientists and is something that needs to have close attention paid to.

T. Teach: I care about a student’s learning. I am here for a purpose. The student may not know now or later or ever...but I am committed to their learning. If they don’t want that, I wish them to find another section.

H. Help: In my mind, learning is a permanent change in behavior and as a teacher, I am here to *help* them in their journey. If you asked a student to rank three aspects of a course - *content, teacher and learning* – they would be most often be ranked in that respective order. Content, content, content. Of course there is a certain amount of content that needs to be conveyed to the students. However, if one goes too fast over content just in order to ‘cover the material’ in the allotted time, a student may not grasp the fundamentals you are trying to instill. **Here one needs to distill the content.** In other words, help the student realize what is important and what is not.

There are four pedagogical questions I think of when designing instruction that can help with this. *What do you want students to know when they leave for the day?*

Forever? One must keep in mind here that acquiring new knowledge depends on existing knowledge and how that knowledge is organized in turn determines what and how new knowledge will be acquired. The knowledge acquired from content must in some way be conveyed to skill: *What do you want your students to do with what they know?* Is it simply to regurgitate on the next test or final? Or do you want them to take that knowledge and apply it to future courses, careers, or life. Be honest, have you ever taken a course where you couldn't pass the final if you retook it 6 weeks later? Of course you have, as have I. Of course, in order for this relay of information to occur, one must be articulate, clear and concise with the information. Next I ask: *Who do you want your student to be?* For me, I want them to be excited and enthusiastic about a discipline. I want them to be clear and confident of knowledge and skill on paper, verbally and physically. I feel it is most important that they leave my classroom having the necessary confidence and skills to seek answers to questions they may not know and to realize that learning is a life-long process, not one that stops after graduation.

All of the answers to these questions help formulate the answer to the final and fourth question: *What strategies do you use to get them to learn and how do you assess what they finally know?* This is where a teacher must be flexible and creative. I try to use a variety of teaching strategies to meet the needs of the different learning styles my students may use and assess in the same way I state my objectives.

Help doesn't stop at distillation of material. It extends into making the student **aware of local and remote resources and opportunities, as well as physical one-on-one or group help on lecture or laboratory material.**

Y. Youthfulness: A teacher must stay his/her own student. They must stay up-to-date on scientific literature as well as teaching literature in general and in the specific discipline. They must keep lessons new and fresh and not use the same old yellow pieces of paper that still do not have the corrections to the problems student's caught 5 years ago. I am always exploring ways in which I can improve pedagogy so that students can both enhance their understanding of scientific concepts and learn to appreciate how science impacts their lives. Good teachers should be committed to a continuing process of self-reflection and refinement. Reflective teachers generally accept that their teaching practices, and the motives for those practices, should be critically questioned and continually improved. Critical reflection is not limited to teaching techniques, but includes our attitudes, beliefs, behaviors, and perceptions. True excellence in the classroom and the laboratory develops as a result of this evolutionary process and through hard work and dedication to the profession.

In addition to staying youthful as a teacher, one must remember to also stay youthful as a person. Take care of yourself mentally and physically in order to continue a pursuit of excellence and not to get burnt out over the years.

By no means am I an expert in all of the areas outlined above by EMPATHY. However, I feel that I am on the right track. I am certainly a person dedicated to the pursuit of excellence and my standards are set high. Although students notice that I work very hard at my craft and that my expectations are high, they seem to like me personally and find it easy to relate with me. I think that I am a very approachable by students. They are

willing to ask questions and seek my help if they are having difficulty understanding the material. I think that they realize that I genuinely want them to succeed and that I am willing to help them achieve academic success. Improving my effectiveness as a teacher continues to be my highest priority and I take advantage of the professional development activities provided locally and nationally. My association with professional organizations such as the American Chemical Society, the American Association for the Advancement of Science and the Protein Society provide me the opportunity to keep current in my discipline and discover new ways to improve my teaching effectiveness.

The students know that I will do whatever it takes to help them achieve success. However, true student success and excellence is not measured by what I do alone. Students play an integral role in the pursuit of excellence. They are the ones that provide the necessary feedback to help me improve as a teacher. Without this information, the requisite changes would never occur. Therefore, my success completely depends on the sincere and honest evaluations by students. I have found this process to be extremely beneficial in helping me discover ‘what works’ in teaching.

REFERENCES

1. Flower, D.R., *Experimentally determined lipocalin structures*. Biochim Biophys Acta, 2000. **1482**(1-2): p. 46-56.
2. Palmer, A.H., *Crystallisation of bovine beta-lactoglobulin*. J Biol Chem, 1934. **104**: p. 359-361.
3. Maddox, B., *Rosalind Franklin the Dark Lady of DNA*. 2002, New York: HarperCollins Publishers.
4. Green, D.W., et al., *Structure of bovine beta-lactoglobulin at 6A resolution*. J Mol Biol, 1979. **131**(2): p. 375-97.
5. Aschaffenburg, R., D.W. Green, and R.M. Simmons, *Crystal forms of Beta-lactoglobulin*. J Mol Biol, 1965. **13**(1): p. 194-201.
6. Aschaffenburg, R., D.W. Green, and A.C. North, *Crystallography of the beta-lactoglobulins of cows' milk*. Biochim Biophys Acta, 1956. **21**(3): p. 583-5.
7. Bolognesi, M., et al., *Preliminary crystallographic data on buffalo beta-lactoglobulin*. J Mol Biol, 1979. **131**(2): p. 411-3.
8. Kumar, R., et al., *Purification, crystallization and preliminary X-ray crystallographic analysis of lactoperoxidase from buffalo milk*. Acta Crystallogr D Biol Crystallogr, 1995. **51**(Pt 6): p. 1094-6.
9. Aschaffenburg, R. and J. Drewry, *Occurrence of different beta-lactoglobulins in cow's milk*. Nature, 1955. **176**(4474): p. 218-9.
10. Newcomer, M.E., et al., *Crystallization of and preliminary X-ray data for the plasma retinol-binding protein*. J Biol Chem, 1984. **259**(8): p. 5230-1.
11. Newcomer, M.E., et al., *The three-dimensional structure of retinol-binding protein*. Embo J, 1984. **3**(7): p. 1451-4.
12. Brownlow, S., et al., *Bovine beta-lactoglobulin at 1.8 A resolution--still an enigmatic lipocalin*. Structure, 1997. **5**(4): p. 481-95.
13. Branden C., T.J., *Introduction to Protein Structure, 2nd Edition*. 1999, New York: Garland Publishing, Inc.
14. Akerstrom, B., D.R. Flower, and J.P. Salier, *Lipocalins: unity in diversity*. Biochim Biophys Acta, 2000. **1482**(1-2): p. 1-8.

15. Flower, D.R., A.C. North, and C.E. Sansom, *The lipocalin protein family: structural and sequence overview*. Biochim Biophys Acta, 2000. **1482**(1-2): p. 9-24.
16. Bugos, R.C., A.D. Hieber, and H.Y. Yamamoto, *Xanthophyll cycle enzymes are members of the lipocalin family, the first identified from plants*. J Biol Chem, 1998. **273**(25): p. 15321-4.
17. Hieber, A.D., R.C. Bugos, and H.Y. Yamamoto, *Plant lipocalins: violaxanthin de-epoxidase and zeaxanthin epoxidase*. Biochim Biophys Acta, 2000. **1482**(1-2): p. 84-91.
18. Bishop, R.E., et al., *Stationary phase expression of a novel Escherichia coli outer membrane lipoprotein and its relationship with mammalian apolipoprotein D. Implications for the origin of lipocalins*. J Biol Chem, 1995. **270**(39): p. 23097-103.
19. Pervaiz, S. and K. Brew, *Homology of beta-lactoglobulin, serum retinol-binding protein, and protein HC*. Science, 1985. **228**(4697): p. 335-7.
20. Pervaiz, S. and K. Brew, *Homology and structure-function correlations between alpha 1-acid glycoprotein and serum retinol-binding protein and its relatives*. Faseb J, 1987. **1**(3): p. 209-14.
21. Flower, D.R., A.C.T. North, and T.K. Attwood, *Structure and sequence relationships in the lipocalins and related proteins*. Protein Science, 1993. **2**: p. 753-761.
22. Flower, D.R., *Structural relationship of streptavidin to the calycin protein superfamily*. FEBS Lett, 1993. **333**(1-2): p. 99-102.
23. Fuentes-Prior, P., et al., *Structure of the thrombin complex with triabin, a lipocalin-like exosite-binding inhibitor derived from a triatomine bug*. Proc Natl Acad Sci U S A, 1997. **94**(22): p. 11845-50.
24. Flower, D.R., *The lipocalin protein family: structure and function*. Biochem J, 1996. **318** (Pt 1): p. 1-14.
25. Flower, D.R., *Multiple molecular recognition properties of the lipocalin protein family*. J. Mol. Recognit., 1995. **8**(3): p. 185-195.
26. Skerra, A., *Lipocalins as a scaffold*. Biochim Biophys Acta, 2000. **1482**(1-2): p. 337-50.

27. Montfort, W.R., A. Weichsel, and J.F. Andersen, *Nitrophorins and related antihemostatic lipocalins from Rhodnius prolixus and other blood-sucking arthropods*. Biochemical and Biophysical Acta, 2000. **1482**: p. 110-118.
28. Lavoipierre, M.M.J., G. Kickerson, and R.M. Gordon, *Studies on the methods of feeding of blood sucking arthropods. I. The manner in which Triatomine bugs obtain their blood meal, as observed in the tissues of the living rodent, with some remarks on the effects of the bite on human volunteers*. Ann. Trop. Med. Parasit., 1959. **53**: p. 235-250.
29. Kirchhoff, L.V., *American trypanosomiasis (Chagas' Disease) - A tropical disease now in the United States*. New England Journal of Medicine, 1993. **329**: p. 639-644.
30. Champagne, D.E., *The role of salivary vasodilators in bloodfeeding and parasite transmission*. Parasitology Today, 1994. **10**(11): p. 430-433.
31. Ribeiro, J.M., et al., *Role of salivary antihemostatic components in blood feeding by triatomine bugs (Heteroptera)*. J Med Entomol, 1998. **35**(4): p. 599-610.
32. Ribeiro, J.M., et al., *Reversible binding of nitric oxide by a salivary heme protein from a bloodsucking insect*. Science, 1993. **260**(5107): p. 539-41.
33. Champagne, D.E., R.H. Nussenzvieg, and J.M.C. Ribeiro, *Purification, partial characterization and cloning of nitric oxide-carrying heme proteins (nitrophorins) from salivary glands of the blood-sucking insect Rhodnius prolixus*. The Journal of Biological Chemistry, 1995. **270**(15): p. 8691-8695.
34. Walker, F.A., *Nitric oxide interaction with insect nitrophorins and thoughts on the electron configuration of the {FeNO}6 complex*. J Inorg Biochem, 2005. **99**(1): p. 216-36.
35. Moreira, M.F., et al., *Changes in salivary nitrophorin profile during the life cycle of the blood-sucking bug Rhodnius prolixus*. Insect Biochem Mol Biol, 2003. **33**(1): p. 23-28.
36. Andersen, J.F., et al., *Recognition of anionic phospholipid membranes by an antihemostatic protein from a blood-feeding insect*. Biochemistry, 2004. **43**(22): p. 6987-6994.
37. Andersen, J.F., et al., *Kinetics and equilibria in ligand binding by nitrophorins 1-4: Evidence for stabilization of a NO-ferriheme complex through a ligand-induced conformational trap*. Biochemistry, 2000. **39**: p. 10118-10131.

38. Roberts, S.A., et al., *Ligand-Induced Heme Ruffling and Bent NO Geometry in Ultra-High Resolution Structures of Nitrophorin 4*. *Biochemistry*, 2001. **40**: p. 11327-11337.
39. Ribeiro, J.M.C. and F.A. Walker, *High affinity histamine-binding and antihistaminic activity of the salivary nitric oxide-carrying heme protein (nitrophorin) of *Rhodnius prolixus**. *Journal of Experimental Medicine*, 1994. **180**: p. 2251-2257.
40. Zhang, Y., et al., *Nitrophorin-2: a novel mixed-type reversible specific inhibitor of the intrinsic factor-X activating complex*. *Biochemistry*, 1998. **37**(30): p. 10681-10690.
41. Sun, J., et al., *Purification, characterization and cDNA cloning of a novel anticoagulant of the intrinsic pathway (prolixin-S) from salivary glands of the blood sucking bug, *Rhodnius prolixus**. *Thrombosis and Hemostasis*, 1996. **75**(4): p. 573-577.
42. Hellman, K. and R.I. Hawkins, *Prolixin-S and prolixin-G: Two anticoagulants from *Rhodnius prolixus* STAHL*. *Nature*, 1965. **207**: p. 265-268.
43. Ribeiro, J.M.C., M. Schneider, and J.A. Guimaraes, *Purification and characterization of prolixin S (nitrophorin 2), the salivary anticoagulant of the blood-sucking bug *Rhodnius prolixus**. *Biochemical Journal*, 1995. **308**: p. 243-249.
44. Sun, J., et al., *Characterization and cDNA cloning of a hemoprotein in the salivary glands of the blood-sucking insect, *Rhodnius prolixus**. *Insect Biochem. Mol. Biol.*, 1998. **28**(3): p. 191-200.
45. Yuda, M., et al., *Expression, reconstitution and characterization of prolixin-S as a vasodilator--a salivary gland nitric-oxide-binding hemoprotein of *Rhodnius prolixus**. *Eur J Biochem*, 1997. **249**(1): p. 337-342.
46. Ding, X.D., et al., *Nitric oxide binding to the ferri- and ferroheme states of nitrophorin 1, a reversible NO-binding heme protein from the saliva of the blood-sucking insect, *Rhodnius prolixus**. *J. Am. Chem. Soc.*, 1999. **121**: p. 128-138.
47. Shokhireva, T., et al., *Electrochemical and NMR spectroscopic studies of distal pocket mutants of nitrophorin 2: stability, structure, and dynamics of axial ligand complexes*. *Proc. Natl. Acad. Sci. U S A*, 2003. **100**(7): p. 3778-3783.
48. Shokhireva, T., N.V. Shokhirev, and F.A. Walker, *Assignment of heme resonances and determination of the electronic structures of high- and low-spin*

- nitrophorin 2 by 1H and 13C NMR spectroscopy: an explanation of the order of heme methyl resonances in high-spin ferriheme proteins.* Biochemistry, 2003. **42**(3): p. 679-93.
49. Andersen, J.F., et al., *Nitric oxide binding and crystallization of recombinant nitrophorin I, a nitric oxide transport protein from the blood-sucking bug Rhodnius prolixus.* Biochemistry, 1997. **36**(15): p. 4423-4428.
 50. Berry, R.E., et al., *Axial ligand complexes of the Rhodnius nitrophorins: reduction potentials, binding constants, EPR spectra, and structures of the 4-iodopyrazole and imidazole complexes of NP4.* J Biol Inorg Chem, 2004. **9**(2): p. 135-44.
 51. Maes, E.M., et al., *Resonance Raman spectroscopic study of nitrophorin I, a nitric oxide-binding heme protein from Rhodnius prolixus, and its nitrosyl and cyano adducts.* Journal of the American Chemical Society, 2001. **123**(47): p. 11664-11672.
 52. Maes, E.M., et al., *Role of binding site loops in controlling nitric oxide release: structure and kinetics of mutant forms of nitrophorin 4.* Biochemistry, 2004. **43**(21): p. 6679-6690.
 53. Maes, E.M., et al., *Ultrahigh Resolution Structures of Nitrophorin 4: Heme Distortion in Ferrous CO and NO Complexes(,).* Biochemistry, 2005. **44**(38): p. 12690-9.
 54. Weichsel, A., et al., *Crystal structures of a nitric oxide transport protein from a blood-sucking insect.* Nature Structural Biology, 1998. **5**: p. 304-309.
 55. Andersen, J.F. and W.R. Montfort, *Crystal structures of nitrophorin 2: A trifunctional antihemostatic protein from the saliva of Rhodnius prolixus.* The Journal of Biological Chemistry, 2000. **275**: p. 30496-30503.
 56. Weichsel, A., et al., *Nitric oxide binding to nitrophorin 4 induces complete distal pocket burial.* Nat Struct Biol, 2000. **7**(7): p. 551-4.
 57. Andersen, J.F., et al., *The crystal structure of nitrophorin 4 at 1.5 Å resolution: Transport of nitric oxide by a lipocalin-based heme protein.* Structure, 1998. **6**(10): p. 1315-1327.
 58. Kondrashov, D.A., et al., *Protein functional cycle viewed at atomic resolution: conformational change and mobility in nitrophorin 4 as a function of pH and NO binding.* Biochemistry, 2004. **43**(43): p. 13637-47.

59. Newcomer, M.E., *Structure of the epididymal retinoic acid binding protein at 2.1 Å resolution*. Structure, 1993. **1**(1): p. 7-18.
60. Shelnut, J.A., et al., *Nonplanar porphyrins and their significance in proteins*. Chemical Society Reviews, 1998. **27**: p. 31-41.
61. Ma, J.-G., et al., *The Structural Origin of Nonplanar Heme Distortions in Tetraheme Ferricytochromes c3*. Biochemistry, 1998. **37**(36): p. 12431-12442.
62. Jentzen, W., J.G. Ma, and J.A. Shelnut, *Conservation of the conformation of the porphyrin macrocycle in hemoproteins*. Biophys J, 1998. **74**(2 Pt 1): p. 753-63.
63. Shelnut, J.A., et al., *Nonplanar porphyrins and their significance in proteins*. Chemical Society Reviews, 1998. **27**: p. 31-41.
64. Jentzen, W., X.-Z. Song, and J.A. Shelnut, *Structural Characterization of Synthetic and Protein-Bound Porphyrins in Terms of the Lowest-Frequency Normal Coordinates of the Macrocycle*. J. Phys. Chem. B., 1997. **101**: p. 1684-1699.
65. Coles, M., et al., *The solution structure and dynamics of human neutrophil gelatinase-associated lipocalin*. J Mol Biol, 1999. **289**(1): p. 139-57.
66. Paesen, G.C., et al., *Tick histamine-binding proteins: lipocalins with a second binding cavity*. Biochim Biophys Acta, 2000. **1482**(1-2): p. 92-101.
67. Glasgow, B.J., et al., *A conserved disulfide motif in human tear lipocalins influences ligand binding*. Biochemistry, 1998. **37**(8): p. 2215-25.
68. Amoia, A.M. and W.R. Montfort, *High resolution structure of apo nitrophorin 4: a rigid beta-barrel remains*. To be submitted to Protein Science, 2006.
69. Weichsel, A., et al., *Reversible nitric oxide binding to nitrophorin 4 from Rhodnius prolixus involves complete distal pocket burial*. Nature Structural Biology, 2000. **7**: p. 551-554.
70. Leslie, A.G.W., *Recent changes to the MOSFLM package for processing film and image plate data*. Newsletter on Protein Crystallography, 1992. **26**.
71. Collaborative Computational Project Number 4, *The CCP4 Suite: Programs for Protein Crystallography*. Acta Crystallographica, 1994. **D50**: p. 760-763.
72. Emsley, P. and K. Cowtan, *Coot: model-building tools for molecular graphics*. Acta Crystallogr D Biol Crystallogr, 2004. **60**(Pt 12 Pt 1): p. 2126-32.

73. Laskowski, R.A., et al., *PROCHECK: A program to check the stereochemical quality of protein structures*. Journal of Applied Crystallography, 1993. **26**: p. 283-291.
74. DeLano, W.L., *The PyMOL Molecular Graphics System*, ed. D. Scientific. 2002, San Carlos, CA, USA.
75. Zanotti, G., R. Berni, and H.L. Monaco, *Crystal structure of liganded and unliganded forms of bovine plasma retinol-binding protein*. J Biol Chem, 1993. **268**(15): p. 10728-38.
76. Kirissinel, E. and K. Henrick. *Protein structure comparison in 3D based on secondary structure matching (SSM) followed by Ca alignment, scored by a new structural similarity function*. in *Proceedings of the 5th International Conference on Molecular Structural Biology*. 2003, September 3-7. Vienna.
77. Chen, X., et al., *Crystal structure of apo-cellular retinoic acid-binding protein type II (R111M) suggests a mechanism of ligand entry*. J Mol Biol, 1998. **278**(3): p. 641-53.
78. Kleywegt, G.J., et al., *Crystal structures of cellular retinoic acid binding proteins I and II in complex with all-trans-retinoic acid and a synthetic retinoid*. Structure, 1994. **2**(12): p. 1241-58.
79. Wang, L., et al., *NMR solution structure of type II human cellular retinoic acid binding protein: implications for ligand binding*. Biochemistry, 1998. **37**(37): p. 12727-36.
80. Winter, N.S., J.M. Bratt, and L.J. Banaszak, *Crystal structures of holo and apo-cellular retinol-binding protein II*. J Mol Biol, 1993. **230**(4): p. 1247-59.
81. Lu, J., et al., *The structure and dynamics of rat apo-cellular retinol-binding protein II in solution: comparison with the X-ray structure*. J Mol Biol, 1999. **286**(4): p. 1179-95.
82. Lu, J., et al., *Binding of retinol induces changes in rat cellular retinol-binding protein II conformation and backbone dynamics*. J Mol Biol, 2000. **300**(3): p. 619-32.
83. Zanotti, G., et al., *Crystal structure of the trigonal form of human plasma retinol-binding protein at 2.5 Å resolution*. J Mol Biol, 1993. **230**(2): p. 613-24.

84. Sacchettini, J.C., J.I. Gordon, and L.J. Banaszak, *Refined apoprotein structure of rat intestinal fatty acid binding protein produced in Escherichia coli*. Proc Natl Acad Sci U S A, 1989. **86**(20): p. 7736-40.
85. Sacchettini, J.C., J.I. Gordon, and L.J. Banaszak, *Crystal structure of rat intestinal fatty-acid-binding protein. Refinement and analysis of the Escherichia coli-derived protein with bound palmitate*. J Mol Biol, 1989. **208**(2): p. 327-39.
86. Chaudhuri, B.N., et al., *The structures of alpha 2u-globulin and its complex with a hyaline droplet inducer*. Acta Crystallogr D Biol Crystallogr, 1999. **55**(Pt 4): p. 753-62.
87. Paesen, G.C., et al., *Tick histamine-binding proteins: isolation, cloning, and three-dimensional structure*. Mol Cell, 1999. **3**(5): p. 661-71.
88. Greene, L.H., et al., *Role of conserved residues in structure and stability: tryptophans of human serum retinol-binding protein, a model for the lipocalin superfamily*. Protein Sci, 2001. **10**(11): p. 2301-16.
89. Clark, P.L., et al., *Intrinsic tryptophans of CRABPI as probes of structure and folding*. Protein Sci, 1996. **5**(6): p. 1108-17.
90. Ambrus, A., K. Friedrich, and A. Somogyi, *Oligomerization of nitrophorins*. Anal Biochem, 2006. **352**(2): p. 286-95.
91. Nakamura, M., et al., *Electron Configuration of Ferric Ions in Low-Spin (Dicyano)(meso-tetraarylporphyrinato)iron(III) Complexes*. Inorganic Chemistry, 1999. **38**: p. 3857-3862.
92. Ikeue, T., et al., *Spin Distribution in Low-Spin (meso-Tetraalkylporphyrinato)iron(III) Complexes with (dx_y,yz)⁴(dxy)¹ Configuration. Studies by ¹H NMR, ¹³C NMR, and EPR Spectroscopies*. Journal of the American Chemical Society, 2000. **122**: p. 4068-4076.
93. Amoia, A.M., J.L. Brailey, and W.R. Montfort, *Heme distortion in nitrophorin 4: high resolution structures of heme altered and L123V and L133V mutant proteins*. To be submitted to Biochemistry, 2006.
94. Pflugrath, J.W., *The finer things in X-ray diffraction data collection*. Acta Crystallographica, 1999. **D55**(Pt 10): p. 1718-1725.
95. Jones, T.A., et al., *Improved methods for building protein models in electron density maps and the location of errors in these models*. Acta Crystallographica, 1991. **A47**: p. 110-119.

96. Sheldrick, G.M. and T.R. Schneider, *SHELXL: High -Resolution Refinement*. Methods in Enzymology, 1997. **277**(Part B): p. 319-343.
97. Esnouf, R.M., *An extensively modified version of MolScript that includes greatly enhanced coloring capabilities*. J. Mol. Graph. Model, 1997. **15**(2): p. 132-134, 112-113.
98. Merritt, E.A. and D.J. Bacon, *Raster3D photorealistic molecular graphics*. Methods in Enzymology, 1997. **277**: p. 505-524.
99. Kleywegt, G.J., *Validation of protein models from C[alpha] coordinates alone*. J Mol Biol, 1997(273): p. 371-376.
100. Murshudov, G.N. and E.J. Dodson, *Simplified error estimation a la Cruickshank in macromolecular crystallography*. CCP4 Newsletter, 1997.
101. Scheidt, W.R. and M.K. Ellison, *The synthetic and structural chemistry of heme derivatives with nitric oxide ligands*. Accounts of Chemical Research, 1999. **32**: p. 350-359.
102. Reading, N.S. and S.D. Aust, *Effect of modified hemes on the spectral properties and activity of manganese peroxidase*. Archives of Biochemistry and Biophysics, 1998. **359**(2): p. 291-296.
103. Munro, O.Q., et al., *Structural and molecular mechanics studies on highly ruffled low-spin (porphinato)iron(III) complexes*. Journal of the American Chemical Society, 1995. **117**(3): p. 935-954.
104. Yatsunyk, L.A., M.D. Carducci, and F.A. Walker, *Low-spin ferriheme models of the cytochromes: correlation of molecular structure with EPR spectral type*. J Am Chem Soc, 2003. **125**(51): p. 15986-6005.
105. Schreiter, E.R., et al., *S-Nitrosylation-induced conformational change in blackfin tuna Myoglobin*. to be submitted, 2006.
106. Senge, M.O., *Highly Substituted Porphyrins*, in *The Porphyrin Handbook*, K.M. Kadish, K.M. Smith, and R. Guilard, Editors. 2000, Academic Press: San Diego. p. 240-347.
107. Kadish, K.M., E. Van Camelbecke, and G. Royal, *Electrochemistry of Metalloporphyrins in Nonaqueous Media*, in *The Porphyrin Handbook*, K.M. Kadish, K.M. Smith, and R. Guilard, Editors. 2000, Academic Press: San Diego. p. 3-125.

108. Ma, J.G., et al., *The structural origin of nonplanar heme distortions in tetraheme ferricytochromes c3*. Biochemistry, 1998. **37**(36): p. 12431-12442.
109. Linder, D.P., et al., *Five-coordinate Fe(III)NO and Fe(II)CO porphyrinates: where are the electrons and why does it matter?* J Am Chem Soc, 2004. **126**(43): p. 14136-48.
110. Linder, D.P. and K.R. Rodgers, *Fe-N-O structure and bonding in six-coordinate {FeNO}6 porphyrinates containing imidazole: implications for reactivity of coordinated NO*. Inorg Chem, 2005. **44**(5): p. 1367-80.
111. Amoia, A.M. and W.R. Montfort, *Ligand protection and nitric oxide interactions with heme in nitrophorin 4: kinetic and structural analyses of a loop mutant*. to be submitted, Biochemistry, 2006.
112. Matheson, I.B.C., *A critical comparison of least absolute deviation fitting (robust) and least-squares fitting: the importance of error distributions*. Computers in Chemistry, 1990. **14**: p. 49-57.
113. Olson, J.S. and G.N. Phillips, Jr., *Kinetic Pathways and Barriers for Ligand Binding to Myoglobin*. J Biol Chem, 1996. **271**(30): p. 17596.
114. Hess, D.T., et al., *Protein S-nitrosylation: purview and parameters*. Nat Rev Mol Cell Biol, 2005. **6**(2): p. 150-66.
115. Brandish, P.E., W. Buechler, and M.A. Marletta, *Regeneration of the ferrous heme of soluble guanylate cyclase from the nitric oxide complex: acceleration by thiols and oxyhemoglobin*. Biochemistry, 1998. **37**(48): p. 16898-907.
116. Miranda, K., *Assistant Professor, Department of Chemistry, University of Arizona, Tucson.*, A.M. Amoia, Editor. 2006.
117. Brew, K. and L. Greene, *Evolution, folding and flexibility*. Protein Eng., 1997. **10**(S44).
118. Greene, L. and K. Brew, *Conserved residues in the lipocalins suggest a folding motif*. Protein Eng., 1995. **8**(S100).